EMBRACE System Engineering and Astronomical Test Plan
SKADS: DS5T3

S.A. Torchinsky (Task Leader), A.O.H. Olofsson, L. Chemin, R. Strom,
P. Picard, J.M. Martin, B. Stappers, J. Bregman, N. Ebbendorf, I. Cognard, P. Colom, G.W. Kant,
P. Renaud, M. Ruiter, C. Taffoureau, H. van der Marel, E. van der Wal

June 4, 2008

Contents

1

Introduction

This document outlines the test plan for EMBRACE as a system. It is assumed that basic electronic check-out of EMBRACE tiles has been done, and the experiments described here are done in the final EMBRACE location, with some subset of the full system. It is useful to do these tests even with a single EMBRACE tile, setup at the EMBRACE location in Westerbork or Nançay, for testing system operations and correlation with Westerbork.

The accompanying document "EMBRACE Engineering Test Plan" by Mark Ruiter describes a hierarchy of component level testing through subsystems, leading finally to the full EMBRACE system. The present document is concerned with testing the EMBRACE system.

The original SKADS deliverable was for a separate "Engineering Test Plan" and "Astronomical Test Plan." These two categories are sometimes difficult to distinguish, with some engineering testing having scientific interest (for example, long integrations). Therefore, the two documents are presented here together as an overall system test plan.

The document is organised in sections going from the more engineering related testing to purely scientific experiments. Section 2 deals with the measurement of basic performance parameters, such as system temperature, effective collecting area, and beam profile as a function of pointing. Section 3 presents a scheme for the validation of the beamforming capability of EMBRACE. Section 4 describes interferometric observations using the two EMBRACE installations, at Westerbork and Nançay, as well as interferometry between the EMBRACE Westerbork site and one of the WSRT dishes. Pulsar observing is the subject of Section 5, and it describes how to use the Nançay pulsar dedispersion cluster BON for EMBRACE observations. This also includes the possibility of reconfiguring BON to record data for spectral line observations. Section 6 continues with the discussion of pulsar observing, but this time using Westerbork. In Section 7, two projects are presented for the mapping of HI in nearby galaxies. This will also test the key capability of EMBRACE to do multibeam observations, as well as its ability to integrate over long periods of time in order to detect faint sources. Section 8 describes the astrophysically interesting molecular species which may be detectable with EMBRACE, and which forms the basis of a project to detect organic molecules with SKA in the mid frequency range (~500 MHz to ~1600 MHz). Detailed lists of molecular species are provided in the Appendixes A and B. Section 9 looks at somewhat more speculative possibilities, but which would be scientifically rewarding. Such possibilities include the monitoring of time variable phenomena, such as the Fiedler Effect. Repeating the Leiden-Dwingeloo HI Survey using the wide field of view and multibeaming capability of EMBRACE would demonstrate the fast mapping capability of the Aperture Array technology. A list of possible astronomical sources is given in Section 10.

1.1 Abbreviations used in this document

BON	=	Berkeley-Orléans-Nançay pulsar dedispersion cluster
DS	=	Design Study
DS5T3	=	Design Study #5, Task #3 “EMBRACE Test & Evaluation”
EIRP	=	Effective Isotropic Radiated Power
EMBRACE	=	Electronic Multi Beam Radio Astronomy Experiment
GMC	=	Giant Molecular Cloud
ISRF	=	Interstellar Standard Radiation Field
ISM	=	Interstellar Medium
LEO	=	Low Earth Orbit
NATS	=	Nançay Antenna Test Site
RRL	=	Radio Recombination Line
RFI	=	Radio Frequency Interference
RMS	=	Root Mean Square
SEFD	=	System Equivalent Flux Density
SKA	=	Square Kilometre Array
SKADS	=	SKA Design Studies
SNR	=	Signal to Noise Ratio
THEA	=	THousand Element Array
WATS	=	Westerbork Antenna Test Site
WSRT	=	Westerbork Synthesis Radio Telescope

2

Evaluating the primary EMBRACE instrument parameters

In order to acquire useful astronomical data, we need to: i) determine the system noise temperature which allows us to scale the intensity axis correctly, and ii) determine the beam profile/collecting area in order to estimate expected signal strengths when planning observations and also reconstruct the true brightness temperature of unresolved sources.

2.1 Noise determination

The most commonly used method is to assume a linear relation between measured power and noise temperature (valid within the Rayleigh-Jeans regime if the frontend/backend system is linear in all other respects), and compare the the measurements of two sources of known temperatures that fill the beam (the Y-factor approach). If the system temperature is expected to change rapidly, it is desirable to make the two measurements in quick succession and repeat the measurement often. Such is the case when the optical depth in the atmosphere is significant and $T_{\rm atm} \geq T_{\rm rec}$. At cm wavelengths this should not be a major concern. Below $\approx$1m the ionosphere come into play but the effects are mainly of defocussing the array (due to spatially varying phase delays)[1]. Apparently this is also a function of the physical separation of the antennæ which is indeed very small EMBRACE.

For the THEA instrument ((Woestenburg & Dijkstra 2003)), it was advocated that the Y-factor method may be used by measuring the cold sky at zenith and a hot load (consisting of an absorber that fills up the near-field) in a phased-up adder mode. The method becomes completely analogous to a single-dish measurement if gain variations across the elements are ignored. The aforementioned paper further reports that even for relatively large gain variations, the error in $T_{\rm sys}$ is less than 10% which could be considered good. The method is said to be valid for an infinite element array, and could therefore (perhaps) be yet more valid for EMBRACE compared to THEA; in a relative sense EMBRACE will have less edge elements (that are exposed to an "anisotropic" environment).

(Wijnholds & Boonstra 2006),(Wijnholds 2005) also discusses a method to calibrate a phased array (LO-

[1] An approach to rectifying data thusly affected was demonstrated at a recent LOFAR Super Station (LSS) meeting but it is still work in progress.

FAR) by using full sky measurements and known flux densities and distributions of a number of sources. In this manner, one can estimate the full matrix of complex antenna gains. It is rather complicated and may not be applicable to EMBRACE: in order to construct a sky image with the prototype LOFAR station, they used the signals from each antenna (or rather the $N \times N$ matrix of cross correlations). With EMBRACE – while cross correlations are indeed available prior to digital beam-forming – the RF beams are formed at patch level by pre-settings of the BF chips. *Thus our field of view can never be larger than that seen by a single patch.* The cross-correlations are made between the RF beams of the phased-up patches. The patches should therefore be seen as virtual antennæ with a zenith beam of (very!) roughly λ/D radians (D is the side length of the patch) whereas the LOFAR antennæ are designed to be as close to full sky omnidirectional as possible. It is not clear to the author at present time if the aforementioned LOFAR method can be adopted to be used for a mosaic in which the RF beams have been moved around (either to target the whole sky in a quick sequence, or possibly by targetting the same strong sources at different times and thereby at different azimuths and elevations).

Implementation of Noise Characterisation for EMBRACE

The cold sky observation needed for the Y-factor measurement should be straight forward. Although avoiding astronomical sources is not a major concern since they will make a very small contribution in the large RF beam, it is easily done by avoiding the galactic plane (in which Cas A, Cyg A, Taurus A all reside). The frequency range should be sampled as densely as possible but a minimum of 5 frequency points is estimated to be needed to detect general trends across the band. The output data should be in the form of the sum of the RF-beams (adder mode; one pixel, no spatial resolution needed). If practical, we can repeat the measurements at 45° elevation in the N,S,E,W directions, and so forth at as many elevations as needed. This will give information of the side-lobe noise contribution from the particular site chosen. In (Woestenburg & Dijkstra 2003), all the uncorrelated noise sources outside the receiver is assembled in one term called T_g and this is an unknown quantity that has to be estimated independently. In order to determine the value of this figure, a deep knowledge of the hardware is required. However, in the THEA example, it accounts for only ~15% of T_{sys} and even if it is neglected, one still obtains a reasonable first estimate of the system noise. Of course, if the theoretical T_{rec} can additionally be calculated to some accuracy it would directly tell us T_{g}. Another way would be to measure absorbers cooled to liquid nitrogen temperature, but this extremely difficult for large area absorbers because water condenses on the absorber before the absorber is fully cooled down.

The flux density of Cyg A can be expressed as follows (Baars et al., A&A, 61, 99, 1977) over the frequency range of interest for EMBRACE, 20 MHz – 2 GHz:

$$\log S = 4.695 + 0.085 \log \nu - 0.178 \log^2 \nu$$

with S in Jy and ν in MHz.

2.1.1 Nominal sensitivity calculation

One of the goals of the test observations will be to determine basic parameters relating to the sensitivity, such as the effective area, A_{eff}, and system temperature, T_{s}. For the purpose of our discussion, it is useful to have an indication of what we can expect. For this purpose, the following calculations will be used, based upon an assumed $A_{\mathrm{eff}} = 100$ m^2 and $T_{\mathrm{s}} = 100$ K. (The final EMBRACE values may well be better than these, but it is probably better to be on the pessimistic side when considering possible tests. Moreover, away from the zenith, foreshortening will diminish A_{eff}.)

In addition to the assumed values for $A_{\rm eff}$ and $T_{\rm s}$, the calculation will be done for a bandwidth of $BW = 10$ MHz and integration time, $\tau = 10$ s. Using the standard Rayleigh-Jeans relationship, $S = 2kT/A_{\rm eff}$, we obtain a (rounded-off) SEFD for EMBRACE of $\simeq 30$ Jy/K. The expected rms noise level, σ, is then,

$$\sigma = \frac{100 \text{ K}}{(10 \text{ s} \times 10^7 \text{ Hz})^{1/2}} = 0.01 \text{ K}$$

For the estimated SEFD, this corresponds to 300 mJy. For a line observation, suppose we observe with $BW = 5$ kHz (equivalent to about 1 km/s for the HI line at 1420 MHz), then,

$$\sigma = \frac{100 \text{ K}}{(10 \text{ s} \times 5 \times 10^3 \text{ Hz})^{1/2}} = 0.4 \text{ K}$$

Where appropriate, these values will be used in the following discussion.

2.2 Beam and Aperture Characterisation

For a single-dish instrument the main beam size can be estimated by mapping out a point source. The main beam efficiency can then be measured by making a single observation towards a source not very much smaller than the beam, with a known source distribution, e.g. a planet which can be modelled as a disc[2]. For arrays, the beam will vary with sky direction and should be characterised as a function of azimuth and elevation. The aperture efficiency is a measure of how much of the instrument's physical cross-section area is actually used for signal collection. For an ideal instrument, the received power would be the procuct of the flux density and the projected physical area. The efficiency can be seen as the ratio of the measured and ideal received power from a well known source. Here it is important that the source is much smaller than the beam. Otherwise the received power would be independent on the flux since the antenna gain is close to zero far away from the beam centre.

2.2.1 Synthesis Imaging with Aperture Array Stations

A synthesis image is the average of a series of individually self calibrated snapshot images. Since the beam of an aperture array station changes shape while tracking a field in the sky, the final average station beam pattern depends on the actual combination of snapshot beams, just as the synthesized array beam pattern.

The station beam pattern with its side lobes as seen from a sky object rotates and foreshortens depending on the declination of the object and the latitude of the station. This shows that the complex power beam pattern for any baseline, which is the product of the voltage beam pattern of one station multiplied with the complex conjugated voltage beam pattern of the other station, is different for every station combination at any instant. This is in principle not different from VLBI imaging with different telescopes, but needs appropriate self calibration and image processing such as has been developed for LOFAR to allow full field of view imaging. The basic self calibration process in LOFAR solves for a complex gain factor in at least four different directions corresponding to the strongest sources within the primary beam to solve for the effective pointing of the main beam and for the effective atmospheric phase screen including tilt and curvature. These strongest sources can then be perfectly subtracted from the U,V-data and the next set of sources that are too weak to be solved for, will be subtracted using complex gain factors derived from interpolation over the phase screen and over the nominal primary beams as established from the station calibration.

[2]By observing a highly resolved disc-like source one can get detailed information on the beam pattern by sweeping over the edges. It can of course also be used as an intensity calibration source in that case

A key issue is the side lobe level, which should be so low that only the strongest source in the sky would be just solvable to obtain a proper complex gain factor for each station which allows perfect subtraction. The reason is that we can solve for complex gain factors in at most N/2 directions when there are N stations, while we need a signal to noise ratio (SNR) larger than 3 for each source on each baseline that has to be used in the solution. So there is no point in synthesizing an image with just two or three stations that are moved around to build up sufficient U,V-coverage, since we cannot self calibrate each snapshot observation. We need at least 15 stations for proper self calibration and each station of sufficient size to have sufficiently low side lobes to be representative. LOFAR has low band stations with 48 dipoles at randomized sparse positions while the high band stations have 48 tiles with 16 dipoles in regular sparse arrays with gaps between the tiles. The LOFAR tiles have delay control per dipole and course gain settings. EMBRACE has a contiguous distribution of Vivaldi antenna elements organized in 144 tiles formed by 6 boards each providing 3 groups of 4 dipoles. The four antennas are combined with phase control in steps of 45 degrees and gain control in steps of 0.5 dB. The groups and boards are combined with 2 steps of delay control that allow appropriate adding of four tiles in a cluster. Although all clusters of four tiles are added with accurate phase and gain control by the digital receiver chain, the effective tapering of a LOFAR station has a much more limited capability to minimize the side lobes than the EMBRACE station.

In conclusion, EMBRACE has, apart from sensitivity and wide field capability, to demonstrate that the combination of RF and digital beam forming provides sufficient low side lobes, in the frequency range where the array is in dense mode. The station side lobe level needs to be so low that a synthesis array of 15 m stations would not suffer from artefacts in its main beam caused by objects in the station side lobes that are too weak to be self calibrated and subtracted accurately.

2.2.2 Station Side Lobes

The EMBRACE station will have 144 tiles with 72 dual polarization antenna pairs producing two station beams for only a single polarization. The elements are placed on a rectangular grid with 0.125 m spacing providing a grating free power pattern for frequencies below the Nyquist frequency of 1.2 GHz. The station power pattern is for a non tapered array given by $[\sin(\pi k)/\pi k.\sin(\pi l)/\pi l]2$, which is dominated by the cross pattern on the k and l axes. For an array with $\sim 100 \times 100$ elements the weakest side lobes on the cross are typically 4×10^{-5} at the Nyquist frequency and can be further reduced by appropriate tapering. However the 40 side lobes on the cross around the main beam are stronger than 10^{-3}. This means that when Cyg A, Cas A or Tau A are located in one of these side lobes we get a response of 6, 3.1 or 1 Jy at 1 GHz. These fluxes are much stronger than the fluxes of the four strongest sources in the main beam with 1.8 square degrees solid angle that typically range from 0.24 to 0.095 Jy.

The RF beam former uses phase steps of 45 degrees, which results into an rms phase error σ of 0.23 radians per antenna element. This causes an rms error of $2\sigma(P(k,l)/N_e))^{1/2}$ in the power beam pattern $P(k,l)$, which amounts for $N_e \sim 104$ elements to $\sim 4.6 \times 10^{-3} P(k,l)^{1/2}$. For the 40 strongest cross side lobes this results in an rms error larger than 1.5×10^{-4}. The total beam solid angle of these 40 lobes is 36 square degrees, which is 1.8×10^{-3} of a hemisphere at 1 GHz. So there is a chance of 0.005 that one of the three A-sources will be caught by a strong cross side lobe. In such a case we could in principle correct for the nominal side lobe response, but we are left with an error response stronger than 0.15 Jy.

Further analysis of the consequences for self calibration and synthesis imaging is outside the scope of this testing report, but it is clear that the actual side lobe performance is a crucial parameter that needs experimental verification for various taper functions. Especially the behaviour of the error pattern as function of the beam

tracking algorithm needs experimental verification.

2.2.3 Implementation of Beam Characterisation for EMBRACE

In order to study the beam properties, we need strong sources in the northern hemisphere ($\delta_{\min} \approx +3^\circ$, preferably much larger). The option of employing spectral lines here is also open but perhaps not practical, the advantage being that baselines can be subtracted stabilising the zero levels. The only candidate would be the HI spin-flip transition at 21 cm. Other lines may turn out to be measurable as independent spectroscopy test targets, see discussion elsewhere. But as can be seen in the THEA HI survey (and as has been known for a very long time of course), it has a complex distribution throughout the Milky Way ((Wijnholds et al. 2004)). Additionally, the SNR in terms of integrated emission is much larger for continuum radiation.

As astronomical continuum targets, the only two useful sources are Cyg A and Cas A (the former a radio galaxy and the latter a super nova remnant). They reportedly have about equal flux densities towards the lower frequency end, and both have rather useful declinations, 41° and 59°, respectively. Thus Cyg A is the closest to pass directly overhead in Nançay and can be used for measuring the beam at nearly all elevations.

At 5m wavelength, a LOFAR single station test meausrement reveals that one obtains a large SNR of Cyg A with only 156 kHz bandwidth and a beam of a few degrees after a very short integration.

Another option is to use satellites as calibrators. Here we have many options open to us but it remains to sort out which ones are practical. If it is possible to measure satellites in LEOs (Low Earth Orbits $h < 1000$ km) we will, for example, have access to the multitude of crafts in sun-synchronous/near-polar orbits. That in turn will enable scans in the the north-south directions. The integration times must not exceed 2s (=1.5° movement on the sky) unless we track the source by rephasing the patches continuously.

Geostationary satellites are fixed on the sky but their elevations are always much below the 45° intended operational limit of the instrument. However, THEA managed to measure one ((bij de Vaate et al 2002)) so it can probably be done for demonstration purposes.

Among satellites moving at a slower rate, we have GPS type and Molniya satellites. Both of these have "semi-synchronous" orbits (orbital period of 1/2 sidereal day), meaning that they follow the same ground-track after two completed orbits. It is thus not certain one can find a satellite that passes directly over-head[3]. GPS satellites will have maximum angular sky rates of $\sim 0.01^\circ \mathrm{sec}^{-1}$ (neglecting the effect of earth's W-E rotation which corresponds to about $0.003^\circ \mathrm{sec}^{-1}$ in the zenith direction).

Molnyia orbits would be the best choice since they are designed to "hang" in the sky at high latitudes for as long times as possible by use of an eccentric orbit. Although perfectly applicable to Europe, the only such spacecrafts launched to date unfortunately seem to have their longitudes of apogee in central Russia (and by necessity also in Canada due to the 12h orbit).

The basic requirements for satellite measurements would be that they transmit continously at a suitable carrier frequency and not inside a very narrow beam (unless it passes overhead and is pointed in the nadir direction[4]).

If we want to do aperture efficiency tests, we need data on the transmitted power but the EIRP ($=P_t G_t$) should be publicly available for many satellites.

[3] LEOs, on the other hand, will *always* pass directly over-head every few weeks if the inclination is larger than the observer's latitude. This is due to the ground-track drifting westwards by ~ 24 deg every orbit.

[4] Such could be the case for radar satellites which are often in polar LEOs.

Example Test 1

As the very simplest test, we could point the array towards south at an elevation of $90^\circ - (\phi_{\text{Nancay}} - \delta_{\text{Cyg A}}) = 83.4^\circ$ and make measurements regularly before and after Cyg A transits, perhaps all the time it is above the horizon. This will give some basic information about the digital beam behaviour inside the RF beam but hopefully also about the RF gain pattern along one dimension. Output data from one-pixel (adder) mode as well as cross correlations would be desired. This test could be useful even if only one patch is available. It would be good to cover both the lowest and highest frequencies, but if a choice has to be made low frequency is better, especially if the alignment parameters (pointing model) of the array has not been established; at 300 MHz we can "miss" the source by 15° and still be inside the RF beam. Multiple frequency bands (at minimum resolution) is desired in case one or several are affected by RFI. Taking the measurement at maximum strength, an aperture efficiency estimate should be possible using tabulated flux densities. The other strong source, Cas A, is fortunately about 35° (sky angle) away and thus outside the RF beam even at the low frequency end. The weak contribution from the extended Milky Way must simply be ignored as a first approximation. This approach also provides us with off-source measurements close in time – both before and after the signal – if needed.

The next step would be to track the source from horizon to horizon. This would give information on the digital beam patterns, the maximum RF gains, the effective antenna areas etc all as a function of elevation, as well as demonstrating the basic capability to track a source.

Example Test 2

We could use a fixed pointing at south azimuth at an elevation to intercept the meridian transit of Cas A, Cyg A or Tau A. Then we do not need updating or steering at all and get an impression of the side lobes. This is a power mode. Better sensitivity is obtained when we cross correlate EMBRACE with a station that tracks the object of interest such that we observe the voltage pattern.

All initial testing is most easily done using the station correlator, which forms the auto correlations of and all cross correlations between the clusters formed by 4 tiles each. The EMBRACE station at the WSRT site has 36 tile clusters of which each produces two beams.

At a later stage the X and the Y-output of the nearest WSRT dish of 25 m could be connected to some spare inputs of the receivers of the EMBRACE station processor. Then the output of the UHF-high or the L-band receiver could be cross-correlated against each other to provide normalised correlation coefficients for a whole range of objects ranging from a few Jy to 6000 Jy on Cyg A.

The normalized correlation coefficient of an interferometer formed by two antenna stations with flux sensitivities S1 and S2 observing a point source with flux S_s is given in first order approximation by

$$C_{12} = S_s[(S_1 + S_s)(S_2 + S_s)]^{-1/2}. \tag{2.1}$$

A more detailed analysis is given by (Crane & Napier 1988).

The most sensitive method of observing the side lobe cross pattern is by forming a beam on Cyg A with one beam and cross-correlate this signal with the second beam that points to a specific side lobe of the first beam. This cross correlation could for instance be done with a PC system that uses the beam formed output for a subset of the 512 sub-bands that is available from the 1 GbE outputs of the station processing units. This method allows forming spectral channels within each sub band of 192 kHz.

It must be realised that both signals that are cross-correlated contain the same receiver noise, and the sky signals shared by the two beams that needs to be corrected for.

Instead of cross-correlating the two beams we could cross-correlate the station beam with the beam of a single tile. It is attractive to place this reference tile at some distance from the EMBRACE station to reduce coupling effects. With two reference tiles in orthogonal directions we could observe the two coherences $< V_{Ex} \cdot V_X >$ and $< V_{Ex} \cdot V_Y >$. If these are complemented with the coherencies observed for an object at the same elevation but at a 90 degree different azimuth, we could infer the polarisation characteristics of the average element pattern of the station, which is expected to be the same as for the two tiles.

When we work with a reference telescope we need to correct for the fringe phase of the baseline between EMBRACE and the reference for the specific direction of the object that is used. On a 50 m baseline at 25 cm wavelength at 1.2 GHz the max fringe rate is given by $\sim 50/.25 = 200$ fringes in $\sim$ 4 hours or fringe period $\sim$ 1 min. With 1 sec readout easy post correlation fringe tracking can be done.

An alternative method uses the cross correlations between the tiles provided by the station correlator and evaluates for a given sub band of 192 kHz for each integration time interval of 5 seconds a complete sky snapshot image. Here too two orthogonal reference tiles could be introduced.

Special attention is needed to have observing modes where the RF tile beam formers are continuously updated or at a fixed setting while the digital beam forming is continuously updated or at a fixed setting. Then Cyg A or Cas A could be either tracked on a fixed side lobe or are left drifting through the side lobe pattern of EMBRACE while we still have the tracking or drifting option for the reference tiles. We could even use almost tracking while the sources slowly drift through the side lobe cross to increase the effective integration time on weak side lobes. By comparing the results of the various modes we can verify the magnitude of the error side lobes as discussed before.

Sensitivity Calculation

- WSRT dish sensitivity 250 m^2 effective and 25 K, $S \sim 250$ Jy
- EMBRACE sensitivity 100 m^2 effective and 100 K, $S \sim 2500$ Jy
- Interferometer $\sim (250 \times 2500)^{1/2} = 790$ Jy, $dS = S(B \cdot t)^{-1/2}$ with 156 kHz and 1 sec $dS \sim 2$ Jy

Using Cas A with 2000 Jy we have rms SNR$\sim$ 1000 in one subband after 1 sec when both stations are pointed. This indicates that a side lobe of -60 dB could be detected.

When the source flux S_s is comparable with the system sensitivity S_1 and S_2 we need to evaluate the ratio in correlation coefficients.

Both stations pointed

$$C_p = \left[\frac{S_s}{(S_s + S_1)} \cdot \frac{S_s}{(S_s + S_2)} \right]^{1/2} \tag{2.2}$$

Station 1 pointed with the main lobe and Station 2 pointed with side lobes that intercept only a fraction p of the source power

$$C_s = \left[\frac{S_s}{(S_s + S_1)} \cdot \frac{pS_s}{(pS_s + S_2)} \right]^{1/2} \tag{2.3}$$

Then

$$\frac{C_s}{C_p} = p^{1/2}\left[\frac{(S_s + S_2)}{(pS_s + S_2)}\right]^{1/2}. \tag{2.4}$$

The noise in C_s/C_p follows from

$$\frac{\delta(C_s/C_p)}{(C_s/C_p)} = \frac{\delta C_s}{C_s} + \frac{\delta C_p}{C_p} \tag{2.5}$$

$$\delta(C_s/C_p) = \frac{\delta C_s}{C_p} + \frac{\delta C_p}{C_s} \tag{2.6}$$

while

$$\delta C_s = \delta C_p = \delta C = (B \cdot t)^{-1/2} \simeq 2.5 \times 10^{-3} \tag{2.7}$$

after 1 sec and 156 kHz of one sub band Since $C_s \sim C_p \cdot p^{1/2} \ll C_p$, so the noise in (C_s/C_p) is dominated by the term with $1/C_s$. We could even use a single tile instead of a WSRT dish replacing S_1 with $S_t \sim 250,000$ Jy. This reduces C_s as well as C_p only by a factor

$$\left[\frac{S_s + S_1}{S_s + S_t}\right]^{1/2} \sim 0.1 \tag{2.8}$$

while the noise remains the same.

2.3 Stability

We will here consider stability to be a general state in which the instrument can perform long measurements without the data quality being affected by changes of inner or outer conditions. The stability of the instrument depends on its own intrinsic characterics, as well as on its environment. The intrinsic stability is mainly determined by the performance of the electronics. External effects are defined to be those mainly due to weather changes, day/night variations, and in general, environmental effects which are beyond the control of the instrument.

2.3.1 Intrinsic stability

As discussed elsewhere, it is probably not practical to perform system temperature measurements using near-field hot-load absorbers very often. It is thus desirable to know the magnitude and time-scales of potential $T_{\rm sys}$ variations. A very simple method should be to make repeated measurements (closely spaced in time but extending over 24h in order to discern possible diurnal variations[5]) of a source (continuum or line) and study the amplitude scatter. This requires that we can disentangle the effects of the elevation dependent beam pattern/projected collection area and potential side-lobe contaminations. A rapidly changing system temperature can also reveal itself by an unstable passband profile, traced e.g. by taking the channel RMS of two consecutive total power spectra subtracted by each other.

[5]There are no circumpolar sources available given the design limit of 45° elevation.

Baseline stability (or "flatness") is mainly important for spectral line observations. It is essential for measuring line areas, analysing line shapes, and even for safely being able to claim detections at all. The proper approach on how to achieve this is difficult to foresee, it will have to be an interactive process once the test measurements have started. Some relevant questions: Will we have standing waves causing baseline ripples? How do we do off-source measurements? Can we/should we dedicate one digital beam direction as simultaneous off-source measurements? Can we use baseline templates to subtract and eliminate baseline patterns in data reduction? In principle, we don't need on-source measurements to study the baseline behaviour. We should at earliest possible point in time make a long integration so that the properties of the resulting spectra can be understood. This also will allow for an Allen-variance analysis, albeit it requires calibrated spectra to be meaningful.

Frequency stability can be verified with any kind of test signal such as an LO in the near-field. It could be tested by monitoring the spectral position of the spike in a range of conditions (varying ambient temperature etc.). It is also important to compare the measured and expected widths of the spectral feature; if we have oscillations in the tuning frequency the effective spectral resolution goes down. For such a purpose satellites could perhaps also be used, simultaneously observed by another telescope which will provide a reference profile to compare with. The astronomical HI line is a less suitable choice due to the complex line shapes and source structures. The intricacy of explaining an anomalous HI line profile is illustrated in (Wijnholds et al. 2004).

2.3.2 External stability

The effects of Radio Frequency Interference (RFI) will present a problem in the EMBRACE frequency range. It will not be discussed in detail here but in order to get test data that correspond to best-case and worst-case scenarios, one can observe one or several of the protected frequency windows (Cohen et al 2005), and also deep into the unprotected regions (around 1 GHz for instance). As a comparison, a 30-year old paper on observations of Radio Recombination Lines (RRLs) at decimeter wavelengths in unprotected frequency ranges reported that 2 out of 8 frequency bands were typically affected by RFI (reference to be inserted later). As RFI will vary (transient satellites, media broadcasts that are not active at night) it may be useful to have such a "statistical idea" of the feasibility of targeting certain frequencies when planning observations.

The weather should have little effect on the signal propagation but local meteorological conditions could have secondary effects on the electronics, cables, or materials in general even though care is taken to ameliorate its impact. It should be kept in mind if anomalies are detected during intrinsic stability testing.

2.4 Repeatability

The term will here be considered to mean the capacity of obtaining a (scientific) end result repeatedly. If all the issues related to stability (some of which are discussed above) are dealt with, one would expect a good repeatability. However, perfect repeatability will never be the case and it is necessary to quantify the uncertainty of the results. In millimetre astronomy for instance, it is often considered acceptable to have a 10% intensity calibration uncertainty and a pointing error corresponding to 10% of the main beam width. The accuracy requirements depends of course on the scientific analysis attempted. There are many ways to arrive at an early indication of the corresponding figures for EMBRACE but the best option is probably to measure the galactic HI line in a certain direction several times over an extended time period.

2.5 Polarisation Issues

Although EMBRACE is a single polarisation system, we need a full polarisation description of the system and our observations to understand the impact of a non-complete observing system on the results obtained. We start with a global description of the interactions between the EM field, the antennas in the array, the receivers and beam former to point out the different issues.

We start with the induced voltage over the terminals of an antenna element in an array by an incoming plane wave with a given polarisation characteristic from a given direction. This voltage V_i is given by the element voltage pattern that can be observed by only exciting that element i by a current I_i, and includes the interactions with all other elements in the open situation without the connected Low Noise Amplifier (LNA). By EM coupling there will be a voltage V_j induced in all other elements j given by the antenna impedance matrix elements $Z_{ij} = V_j/I_i$. Depending on the actual load by all the LNA impedances Z_{Li} the observable voltage pattern of element i changes.

A second effect of the coupling is that the noise emanated by the LNA input into an antenna element reaches the beam former in various ways. The first is by reflection from the deliberately chosen mismatch between passive element impedance Z_{ii} and LNA input impedance Z_{Li}. The second way is by coupling to all the other elements and via the phase and gain control at the beam former inputs to the summed output. Both paths have the same LNA gain, which is assumed identical for all paths. All these noise terms interfere and make the effective receiver noise dependent on the direction to which the beam former is steered. For a not tapered array, such as is found in infinite array simulations, the optimum match for a LNA needs to use the active array impedance and not the passive element impedance Z_{ii}.

This receiver noise coupling aspect makes clear that receiver noise emanated into the X-elements could couple to Y-elements and will not be cancelled in the X-beam former, but will show up when the cross correlation between X- and Y-beam former output of an array will be made. This noise coupling aspect will be analyzed in the evaluation of 2PAD and in APERTIF. In EMBRACE only the X-antennas are loaded with an LNA driving two RF beam formers, while the Y-elements are not loaded at all.

EMBRACE has only a single polarised output for each of the two beams. Such an output V_{Ex} could be cross-correlated with the outputs V_X and V_Y of a second antenna system. This produces only two coherences $< V_{Ex} \cdot V_X >$ and $< V_{Ex} \cdot V_Y >$, while four coherencies are needed to describe the polarisation state of an incoming plane wave in I, Q, U, and V. Although such an incoming plane wave might be unpolarised, the element beam characteristic will polarise it, which shows that we will not be able to retrieve the polarisation characteristics of the EMBRACE beam without further assumptions.

A reasonable assumption would be that the Y-output of a full polarisation station is equal to the X-output if we rotate the station by 90 degrees. Then we could combine the two coherencies of an observation with the two coherencies of a second observation where the dominant object is at the same elevation but at a 90 degree different azimuth. In this way the polarisation characteristics of the EM simulated element pattern averaged over a tile or a station could be verified.

2.6 Calibration Sensitivity

For frequencies below 0.4 GHz a single dipole antenna could have a system temperature that is sky noise limited which leads to a fixed SNR for the strongest sky sources such as Cas A and Cyg A Tau A and Vir A independent of frequency. The reason is that the effective sensitivity, which is the ratio of collecting area over

system temperature, has about the same spectral characteristic as the source fluxes (except for Tau A). The SNR is only determined by the source flux which is for Cas A $\sim$ 0.007 and can be improved by a factor $(B \cdot t)^{1/2}$ to allow for good calibration of individual dipoles. With 200 kHz band width and 5 seconds integration time an SNR$\sim$ 7 is reached for Cas A. The sky brightness temperature outside the galactic plane (above 10° galactic latitude) is reasonably approximated by $T_{sky} = 60\lambda^{2.55}$[K] with wavelength λ in meters. This indicates that at a frequency of 0.8 GHz the sky temperature of 5 K is dominated by the 100 K receiver noise by a factor twenty so we need 4 MHz and 100 seconds to observe Cas A with a SNR $\sim$ 7 with a single dipole.

However a larger and more sensitive antenna such as a tile or a set of tiles has a narrower beam inversely proportional with its collecting area and sees a smaller fraction of the sky, and misses the strongest sky sources unless the beam is appropriately pointed.

The curve that expresses $\log(N)$ versus $\log(S)$, where N is the number of sources per steradian with a flux larger than S, has a slope that varies between -0.7 and -1.5. For an antenna with a diameter larger than 10 wavelengths we are just in the regime where the number of detectable calibration sources within the main beam is independent of the antenna size and depends for sky noise limited systems only on the $(B \cdot t)^{1/2}$ product. Full field of view self calibration requires that the average distance between the calibration sources in the main beam should be matched to the scale size of the ionosphere phase structures. This means in practice that for frequencies below 0.4 GHz typical station sizes of more than 25 m diameter and aperture efficiencies over 30% are needed at a bandwidth of more than 10 MHz to make self calibration solutions per typical ionosphere coherency time of 10 seconds. For higher frequencies receiver noise dominates the system temperature and the troposphere starts to dominate the phase errors over the beam and brings us in a different regime that needs further investigation.

With a system temperature of 100 K the total collecting area of the EMBRACE stations with 144 tiles of 1.125 m^2 has an instantaneous sensitivity of 2000 Jy. The station correlator processes a typical bandwidth of 200 kHz, which gives after 5 seconds a rms sensitivity per polarisation of 2 Jy.

The instantaneous sensitivity of a single cluster of four tiles is 72000 Jy, provides an rms sensitivity of 72 Jy and gives a SNR $\sim$ 42 on Cas A at 1 GHz.

The weakest source of the four strongest ones in a station beam is 0.095 Jy and needs 4 MHz bandwidth and 100 sec integration to reach the rms noise floor. For appropriate self calibration we need these four sources at least a factor three above the noise floor, which would require 36 MHz bandwidth that is indeed practically available. However we need 4 detectable calibration sources in any field, not just in the average field. This indicates the importance of system a temperature lower than 100 K to give this guarantee and allows for bringing the integration time down to a value more consistent with atmosphere coherency times.

2.7 Observation Modes

The measurements described above require recipes for observing procedures which are briefly described below. In each of the following subsections, there is a list of input requirements, followed by the action to be implemented by the EMBRACE Monitoring And Control (MAC) Software. These modes can be applied to individual digital beams, or multible beams, or the RF beams. The first subsection below describes an initial setup, and how it might be implemented in the EMBRACE Monitoring and Control software.

2.7.1 An initial EMBRACE verification measurement

We want to start observe Cyg A, RA 19:59:28.3, Dec +40:44:02 (J2000), when it rises above 45 degrees elevation on 1/1/2009.

As output, we want 2 beamlets at phase centre, as far apart as possible within the passband in order to probe the SED around 900 MHz. Assuming that the maximum bandpass is 100 MHz, then we want data points at 850 and 950 MHz.

Two spectrally identical beamlets at an off position given as an offset from phase centre in elevation. We correlate tiles (not tilesets) and that we only have 16 tiles, *i.e.*, the field of view is 15 degrees and the digital beam is 4 degrees. So we want the off position to be at least 10 degrees away from phase centre.

We use exactly the same setting for the A and B RF beams in order to cross check the gains in the two signal paths.

After two hours, we move beam A to Cas A, RA 23:23:24, Dec +58:48:54 (J2000), and continue for another two hours to demonstrate the multi-beaming capability.

Then we move also beam B to Cas A and measure for two hours.

At the end, we want a snapshot of the visibilies, *i.e.*, the cross correlations between the tiles in order to see how strong Cyg A is when we look at Cas A. The sky angle between them is so small that Cyg is not so far outside the 3dB FOV. It will also give some idea about the sidelobe pattern.

Pseudo code

The following is pseudo-code used to illustrate how scripting might be implemented.

To define our sources, I have assumed the standard .cat-format which is used by the Pegasus telescope control software.

A .cat file could look like this:

```
DR21(OH)    EQ 1950.0 20:37:14.2  42:12:10 VLSR  -3.0   REFERENCE 20:37:46.6  42:12:10
# IRAS21391   EQ 1950.0 21:39:10.3  58:02:29 VLSR  +0.0
S140        EQ 1950.0 22:17:42.0  63:03:45 VLSR  -7.0     REFERENCE 22:17:31.4  63:01:05
# NGC7538     EQ 1950.0 23:11:36.5  61:11:49 VLSR -57.0
IRC+10216   EQ 1950.0 09:45:14.8  13:30:41 VLSR  25.0
```

The following is an EMBRACE setup script in pseudo-code.

```
setobsname('astrotest090101');  # Should be used in naming output files or directory
load('sourcelist.cat');  # Standard .cat ASCII format. Now sources are defined
# Define output beamlets
setfreqA(1,850e6,2,950e6,3,850e6,4,950e6);
setposA(1,'eqabs',cyga.ra,cyga.dec); setposA(2,'copy',1);
setposA(3,'skyrel',0,-10); setposA(4,'copy',3);
copyallAtoB;
# As long as we record signal, we don't need to specify
```

```
# beamlet spectral width or resolution right??
# Wait for start condition...
while eq2sky(cyga.ra,cyga.dec).el <45
end
# This is an awkward solution, we could calculate the start time ourselves
# and define it explicitly or just launch the script in real time
starttime=getcurrtime; # Which time reference do we use, UT or LST?
endtime1=starttime+2*3600;
trackA('eqabs',cyga.ra,cyga.dec); trackB('eqabs',cyga.ra,cyga.dec);
integrate(60,endtime1); # How long should each recorded time sequence be?
                                    # Depends on desired bandwidth? Used 1 minute here...
trackA('eqabs',casa.ra,casa.dec):
endtime2=getcurrtime+2*3600;
integrate(60,endtime2);
trackB('eqabs',casa.ra,casa.dec);
endtime3=getcurrtime+2*3600;
integrate(60,endtime3);
savehousekeeping('A','xcorr');
integrate(60);  # No obs. endtime = only do it once
```

2.7.2 Source Tracking (normal)

1. specify source by Right-Ascension and Declination (RA & Dec)
2. specify centre frequency and bandwidth
3. specify integration time (in seconds, or minutes, or hours)
4. track source (ie. compensate for Earth rotation)

2.7.3 Source Tracking (satellite)

1. specify initial sky position by providing satellite orbital parameters
2. specify centre frequency and bandwidth
3. specify integration time (in seconds, or minutes, or hours)
4. track source (ie. compensate for satellite motion)

2.7.4 Drift Scan (Alt-Az)

1. specify sky position by Elevation and Azimuth
2. specify centre frequency and bandwidth
3. specify integration time (in seconds, or minutes, or hours)
4. maintain fixed beam pointing relative to the array (ie. allow sky to drift through beam)

2.7.5 Drift Scan (RA-Dec)

1. specify initial sky position by Right-Ascension and Declination
2. specify centre frequency and bandwidth
3. specify integration time (in seconds, or minutes, or hours)
4. maintain fixed beam pointing relative to the array (ie. allow sky to drift through beam)

2.7.6 Drift Scan (satellite)

1. specify initial sky position by providing satellite orbital parameters
2. specify centre frequency and bandwidth
3. specify integration time (in seconds, or minutes, or hours)
4. maintain fixed beam pointing relative to the array (ie. allow satellite to drift through beam)

2.7.7 Map Mode (normal)

1. specify initial sky position by Right-Ascension and Declination
2. specify centre frequency and bandwidth
3. specify integration time (in seconds, or minutes, or hours) per position
4. scan digital beam in a grid pattern centred on the chosen sky position (ie. compensating for Earth rotation).

2.7.8 Map Mode (satellite)

1. specify initial pointing position given the satellite orbital parameters
2. specify centre frequency and bandwidth
3. specify integration time (in seconds, or minutes, or hours) per position
4. scan digital beam in a grid pattern centred on the satellite (ie. compensating for satellite motion).

2.7.9 Peaking-Up

1. specify initial sky position by Right-Ascension and Declination
2. specify centre frequency and bandwidth
3. specify integration time (in seconds, or minutes, or hours) per position

4. scan digital beam in a grid pattern centred on the chosen sky position (ie. compensating for Earth rotation) and determine peak signal.
5. display peak position in RA-Dec, and point to peak position.
6. update pointing model (ie. determine offset from ideal pointing model)
7. is there a dependence on Elevation in the pointing model?
8. is there a dependence on frequency in the pointing model?

2.7.10 On-Off

1. specify ON position by Right-Ascension and Declination
2. specify OFF position by Right-Ascension and Declination
3. specify centre frequency and bandwidth
4. specify integration time (in seconds, or minutes, or hours) per position
5. put one digital beam in the ON position, and one digital beam in the OFF position, and integrate.
6. display (ON-OFF)/OFF

2.7.11 Frequency Switching

1. specify sky position by Right-Ascension and Declination
2. specify centre frequency and bandwidth (ν & $\Delta\nu$)
3. specify offset frequency separation ($\delta\nu$)
4. specify integration time (in seconds, or minutes, or hours)
5. put digital beam on source centred at frequency ν
6. integrate and then put the digital beam on source centred at frequency $\nu + \delta\nu$
7. integrate
8. display ($\text{Result}_1 - \text{Result}_2$)

2.8 To-do list

- Try to find suitable satellites that fulfills criteria outlined above.
- Can the sun be used as test source? In LOFAR test data, the sun is almost exactly in the direction of Taurus A and it is not clear which one is in fact seen. If possible, solar observations can be used to fill gaps in the az/el coverage towards the south (particularly during the winter season when there is no confusion between the sun and Taurus A).

3

Beamforming Firmware Validation

In the EMBRACE station, digital beamforming is done by specific computations on the digitized data flow from RF beams. The digital processing boards are LOFAR Remote Station Processing boards (RSP). Embedded firmware in FPGAs located on RSP boards delivers the digital processing task.

Beamforming firmware validation requires two test steps:

- RSP board tests
- Beamforming validation test

3.1 RSP boards tests

Tests on the RSP board will be performed to verify the proper working of the board. Two kinds of tests are identified:

Stand alone tests: verify that the board will work before it is installed in the system rack;

Executable tests: verify all functionality with full test coverage.

3.1.1 Stand alone tests:

A power-up self test is able to validate the board hardware as far as possible for a stand alone board setup. The power-up self test is executed after every board reset, whether it is not connected to any interface, or that it is built into a full rack. The set of tests that will be performed are based on the assumption that the board is stand alone, and will only test those functions that work stand alone.

Power-up self tests consist of:

- Full intraboard interface test;
- Interboard interface local loopback test;
- Ethernet (CEP and LCU) local loopback test;

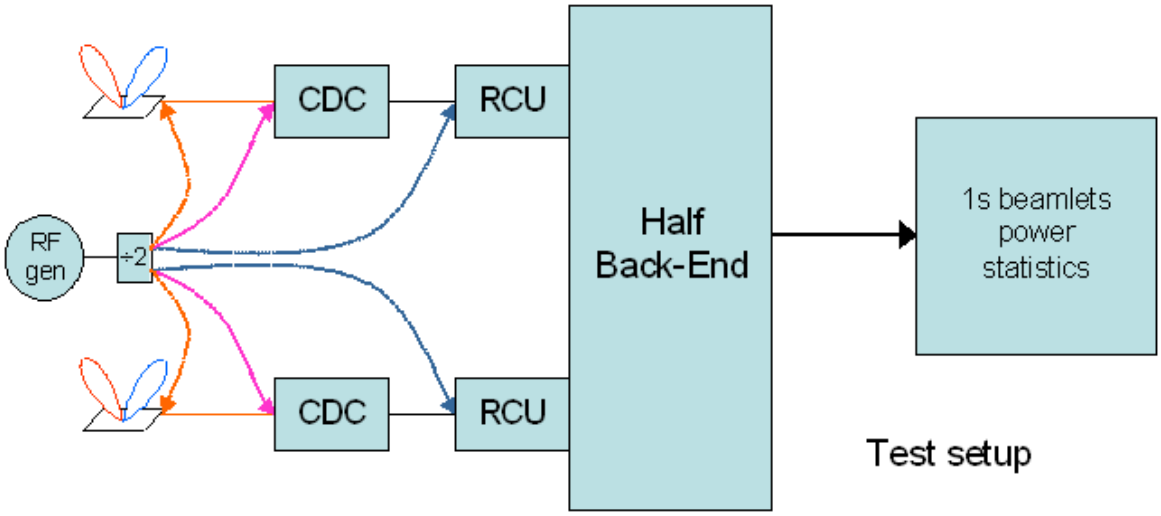

Figure 3.1: Test Setup

- Board health test.

After completion of the power-up self test, the board will signals its status using on board LEDs and will update an internal status register which can be read by LCU if connected. The status register will contain detailed test results, error counts for each interface test, and actual values for the board health parameters.

3.1.2 Executable tests:

During normal operation, LCU can initiate all built in tests and diagnostics. Depending on which test is executed, the results of the test will be written into the status register (interface tests) or can be read from a data collection buffer (data path test).

These user tests are capable of a much larger test coverage than the power-up self test. All external interfaces can be tested in full data transmit/receive mode in cooperation with the other end of the data line. Data path testing allows to test the internal logic (firmware) of the FPGAs to determine the validity of the component and/or the correct firmware.

Tests and diagnostics during normal operation will be disruptive during sky measurements sessions, since they make use of the same interfaces, data path or control registers as the measurements sessions. The only diagnostic that will not disrupt operations is the board health test since it only reads the on board sensors.

3.2 Beamforming validation test

The goal is to verify the process of beamforming firmware on two analogue inputs (receiver units, CDC units, tilesets cables) by nulling the output of the beamforming stage with the proper parameters (subbands map, weights parameters). RF or IF signal comes from a RF generator and a two ways RF splitter supplies two inputs with the signal.

Beamforming process for 2 tilesets, in one subband sb:

$$S = (a_1 e^{j\phi_1})(g_1 e^{j\psi_1}) + (a_2 e^{j\phi_2})(g_2 e^{j\psi_2}) \tag{3.1}$$

$\mathbf{a_1}$:amplitude of tileset 1 output
ϕ_1 :phase of tileset 1 output

$\mathbf{g_1}$:gain to apply to tileset 1 (for beam steering)
ψ_1 :phase shift to apply to tileset 1

} Beamformer weight for tileset 1, subband sb and beam (θ, ϕ)

$\mathbf{a_2}$:amplitude of tileset 1 output
ψ_2 :phase of tileset 1 output

$\mathbf{g_2}$:gain to apply to tileset 1 (for beam steering)
ψ_2 :phase shift to apply to tileset 1

} Beamformer weight for tileset 2, subband sb and beam (θ, ϕ)

To null the sum S we only apply weight to tileset 2 output, that is

$$g_1 = 1 \text{ and } \psi_1 = 0$$

$$S = (a_1 e^{j\phi_1}) + (a_2 e^{j\phi_2})(g_2 e^{j\psi_2}) = a_1 e^{j\phi_1} + a_2 g_2 e^{j(\phi_2+\psi_2)} \tag{3.2}$$

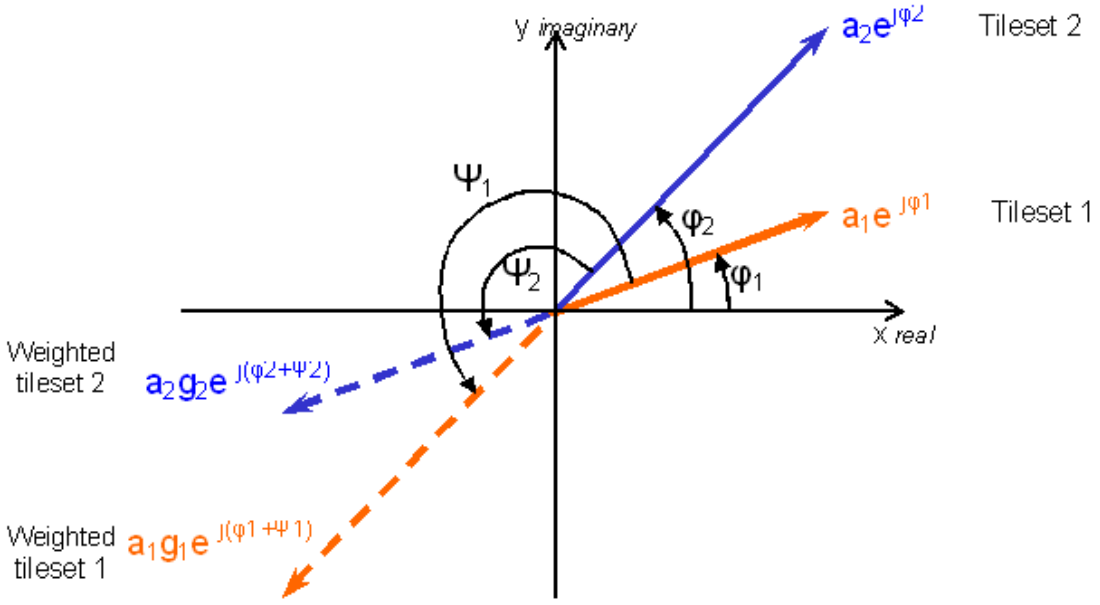

$$\text{To null } S\text{: } a_2 g_2 = a_1 \text{ and } \phi_2 + \psi_2 = \phi_1 + \pi \tag{3.3}$$

or (if tileset 1 weighted and tileset 2 not weighted):

$$a_1 g_1 = a_2 \quad \text{and} \quad \phi_1 + \psi_1 = \phi_2 + \pi \tag{3.4}$$

$$2\phi + \psi_2 = \psi_1 \quad \text{with} \quad \phi_2 - \phi_1 = \phi \text{ and } g_2 = 1/g_1 \tag{3.5}$$

$$S = (a_1 e^{j\phi_1}) + (a_2 e^{j\phi_2})(g2e^{j\psi_2}) = a_1 e^{j\phi_1} + a_2 g2e^{j(\phi_2+\psi_2)} \tag{3.6}$$

$$\text{Power} = 10log_{10}(S^2 + 0.0001) = f(\phi, r) \text{ with } \phi = \phi_2 + \psi_2 - \phi_1, r = |a_2 g_2 / a_1| \tag{3.7}$$

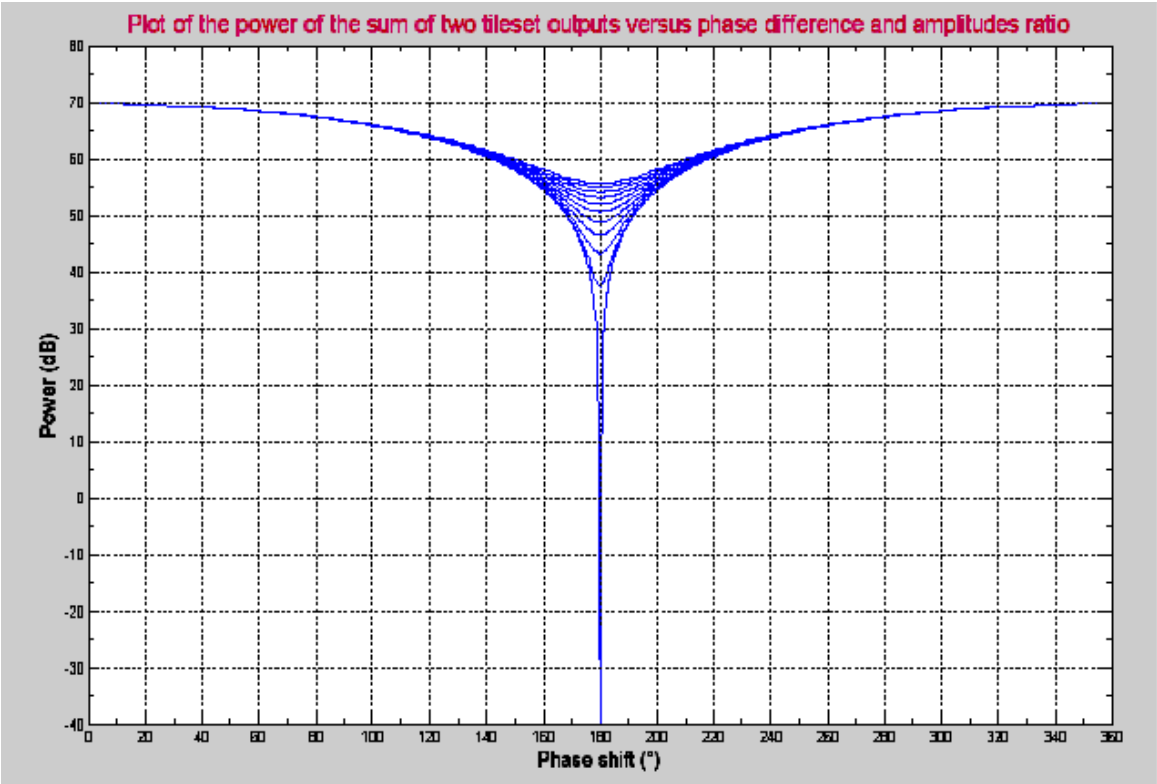

Figure 3.2: The above plot shows the great sensitivity of the nulling test to the gain and phase shift weights. It also shows that a high value of nulling requires high input signals levels.

Specific test scripts are built for this nulling test. They are made of:

- A script to define digital beams parameters (subbnads, weights) and record them in parameter files.

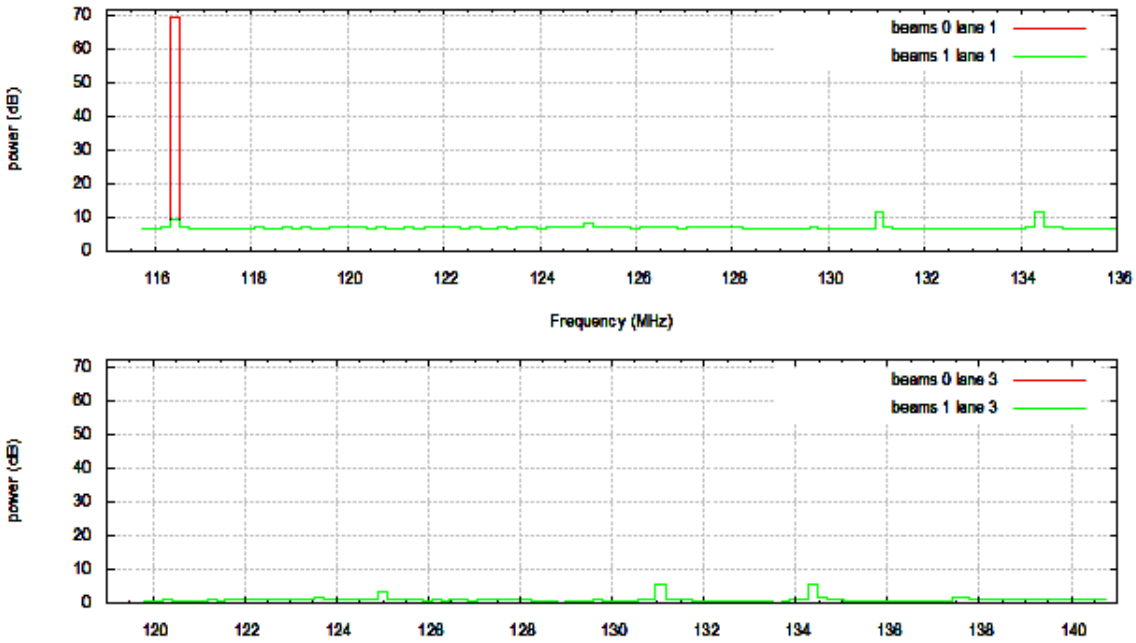

Figure 3.3: These plots show a nulling test result obtained with the testbench platform. Use of ant 0 and ant 1 RCU inputs, beamlet No. 12, subband 84 (116.40625 MHz) results in 60dB nulling with $g_2 = 0.957$ and $\psi_2 = 181.7°$. **top:** Digital beam A1 with two beams, with nulling parameters. **bottom:** Digital beam A2 with two beams, no nulling parameters.

- A script to start a measurements session with these parameters.
- A script to modify gain and Phase shifts for a specified antenna path and subband number.
- A script to plot beamlet statistics in real time.
- A script to record beamlet statistics on disc storage.
- A script to offline plot data from storage, spectral power density versus frequency or channel power versus time.

4

Interferometric operation

Much can be learned about EMBRACE by using the prototype interferometrically with one or more of the WSRT elements. There are, however, some potential problems with this, because the geometries are very different. The relative orientation of the dipoles will change with location on the sky; at the meridian the dipoles will be parallel, but elsewhere this will generally not be so. Initially, it may be best to limit the tests to sources near transit. The EMBRACE effective area will decrease with increasing zenith angle (z); of course this is a property to be determined (as is the resulting beam size/shape). Note that the effective orientation of the EMBRACE dipole can be checked by correlating it with the orthogonal WSRT dipole around meridian transit. This can also be used to check the purity of the linear polarization EMBRACE produces. In principal, the dipole orientation problem can be solved by correlating the EMBRACE signal with both X and Y-dipoles from the WSRT.

In the usual nomenclature, the cross-correlation between two elements with orthogonal dipoles, X and Y, gives:

$$X * X = I + Q$$

and

$$X * Y = U + jV$$

where I, Q, U and V are the Stokes parameters. For an unpolarized source ($Q = U = V = 0$), if one set of dipoles rotates with respect to the other by an angle θ, then the responses become:

$$X * X = I \cos\theta$$

and

$$X * Y = I \sin\theta$$

Since $I^2 \cos^2\theta + I^2 \sin^2\theta = I^2$, we can measure the I-response of the single-dipole EMBRACE by cross-correlating with both WSRT dipoles. (However, for large differences in pointing direction, the geometry becomes more complicated and this simple approximation has to be replaced by a more detailed analysis.)

- 3C 295 may be an important source for many tests: it is strong, compact, unpolarized, and it transits very close to the zenith at Westerbork. Interferometer tests should include:
  - With WSRT element(s) as reference, measure the EMBRACE voltage beam pattern. Using a WSRT element significantly improves the s/n ratio: the effective aperture size of the interferometer is

$(10\ \mathrm{m} \times 25\ \mathrm{m})^{1/2} = 15.8$, or an increase in A_{eff} by 2.5×; and at L-band (where the WSRT has $T_{\mathrm{s}} = 25$ K), the effective $T_{\mathrm{s}} = (25\ \mathrm{K} \times 100\ \mathrm{K})^{1/2} = 50$ K. This gives an overall improvement in s/n of 5×, so the noise in 10 s interations becomes, $\sigma = 60$ mJy. With a 20 Jy calibrator (like 3C 147 and 3C 295), the EMBRACE power beam can be determined to the -30 – -40 dB level.

  - Repeat at different frequencies, locations

- It may also be possible to use the WSRT redundancy to test EMBRACE characteristics.
- The WSRT and Nançay prototypes to be used as a long baseline interferometer.

In order to have EMBRACE perform as a WSRT look-a-like dish it is necessary to have a phase stability equal to the WSRT front-end. (phase noise of < 100 dBc at 10 kHz and $0.1°/°$C per measurement interval). This may not be a practical value for EMBRACE and a phased array works different in that way.

4.1 single short baseline with WSRT

- Demonstrate dynamic range equivalent to single 25-m antenna of WSRT

4.2 two beams on sky with WSRT

- Demonstrate basic operation
- Demonstrate dynamic range equivalent to each EMBRACE beam

4.3 Long baseline operation

- Long baseline interferometry between EMBRACE installations at Westerbork and Nançay.

5

Observing Pulsars with EMBRACE at Nançay

5.1 Introduction

In order to demonstrate that EMBRACE can be used for pulsar observations, we must be certain that the existing pulsar dedispersors can accept the EMBRACE station data. In Nançay, we do have an old analog dedispersor (based on DDS technology and using the NRT correlator) and the B.O.N. Digital dedispersor. Only the later system is considered in this document.

The Nançay Berkeley-Orléans-Nançay pulsar backend is based on a 128MHz spectrometer, producing 2 complex polarization 4 MHz digitized subbands. These 4MHz data flows are sent to approx. 150 AMD ATHLON processors (see Section 5.2). We propose that the digital output (beamlets, see Section 5.3) of the EMBRACE station should be sent directly to the PC cluster, as described in Section 5.4.

5.2 Berkeley-Orléans-Nançay backend short description

Figure 5.1: The Berkeley-Orléans-Nançay pulsar backend block diagram

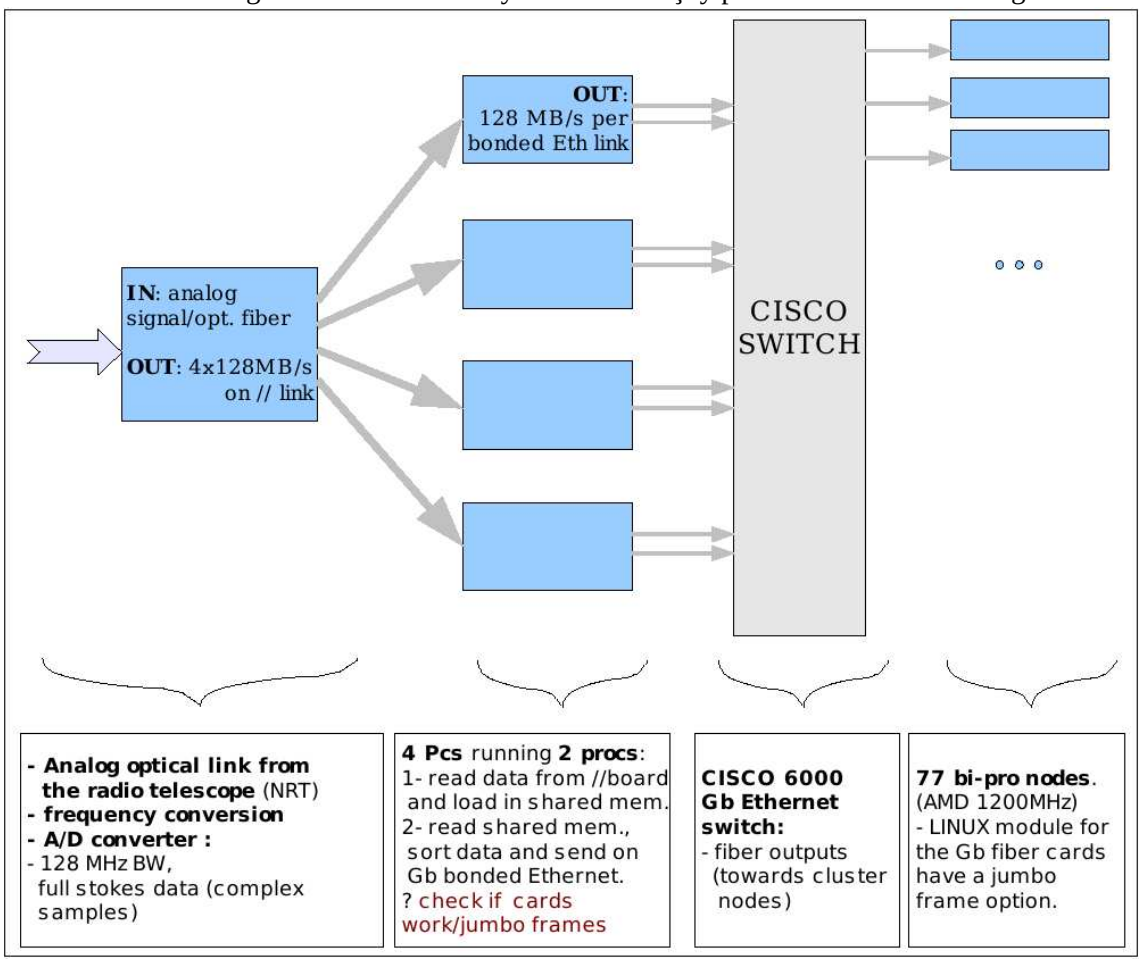

5.3 EMBRACE data format

For detailed information, read the LOFAR specification document. The EMBRACE data output has also been described in P.Picard's document on the External Correlator Interface (06/07/2006).

In the LOFAR backend:

- 1 analog beam (of 1 EMBRACE square meter tile) is filtered in 512 subbands of 195kHz BW
- 100 streams (of 195kHz BW each) are combined in the digital beamformer (weighted additions)
- for EMBRACE, up to 103 subbands (for 40MHz) will be processed
  up to 8 digital beams ; 1 subband of 195kHz means 195,000 beamlets/s (a beamlet is a complex sample)
- the LCU (control unit) reads the crosslets every 1s: crosslets store the crosscorrelation values.
  Framelets = beamlets+crosslets.

5.4 Proposed EMBRACE BON system

It is suggested that 1 to 4 of the 4 acquisition BON PCs, which presently receive the complex voltages on parallel link (128MB/s), sort the data, and send it to the cluster nodes. These PC use presently the 2 motherboard Gb links. It is possible to add 1 Gb card, which should accept jumbo frames [up to 9000 Bytes each] see fig. below. A software, based on the scheme presently used (acquisition in shared memory, then another process reads the shared memory in order to sort the data and send it to the cluster nodes) needs to be written. It is not necessary to bother about jumbo frames coming out from the 14 acquisition BON PCs since the data rate is already substantially reduced.

Requirements for BON subsystem:

1. Received packeted data (time interleaved beamlets) from EMBRACE station Gb Ethernet, jumbo frames).
2. Unpack and rearrange data flow for 1 (or 2, if possible) beam(s) successive subbands for each beam
3. For each beam, aggregate subbands to a 4 MHz bandwidth dataflow (TBC)
4. If possible, work simultaneously with NRT data (half of the BON system) and EMBRACE data (half BON)

Requirements for the EMBRACE system:

1. Send the data on 1 or 2 Gb Ethernet link(s) only, to the BON acquisition PC(s), as described in Figure 5.2.
2. Easy EMBRACE configuration for the destination MAC Addresses (of the BON acquisition Pcs).

Figure 5.2: Block diagram of data flow from EMBRACE to the BON pulsar backend.

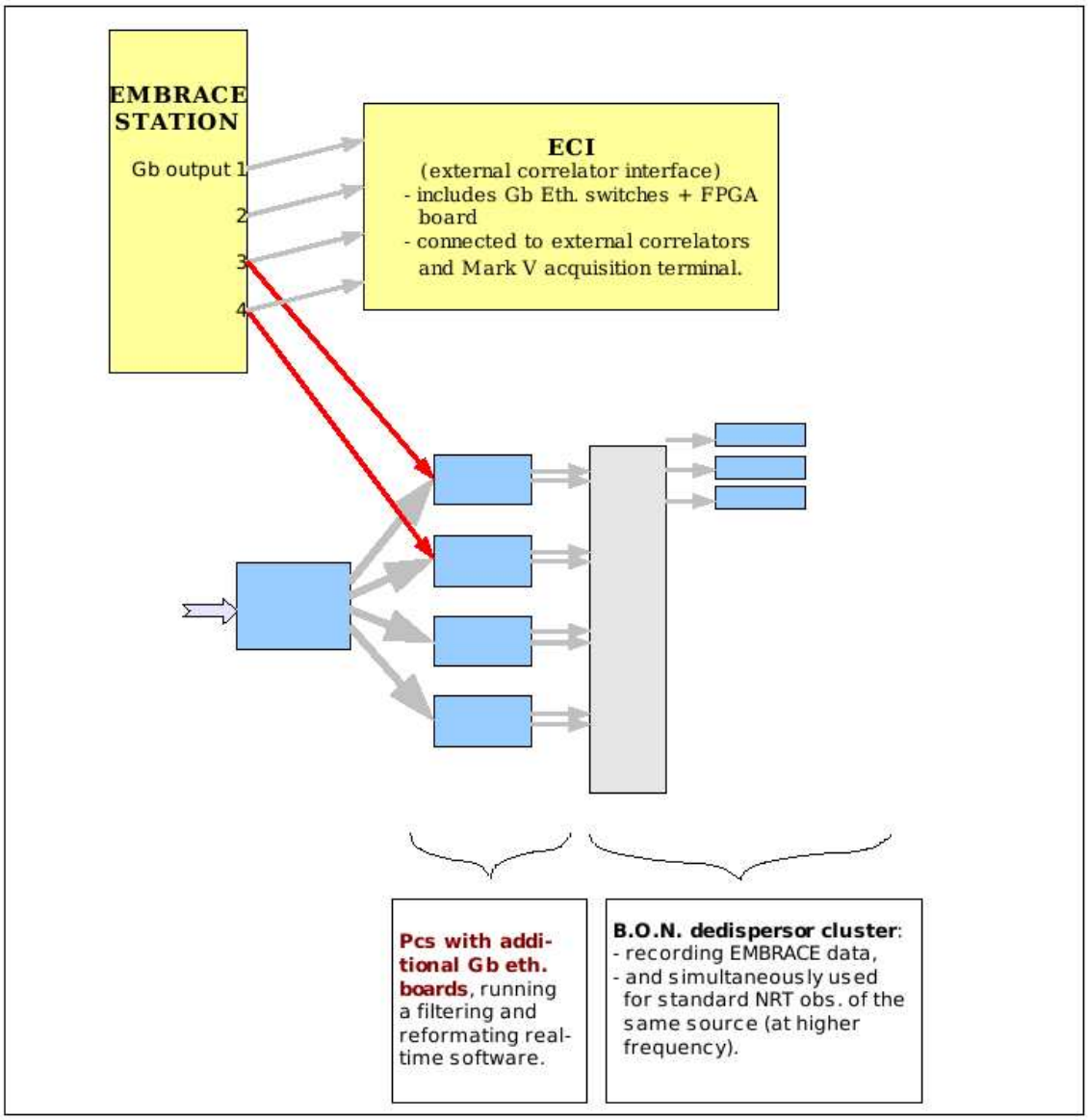

5.5 Possible Sources for Pulsar Observing with EMBRACE

Table 5.1: Pulsars observable with EMBRACE

SNR 1mn	**SNR 30mn**	**PSRname**	**Period (sec)**	**DM pc.cm^{-3}**	**s400 mJy**	**DutyCycle**	**Disp([cycle]) μsec/MHz**	**Rank**
0.913	5.001	J2330-2005	1.643622	8.458	42.0	0.010	1096.6(0.001)	31
0.944	5.170	J2157+4017	1.525266	70.857	105.0	0.025	9186.6(0.006)	30
0.961	5.264	J2145-0750	0.016052	9.003	100.0	0.024	1167.2(0.073)	29
0.972	5.324	J1903+0135	0.729304	245.167	58.0	0.014	31785.8(0.044)	28
1.001	5.485	J1537+1155	0.037904	11.614	36.0	0.008	1505.8(0.040)	27
1.002	5.489	J0630-2834	1.244419	34.468	206.0	0.047	4468.8(0.004)	26
1.055	5.776	J1824-1945	0.189335	224.648	71.0	0.015	29125.5(0.154)	25
1.079	5.911	J0837+0610	1.273768	12.889	89.0	0.019	1671.1(0.001)	24
1.226	6.716	J1948+3540	0.717311	129.075	145.0	0.027	16734.5(0.023)	23
1.239	6.787	J2144-3933	8.509828	3.350	16.0	0.003	434.3(0.000)	22
1.253	6.862	J2022+5154	0.529197	22.648	77.0	0.014	2936.3(0.006)	21
1.300	7.121	J0820-1350	1.238129	40.938	102.0	0.018	5307.6(0.004)	20
1.350	7.395	J1939+2134	0.001558	71.040	240.0	0.040	9210.3(5.912)	19
1.520	8.323	J0826+2637	0.530661	19.454	73.0	0.011	2522.2(0.005)	18
1.621	8.878	J0534+2200	0.033085	56.791	646.0	0.091	7362.9(0.223)	17
1.654	9.060	J2113+4644	1.014685	141.260	230.0	0.032	18314.3(0.018)	16
1.760	9.640	J1509+5531	0.739682	19.613	114.0	0.015	2542.8(0.003)	15
1.813	9.931	J2219+4754	0.538469	43.519	111.0	0.014	5642.2(0.010)	14
1.854	10.155	J1833-0338	0.686704	234.538	89.0	0.011	30407.8(0.044)	13
1.942	10.637	J1820-0427	0.598076	84.435	157.0	0.018	10947.0(0.018)	12
2.080	11.391	J0742-2822	0.166762	73.758	296.0	0.032	9562.7(0.057)	11
2.110	11.558	J1932+1059	0.226518	3.180	303.0	0.033	412.3(0.002)	10
2.191	12.001	J1136+1551	1.187913	4.864	257.0	0.027	630.6(0.001)	9
2.195	12.020	J1935+1616	0.358738	158.521	242.0	0.025	20552.2(0.057)	8
2.237	12.252	J1901+0331	0.655450	402.080	165.0	0.017	52129.5(0.080)	7
2.424	13.278	J0953+0755	0.253065	2.958	400.0	0.038	383.5(0.002)	6
2.675	14.652	J2018+2839	0.557953	14.172	314.0	0.027	1837.4(0.003)	5
2.956	16.193	J1913-0440	0.825936	89.385	118.0	0.009	11588.7(0.014)	4
8.253	45.206	J1645-0317	0.387690	35.727	393.0	0.011	4632.0(0.012)	3
15.471	84.739	J1752-2806	0.562558	50.372	1100.0	0.016	6530.7(0.012)	2
36.946	202.361	J0332+5434	0.714520	26.833	1500.0	0.009	3478.9(0.005)	1

6

Observing Pulsars with EMBRACE at Westerbork

The Westerbork Synthesis Radio Telescope has the possibility to provide a test platform for the pulsar observing capabilities of EMBRACE. There are two main ways in which the data can be analysed; the first would use the current mode of pulsar observation and the other would use the Digital Baseband system being developed for Galileo. We will consider both of these options below.

First let us consider what we need to achieve to be able to demonstrate that the aperture array concept is useful for pulsar observations. There are two prime areas: pulsar searching and high precision pulsar timing. While the available collecting area precludes testing some aspects we can still look at the principle requirements. In the searching case we are most intersted to see how well we can use the available field-of-view and/or the mutiple beaming possibilities. In the case of timing we would want to determine the precision to which we can measure individual pulse arrival times and then also look at tming stability, i.e. how repeatable and predictable are the arrival times.

Testing of the search capabilities can best be achieved by the following set of tests.

i. Observe a range of known pulsars with different fluxes and see that they are detected with the expected signal-to-noise. In these observations we wish to point directly at the source to the best possible accuracy of the beam former. We would also wish to repeat these observations at a number of different days and also hour angles. These data would then be analysed using current pulsar search software to test whether they were detected and whether the signal-to-noise scaled as would be expected as a function of hour angle and time.

ii. Observe a smaller sample of pulsars but now at varying distances from the so-called phase center of the beam. Preferably this would be done in the multi-beaming mode so that one beam can be used to track the pulsar exactly while the other beam is offset from the known position. This two beam approach allows us to compare directly the expected flux and the flux achieved at different locations in the beam. A number of pulsars with different flux would be used to check how this scales with pulse strength also.

iii. As above we would use two beams to track a pulsar as we observe it. This would be to check that both beams give the same sensitivity and track the pulsar equally well.

Testing the timing capability would require a campaign of observations spread over a few months. Obser-

vations would be made initially at a range of different hour angles on consecutive days to check the timing stability as a function of position of the beam in the sky. Following that initial set observations, monthly observations would be required for a period of a few months to ensure that the system could deliver the clock and beam stability to allow for high precision timing to be achieved.

The easiest way to achieve EMBRACE observations with the WSRT is for the data to be treated as from normal WSRT operations. That is, the data should be placed into the adding box as well. When two beams are available then ideally each beam would be seen by the WSRT as a different telescope. This would mean that the pulsar backend PuMa II could be used without any modification. The most important aspect of this would be that there is no automatic gain controller in the loop as this would likely prevent us from doing single telescope work. With PuMa II being used as the pulsar backend then all other software for doing data acquisition etc would already be in place.

The alternative would be to use the digital backend that is being developed for the Galileo project. This backend would have some added flexibility in terms of the input side of the data but would require some resources to make it suitable for gathering data from more than one beam for example. Moreover there would be significant work involved in transferring the data from whatever format is used by the DBCC into one that could then be used by our standard pulsar analysis tools.

The tests described above are not uniquely possible with the WSRT/PuMa II and most if not all could also be done at Nançay. It is especially useful to be able to take more than one beam as input in the pulsar backends. The reason why you might want to do this at two places is that you have more opportunities to do testing without disrupting the normal use of the pulsar backends and it would be a further test of stability of the systems. If there was 50% more collecting area at the WSRT then that too would also be a significant reason to want to do tests there as well as at Nançay for pulsar work.

7

Extragalactic HI with EMBRACE

7.1 Scope of this Section

This section details the astronomical test plan of the SKADS DS5T3 EMBRACE demonstrator for the spectroscopic measurements of the HI emission line at 21-cm. A brief summary of results from previous similar experiment is done.

7.2 Results from the Previous Similar Experiment

THousand Experiment Array (THEA) was a small scale prototype for EMBRACE. It was a 2×2 tiles instrument (4 m^2) that was built at ASTRON and tested in 2003. Each tile was an 8×8 element array. THEA observations of the HI line at 21-cm were successful (Wijnholds et al. 2004). A full scan of the sky was done with the 6° HPBW single beam of THEA. The sky was mapped as a grid of 1246 points. A short exposure of 1 sec was done on each spatial position, giving a total exposure time of 23 minutes. A system temperature of 186 ± 10 K was derived. Spectra from the THEA datacube were compared with spectra from the Leiden-Dwingeloo Survey (LDS) and showed qualitative agreement between the shapes of HI profiles. For more details, see (THEA webpage).

7.3 EMBRACE astronomical test plan for 21-cm observations

7.3.1 Observable targets and HI surveys

The EMBRACE multi-beam facility will be used for Galactic and extragalactic HI observations. HI mapping of the Milky Way can be done whereas no HI mapping is possible for every extragalactic source observable in the northern hemisphere due to the large size of a digital beam compared with the apparent size of galaxies. For these objects, only integrated spectra will be measured.

- An obvious bright HI target for EMBRACE is the Galactic plane. Results will be compared to the Leiden-Dwingeloo-Survey (Hartmann & Burton 1997).
- The most suitable and brightest extragalactic sources to be observed simultaneously within separate digital beams are the Local Group spiral galaxies Messier 31 and Messier 33. These two strong HI sources

Table 7.1: Basic parameters of M31 and M33. Coordinates are in J2000.

Galaxy name	Morphological type	R.A. (hh:mm:ss.s)	Dec. (dd:mm:ss)	v_{sys} (km s^{-1})	Frequency (MHz)
Messier 31	SAb	00:42:44.3	+41:16:09	-300	1421.8286
Messier 33	SAcd	01:33:50.9	+30:39:36	-180	1421.2590

Table 7.2: Observations of M31 with EMBRACE. The coordinates of the field centre are given in J2000.

Field designation	R.A. (hh:mm:ss.s)	DEC (dd:mm:ss)
M31-NE1	00:50:04.1	+43:32:46
M31-NE2	00:49:50.3	+43:00:57
M31-NE3	00:48:03.8	+42:34:45
M31-NE4	00:46:17.3	+42:08:33
M31-NE5	00:44:30.8	+41:42:21
M31-centre	00:42:44.3	+41:16:09
M31-SW1	00:40:57.8	+40:49:57
M31-SW2	00:39:11.3	+40:23:45
M31-SW3	00:37:24.8	+39:57:33
M31-SW4	00:35:38.3	+39:31:21

have been extensively studied by radioastronomers over the last ~30 years due to their proximity. Therefore, the comparison of EMBRACE results with previous studies will be easy.

- The strongest HI sources from the Virgo cluster of galaxies will be observed.

7.3.2 Local Group spiral galaxies

Numerous HI observations of Messier 31 have been done during the last ~30 years. The most recent high sensitivity observations were made by (Thilker et al. 2004) using WSRT and by (Chemin Carignan & Foster 2008) using the DRAO synthesis telescope. We will use the latter dataset to compare with EMBRACE measurements (integrated properties). Table 7.1 gives the basic parameters of M31 and M33 and the observation frequency. The best period to observe these galaxies is from september to november 2008. For each galaxy, the coordinates of the RF beams are the optical centre coordinate of Table 7.1.

The half power beam width is ~1.1° at 1420 MHz for a 100 m^2 telescope (~0.6° for 300 m^2). As seen in Fig. 7.3.2, ten separate pointings are needed to measure the full HI integrated spectrum of M31. The centres of each field-of-view is given in Table 7.2. Each field-of-view corresponds to a unique digital beam.

Notice that significant contamination by Milky Way HI is expected at radial velocities of ~ 50 km s^{-1} because the rotation of the receding half of M31 is projected at these velocities. No specific treatment will be done to disentangle the lines. Figure 7.3.2 shows the integrated spectrum of M31 after removing the contamination by the Galactic HI emission (left-hand panel) and the expected profile with both M31 and MW gas emission (right-hand panel).

Messier 33 is also well suited for EMBRACE observations. It is smaller than M31 and three different EMBRACE pointings are needed to integrate its whole HI spectrum. The centres of each field-of-view is given in Table 7.3. Each field-of-view corresponds to a unique digital beam.

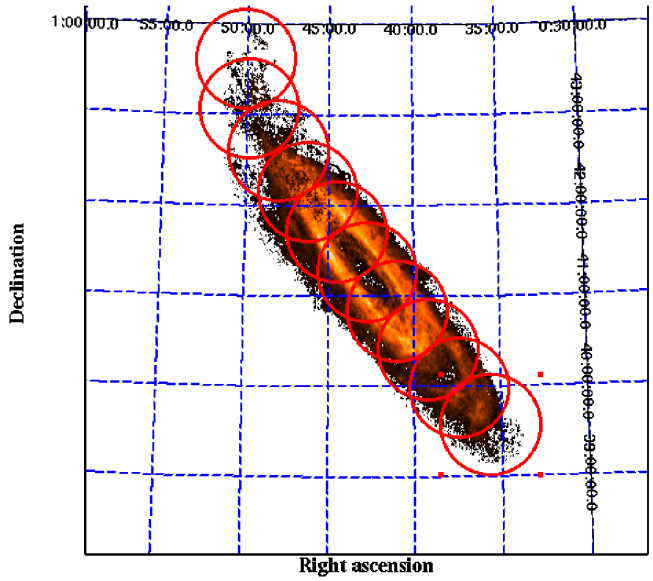

Figure 7.1: HI integrated emission map of Messier 31. A circle corresponds to a half-power beam-width of 1.1° at a frequency of 1.42 GHz and for a 100 m^2 collecting area. The data are from DRAO observations (Chemin Carignan & Foster 2008).

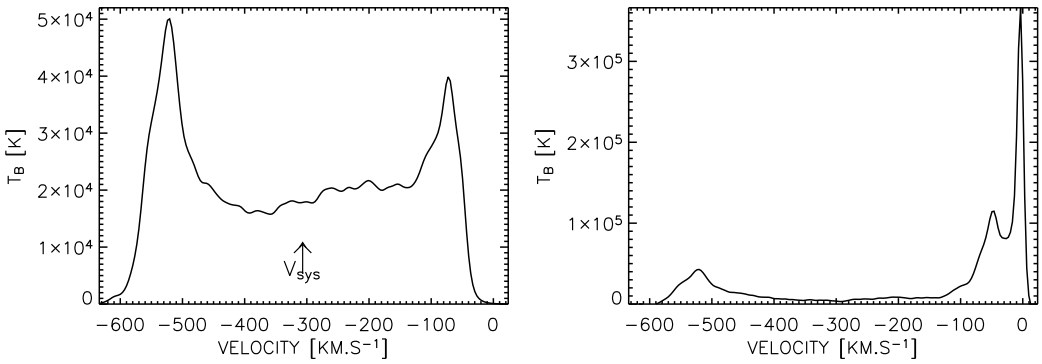

Figure 7.2: HI integrated profile of Messier 31 without (left) and with (right) contamination by Galactic HI. The data are from DRAO observations (Chemin Carignan & Foster 2008).

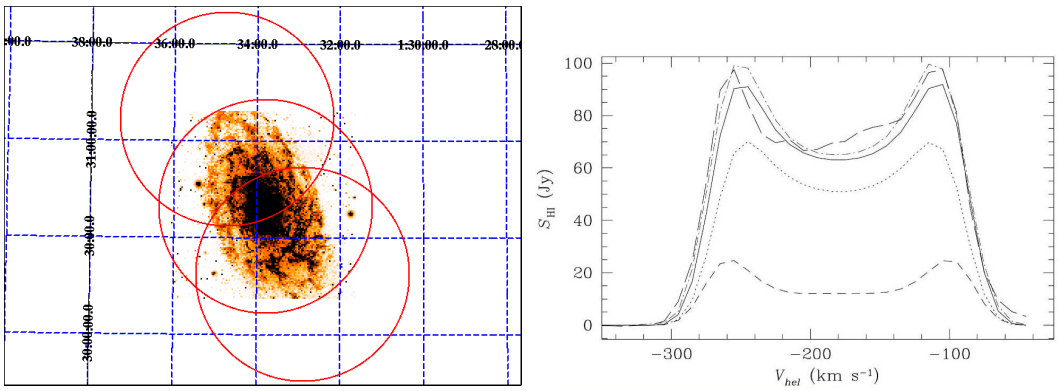

Figure 7.3: HI integrated emission map (left) and integrated profile (right) of Messier 33. The HI image of M33 is from WSRT observations (Braun & Thilker 2003). Comparison of the HI profile of Messier 33 derived from a model (solid line) with the observed profile (long-dashed line). Figure from (Corbelli & Schneider 1997).

Table 7.3: Observations of M33 with EMBRACE. The coordinates of the field centre are given in J2000.

Field designation	R.A. (hh:mm:ss.s)	DEC (dd:mm:ss)
M33-NE	01:34:29.13	+31:06:19
M33-centre	01:33:47.90	+30:39:53
M33-SW	01:33:02.07	+30:15:05

Figure 7.3.2 also shows the integrated HI profile of M33. No contamination from Milky Way is expected here because of the amplitude of the rotation velocity is only $\sim$ 200 km s^{-1}.

7.3.3 Nearby galaxies

The multi-beam facility of EMBRACE for extragalactic HI spectroscopy can be fully tested by observing unresolved nearby spirals lying in the same sky region. We have selected the brightest HI sources in the direction of the Virgo galaxy cluster, which is the closest galaxy cluster from the Earth (17 Mpc). The best period to observe these galaxies is during spring 2008. The selected targets have a total flux density above 20 Jy km s^{-1}. Table 7.5 gives the observational properties of targets. The advantage of observing cluster galaxies is that they all lie in the same sky area. A drawback is that confusion can occur within such a large digital beam size because a galaxy cluster is a dense environment (see Fig. 7.3.3). Fig. 7.3.3 also shows the RF beams which centers are given in Tab 7.4.

Table 7.4: RF beam centres for Virgo cluster observations

Field designation	R.A. (h)	DEC (°)
Virgo-RF1	12.370	+14.0
Virgo-RF2	12.688	+4.2

Table 7.5: Observations of M31 with EMBRACE. Centre field coordinates (J2000).

Galaxy name	Morphological type	R.A. (h)	Dec. (°)	v_{sys} (km s^{-1})	$\int_v S_\nu dv$ (Jy km s^{-1})	Frequency (MHz)
NGC4303	Sbc	12.36527	4.47460	1566	67.92	1413.02466
NGC4527	SABb	12.56889	2.65313	1737	64.27	1412.22327
NGC4535	Sc	12.57231	8.19775	1962	60.81	1411.17041
NGC4536	SABb	12.57414	2.18832	1802	55.46	1411.91907
NGC4808	Sc	12.93020	4.30451	760	54.45	1416.81396
NGC4254	Sc	12.31378	14.41647	2406	52.97	1409.09705
NGC4192	SABb	12.23008	14.89917	-138	52.48	1421.05994
NGC4178	Scd	12.21286	10.86580	376	48.75	1418.62646
NGC4321	SABb	12.38182	15.82126	1577	47.86	1412.97302
NGC4519	Scd	12.55841	8.65444	1227	45.71	1414.61597
NGC4651	Sc	12.72851	16.39339	799	44.87	1416.63025
NGC4654	Sc	12.73238	13.12678	1038	42.85	1415.50464
NGC4532	IB	12.57207	6.46733	2023	40.93	1410.88513
NGC4123	Sc	12.13642	2.87826	1328	38.02	1414.14160
NGC4713	Scd	12.83274	5.31136	653	37.67	1417.31860
NGC4216	SABb	12.26508	13.14988	137	33.42	1419.75708
NGC4701	Sc	12.81984	3.38836	723	33.42	1416.98840
NGC4116	SBcd	12.12686	2.69190	1310	33.11	1414.22595
NGC4496A	SBd	12.52762	3.93950	1730	31.92	1412.25610
NGC4206	Sbc	12.25468	13.02385	703	28.05	1417.08276
NGC4374	E	12.41776	12.88670	910	27.54	1416.10730
NGC4472	E	12.49633	8.00039	1010	25.12	1415.63647
NGC4501	Sb	12.53311	14.42039	2283	25.12	1409.67065
NGC4688	Sc	12.79624	4.33606	984	25.12	1415.75879
NGC4294	SBc	12.35495	11.51080	361	24.21	1418.69751
NGC4197	Sc	12.24402	5.80478	2065	22.28	1410.68872
IC3881	SBc	12.91349	19.17725	920	22.08	1416.06018
NGC4383	Sa	12.42376	16.47010	1710	21.88	1412.34985
NGC4698	Sa	12.80637	8.48747	1008	21.48	1415.64600

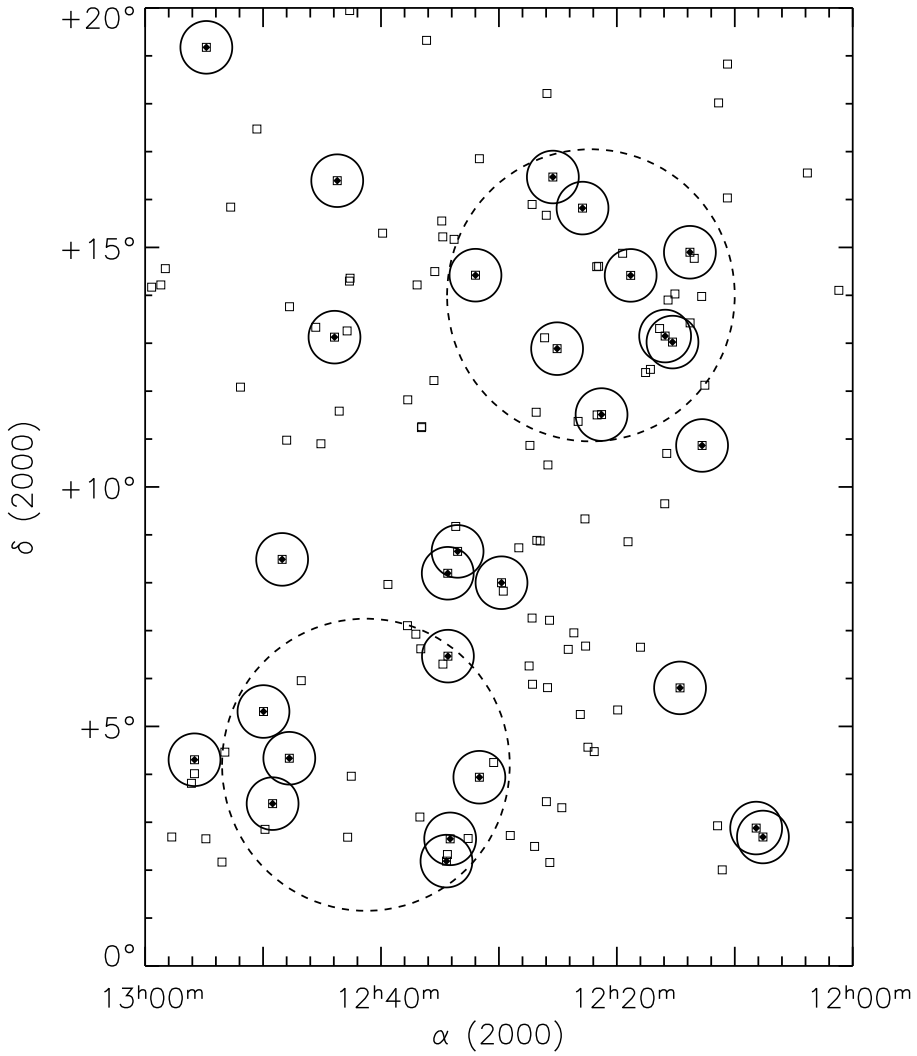

Figure 7.4: Location of Virgo cluster galaxy targets. A dashed circle corresponds to the HPBW of a RF beam (6.1° at 1.4 GHz). A solid circles corresponds to the HPBW of a digital beam (1.1° at 1.4 GHz) for all galaxies having a total flux density above 20 Jy km s^{-1}. These galaxies are marked by a filled square. Open squares correspond to all galaxies having a total flux density above 5 Jy km s^{-1} in the direction of the Virgo cluster.

7.3.4 Exposure time of HI observations and signal-to-noise ratio

The r.m.s. noise ΔT of the system for an emission line can be expressed as a function of the system temperature $T_{\rm sys}$, the frequency pass band $\Delta\nu$ (total frequency bandwidth divided by channels number) and the integration time τ by

$$\frac{\Delta T}{T_{\rm sys}} = \frac{1}{\sqrt{\tau\ \Delta\nu}} \tag{7.1}$$

For EMBRACE, $T_{\rm sys}$ is expected to be within 50-100 K. For a single polarization, the antenna temperature T_a is written as

$$T_{\rm a} = \frac{1}{2k}\, S_\nu\, A_{\rm eff} \tag{7.2}$$

where k is the Boltzmann constant, S_ν the flux density of the observed source, $A_{\rm eff}$ the effective aperture of the telescope. $A_{\rm eff} = \eta_{\rm A} A_{\rm geom}$ is the product of the geometrical aperture $A_{\rm geom}$ by the aperture efficiency $\eta_{\rm A}$. This latter value is to be quantified for EMBRACE during the engineering and astronomical tests. The expected signal-to-noise ratio (SNR) for the *integrated* line is then given by:

$$\mathrm{SNR} = \frac{\eta_{\rm A} A_{\rm geom}\ \sqrt{\tau\ \Delta\nu}\ \int_\nu S_\nu d\nu}{2k\ T_{\rm sys}\ \sqrt{\mathrm{n_{ch}}}\ \Delta\nu}\ , \tag{7.3}$$

with $\int_\nu S_\nu d\nu$ the integrated flux under the emission line, $\mathrm{n_{ch}}$ the number of velocity channels of the emission line and $\Delta\nu$ the velocity resolution of one channel (km s^{-1}). Figure 7.3.4 reports the expected SNR for the two galaxies Messier 33 and NGC 4303 as a function of exposure time τ (s) for a frequency bandwidth $\Delta\nu = \frac{20\ \mathrm{MHz}}{2048\ \mathrm{channels}} \sim 10$ kHz and for $\eta_{\rm A} = 10\%$, 30% and 50%. A bandwidth of 10 kHz at the observed frequency of 1.4 GHz corresponds to a velocity sampling of $\Delta v = \frac{\Delta\nu}{\nu} c \sim 2$ km s^{-1}, which value is relatively good for the HI measurements proposed here (integrated spectra observations). With a low aperture efficiency of $\sim 10\%$ and for a high system temperature, a very good SNR value is reached in a few hundred seconds for the galaxy Messier 33. For Virgo cluster galaxies like NGC 4303, a much longer time (~ 15 hours) is required to achieve a SNR of at least 3. Spectral binning by a factor of two or more is thus advised for this kind of sources if one wants to detect bright galaxies in the local Universe in a few hours.

7.3.5 Stray radiation

The emission detected by sidelobes has to be modelled and removed from the observations. This is particularly important for Milky Way observations because all regions of the sky are emitting. This will not be a problem for extragalactic sources provided that no (strong) HI sources are covered by the sidelobes. The stray radiation modeling will be more complicated than with classical antennas because the beam shape is supposed to change as as function of sky position.

One possibility would be to repeat the long integration on NGC 4303, this time with an artificial emitter on the ground providing a known signal in the vicinity of the EMBRACE array. In principle, the artificial signal should not appear in the final data, as long as phased pointing is done correctly. This would also test the system response to detecting a faint source in the vicinity of a strong source.

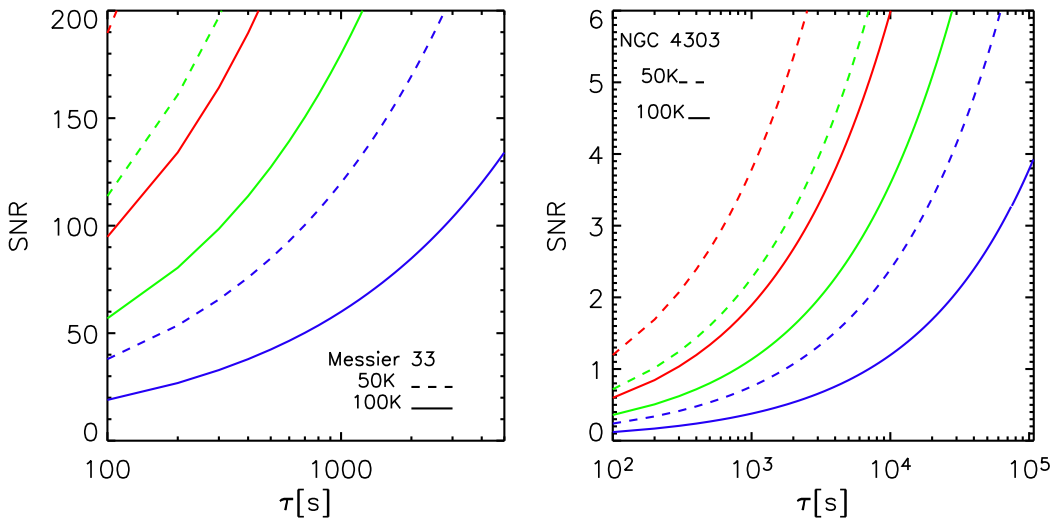

Figure 7.5: Expected signal-to-noise ratio with EMBRACE observations for the galaxies Messier 33 and NGC 4303 as a function of time. Solid (dashed) lines are for a system temperature $T_{\rm sys}$ = 100 K (50 K resp.). SNR values are derived for several aperture efficiencies $\eta_{\rm A}$: 10%, 30% and 50% (blue, green, red respectively). The full width of the HI emission line of NGC 4303 is $\sim$ 200 km s^{-1} (Warmels 1988). All values are derived for a 100 m^2 collecting area.

8

Molecules

8.1 Frequency coverage and transitions

The frequency regime considered here is 300-1600 Mhz which covers the intended EMBRACE range with some margin. The intention here is not to make detailed predictions but rather to disentangle the different aspects needed to be considered in order to evaluate the feasibility of trying to observe spectral lines at these wavelengths.

8.2 Previously detected molecular lines

Table 8.1: Rest frequencies for observed interstellar molecular lines by Frank J. Lovas

Frequency (MHz)	Unc. (MHz)	Formula	Quantum numbers	$\frac{T_r(K)}{T_a(K)}$	Source	Telescope	Astr. ref.	Lab. ref.
701.679	(4)	CH	$^2\Pi_{3/2}$ $J = 3/2$ $F = 2 - 2$	-0.6	W51	Arecibo	Ziu85	Ziu85
704.175*	(10)	CH	$^2\Pi_{3/2}$ $J = 3/2$ $F = 2 + -1-$	-0.10	W51	Arecibo	Tur88	Tur88
722.303*	(10)	CH	$^2\Pi_{3/2}$ $J = 3/2$ $F = 1 + -2-$	-0.12	W51	Arecibo	Tur88	Tur88
724.791	(4)	CH	$^2\Pi_{3/2}$ $J = 3/2$ $F = 1 - 1$	-0.5	W51	Arecibo	Ziu85	Ziu85
834.285*	(1)	CH_3OH	1(1,0)-1(1,1) A-+	0.58	Sgr A	NRAO 43m	Bal70	Xu_97
1065.076*	(0)	CH_3CHO	1(1,0) - 1(1,1) A-+	0.3	Sgr A	NRAO 43m	Got73	Kle96
1371.722*	(7)	CH_2CHCN	2(1,1)-2(1,2) $F = 1 - 1$	0.012	Sgr B2(M)	Parkes	Gar75	Gar75
1371.797*	(2)	CH_2CHCN	2(1,1)-2(1,2) $F = 3 - 3$	0.034	Sgr B2(M)	Parkes	Gar75	Gar75
1371.934*	(7)	CH_2CHCN	2(1,1)-2(1,2) $F = 2 - 2$	0.019	Sgr B2(M)	Parkes	Gar75	Gar75
1538.108*	(3)	NH_2CHO	1(1,0)-1(1,1) $F = 1 - 1$	0.08	Sgr B2(M)	NRAO 43m	Got73a	
1538.676*	(2)	NH_2CHO	1(1,0)-1(1,1) $F = 1 - 2$	0.09	Sgr B2(M)	NRAO 43m	Got73a	
1539.264*	(2)	NH_2CHO	1(1,0)-1(1,1) $F = 2 - 1$	0.10	Sgr B2(M)	NRAO 43m	Got73a	
1539.527*	(4)	NH_2CHO	1(1,0)-1(1,1) $F = 1 - 0$	0.08	Sgr B2(M)	NRAO 43m	Got73a	
1539.832*	(1)	NH_2CHO	1(1,0)-1(1,1) $F = 2 - 2$	0.36	Sgr B2(M)	NRAO 43m	Got73a	
1540.998*	(4)	NH_2CHO	1(1,0)-1(1,1) $F = 0 - 1$	0.10	Sgr B2(M)	NRAO 43m	Got73a	
1570.805	(5)	$NH_2^{13}CHO$	1(1,0)-1(1,1) $F = 2 - 2$	0.04	Sgr B2(M)	Parkes	Gar80	Gar80
1584.274	(2)	^{18}OH	$^2\Pi_{3/2}$ $J = 3/2$ $F = 1 - 2$	-0.05	Sgr B2(M)	Parkes	Wil81a	Bea78

For a complete list of molecular line transitions measured in the laboratory, see Appendix A.

8.3 All lines including predictions based on ab initio calculations

There are several molecular line data bases available on the internet such as The Cologne Database for Molecular Spectroscopy (CDMS) and the Molecular Spectroscopy page at the Jet Propulsion Laboratory (JPL) web site. CDMS returns about 500 lines for this interval while JPL gives about 3000 (for the latter one, the output is sorted by molecule and is limited to 1000 lines so a complete list is not available).

However, there is another database availble on CD (in this case received through private communication), named Spectral Line Atlas for Interstellar Molecules (SLAIM03) by Frank J. Lovas. It has 775 entries of interest and may be best suited for our purposes. It is interesting to note that in the same database, the line density at 3mm wavelength is less than half of that in the range discussed here. However, a comparison of this type does not convey much information for two reasons: as will be discussed later the lines (and their conditions for formation) are different, and lines also occupy less and less spectral space the longer wavelength they are at (assuming they have constant widths in terms of velocity dispersion). Indeed, in terms of velocity space the (database!) line density at 3mm is 50 times higher. Ignoring probable frequency biases in the database and the original spectroscopy work carried out in the field, this could perhaps put an upper limit to what could be expected if a spectral survey is attempted with the final SKA instrument towards a suitable target such as Sgr B2.

The SLAIM03 list is found in Appendix B. Apart from the two left-most columns of identification and frequency, the most interesting column is the 4th one which states the transition lower state energy in terms of cm^{-1} (1 cm^{-1} = 1.44 K).

8.4 Astrophysical context

A number of important circumstances has been identified below. Note that this is not an attempt to present a theory but to serve as a basis for discussion. Some of the points below are strongly connected but have been separated for clarity.

- **Abundance:** Transitions from a number of molecules with relatively high abundances in dense molecular clouds exist in our band, such as H2CO, HCN, CH3OH, the latter having already been detected in the ISM. Most of the species listed in Sect. 1.2 have been detected at other frequencies
- **Expected source sizes:** Many molecules are strongly peaked in the dense cores (very cold as in dark clouds or warm/hot cores in GMCs) where sufficient shielding from the ISRF exist and the conditions for gas-gas or gas/grain chemistry are right. Such sources may a have maximum extension av a few arcminutes, often much less. The finished SKA will be able to resolve these into detail, while for EMBRACE, we would need to find a very strong line in order to see it in a finite amount of time as it will be heavily diluted in the large beam. Nevertheless, some simple molecules and radicals exist also in the extended and diffuse ISM which have much larger source sizes. However, due to the excitation conditions in this gas (more below) it may require a background source to cause absorption spectra in order for them to be seen.

- **Excitation/temperature:** Perhaps the most useful tool to prune the list of potential lines is to look at the transition upper state energy. In principle one needs to add h*f/k to column 4 in the Sect. 1.3 list to get this quantity but in practice it is not necessary; at our low frequencies it never contributes more than 0.077 K. If the upper state energy is high, say several hundred Kelvin, not only does the medium have to be hot in order to populate the states that far up in the energy level tree, but also sufficiently dense to create the coupling between the molecule and its dominating collision partner (typically H_2) to facilitate such a "thermalisation". The problem with diffuse clouds, where $T_{kin} \sim 100$ K, $nH_2 \sim 100 cm^{-3}$ is precisely that the populations are very subthermal. Conditions for high-T excitation do exist but in very small regions, for instance near centers of activity of GMCs, where we have outflows, shocks, and Hot Cores etc.

- **A-coefficient/optical depth:** In the simplest case of radiative transfer, the observed strength (area) of a line is proportional to the Einstein A-coefficient divided by the frequency squared. The A-coefficient in turn goes as the third power of the frequency, i.e., the A-coefficients in our band is about a million times smaller than those typical for mm-spectroscopy but the net effect on the strength is only a factor of 100. There are at least two positive aspects of this as well: populations thermalise much more easily (depopulation by radiation provides less competition), and it becomes less likely that lines become optically thick which could otherwise cause problems with the interpretation.

- **Energy levels:** Transitions occurring between levels close to the rotational ground state are often desired for many reasons. The level populations are typically larger here and one can pick up emission from the more extended cold gas and/or poorly excited gas. Ground state transition observations themselves are widely considered key clues to understanding the excitation of a species. Molecules having such transitions in our band have however of necessity very small rotational constants, B, since Eu=B*Ju(Ju+1) and Ju=1 and Eu=h*f, at least for linear rotors. The smaller the B, the larger the moment of inertia of the molecules (B prop. 1/I), i.e., the ground state transitions we find listed in Sect. 1 (Elower=0) belong to large carbon chains (polymers which are scientifically interesting, discussed later) with large I:s around their primary axes of rotation. The problem now is that for a thermal population, the factor which determines the arising line strength is gu*exp(Eu/T) where gu is the statistical weigh (gu=2Ju+1). Gu has the effect of pushing the maximum of the product upwards. An estimate shows that for molecules having the ground state transition at 1 GHz, the most favoured line is J=15-14 and the aforementioned product six times stronger than for the ground state. There are however other complex molecules, with more degrees of freedom and they may well have more suitable low-lying transitions. This should be checked carefully.

- **Other issues:** What is the effect of continuum sources in this band? From an intuitive standpoint it seems that since at least compact HII regions have turn-over frequencies at 1 GHz or higher, they should be able to block or otherwise effect line radiation here. If that is true ONLY for compact regions then it will not be a problem for EMBRACE but possibly for SKA.

The excitation discussion above left out the effects of non-thermal excitation such as via radiation, shocks, collisions with non-thermal partners etc. Combined with a more complex energy level structure, such effects can lead to maser action among other things. In fact, due to our very small A-coefficients, masering candidates should be carefully looked for in our lists.

8.5 Astronomical candidates

- Polymers/ large linear molecules (incl. anions) in Dark Clouds
- H2CO in diffuse gas (or in SF regions with SKA)
- Atomic lines and RRL's
- Methanol 700 MHz, already detected. This may be possible with EMBRACE if it has enough collecting area.
- CH4 !! high scientific prize, no permanent dipole moment. If high E_{upper}, we may be able to observe this in Jupiter, and this would be an important detection.

9

Other Potential Scientific Measurements

The measurements sketched in this section are more of a demonstration of the EMBRACE possibilities, and go beyond the simple basic testing. The particular features of EMBRACE worth emphasizing are its ability to simultaneously observe with many beams over a large area of sky, and the possibility of adjusting the beam shape and its sidelobes (within certain limits) to suit a particular problem. At the same time, one also wants to show that the changing beam size (or equivalently $A_{\rm eff}$) with zenith angle is not an undue handicap to the various modes of astronomical observation. Multibeaming can be used to simultaneously observe/monitor many sources, or to speed up the observation time required for a wide field survey. Controlling sidelobes can be used to reject various kinds of external interference.

9.1 Fiedler et al. and similar effects

Twenty years ago, (Fiedler et al. 1987) published flux density variations of several extragalactic radio sources which had a characteristic, bowl-shaped form. The effect was most evident at 3 GHz, and the events typically lasted for 1-2 months. Modulations of up to 50% were observed, and the probable mechanism is refractive scattering in the ISM. As a test of EMBRACE, a group of sources could be intensively — and simultaneously — monitored for a period of time. For precision monitoring, one probably can only consider fairly strong sources; note that at L-band, there are only about 20 compact sources with $S > 10$ Jy at $\delta > 0°$. Most of the sources will not vary, but even if none of them do, to demonstrate that objects observed over a wide range of elevations can have their flux densities determined accurately (hence correcting for $A_{\rm eff}(z)$) would be valuable.

Such observations can be extended to other kinds of variable sources, to generate light curves covering a wide range of temporal scales, and done on several sources simultaneously. One can think of pulsars, but also intra-day variables; of course, the categories can be mixed. The main limitation is likely to be backend capacity (and for pulsars in particular, the source strength). L-band is the best candidate frequency region for reasons of interference, and because tropospheric and ionospheric effects should be at a minimum there.

9.2 Milky Way HI observations

An impressive demonstration would be to repeat one of the large-scale surveys, such as the Leiden-Dwingeloo HI survey (Hartmann & Burton, 1997). With N beams, there is clearly a speed-up factor of N. To do it well

would require careful consideration of the backend capacity, and significant reduction effort (either using an existing package, or writing new software). One could also search a large part of the galactic plane for the OH 18 cm transitions.

One of the problems encountered in the HI mapping of the Milky Way is stray radiation picked up in the telescope sidelobes. Given its extended nature, it is probably not realistic to expect that it could be rejected by EMBRACE as a single interfering source can be, but one could carry out experiments to see to what extent this emission can be changed by modifying the sidelobe structure.

10

Potential Sources

This table is taken from de Bruyn, 2001 “THEA Experiments: A preliminary inventory”

Table 10.1: Potential Sources

Object	**Angular Size (degrees)**	**Flux density (Jy at 1GHz)**	**comment**
Sun	0.5	100000	Time variable
Moon	0.5	100	Thermal spectrum
Cas A	0.1	3100	1% / year decay
Cyg A	0.03	6000	
Taurus A	0.1	1000	Flat spectrum
Virgo A	0.3	300	
Perseus A	0.5	50	
Herculus A		70	3C348
3C123	0.01	80	
3C147	0.001	25	
3C295	0.002	25	
3C196	0.002	20	
3C10	0.1	65	Tycho’s Supernova remnant
3C58	0.1	37	supernova remnant
Cygnus Loop	3.0	250	
IC443	1.0	130	3C157

References

[Baars et al. 1977] Baars, J. W. M., Genzel, R., Pauliny-Toth, I. I. K., & Witzel, A. "The absolute spectrum of CAS A - an accurate flux density scale and a set of secondary calibrators," 1977, *Astron. Astrophys*, 61, 99

[bij de Vaate et al 2002] J G bij de Vaate, G W Kant, W A van Cappellen, S. van der Tol, "First Celestial Measurement Results of the Thousand Element Array," URSI GA, Maastricht, August 2002

[Chemin Carignan & Foster 2008] Chemin L., Carignan C., Foster T., "Deep HI observations of the Andromeda galaxy," Astrophysical Journal, submitted 2008

[Cohen et al 2005] Jim Cohen, Titus Spoelstra, Roberto Ambrosini and Wim van Driel (eds) 2005, "CRAAF Handbook for Radio Astronomy"

[Corbelli & Schneider 1997] Corbelli E., Schneider S. E., "A Warped Disk Model for M33 and the 21 Centimeter Line Width in Spiral Galaxies", 1997, The Astrophysical Journal, 479, 244

[Crane & Napier 1988] P.C. Crane and P.J. Napier in "Synthesis Imaging in Radio Astronomy," ASP conference series vol. 6 (1988) edited by R.A. Perley, F.R. Schwab and A.H. Bridle.

[de Bruyn 2001] de Bruyn, G., "THEA Experiments: A preliminary inventory," ASTRON internal report, 2001

[Fiedler et al. 1987] Fiedler, R. L., Dennison, B., Johnston, K. J., & Hewish, A. "Extreme scattering events caused by compact structures in the interstellar medium," 1987, *Nature*, 326, 675

[Hartmann & Burton 1997] Hartmann D., Burton W. B., *Atlas of Galactic Neutral Hydrogen*, 1997, AGNH book

[Lovas et al 2008] Frank J. Lovas, Eberhard Tiemann, Richard D. Suenram, NIST, `http://physics.nist.gov/PhysRefData/MolSpec/freqsearch.html`

[SKADS Wiki] SKADS wiki, `http://webmail.jb.man.ac.uk/skadswiki/Ds5T3`

[THEA webpage] Thousand Element Array, `http://www.astron.nl/tl/thea.htm`

[Thilker et al. 2004] Thilker D. A., Braun R., Walterbos R. A. M., Corbelli E., Lockman F. J., Murphy E., Maddalena, R., "On the Continuing Formation of the Andromeda Galaxy: Detection of H I Clouds in the M31 Halo", 2004, The Astrophysical Journal, 601, L39

[Warmels 1988] Warmels R. H., "The HI Properties of Spiral Galaxies in the Virgo Cluster (Part II): One-Dimensional Westerbork Observations of 21 Galaxies", Astronomy & Astrophysics Supplement Series, 1988, 72, 57

[Wijnholds et al. 2004] Wijnholds S. J., Ger de Bruyn A., Bregman J. D., Bij de Vaatep J.G., “Hemispheric imaging of Galactic neutral hydrogen with a phased array antenna system,” Experimental Astronomy, 2004, 17, 59

[Wijnholds 2005] Stefan J. Wijnholds, “Confusion limited all sky imaging with LOFAR’s initial test station applying wide field calibration techniques,” URSI GA 2005, New Delhi (India), October 2005

[Wijnholds & Boonstra 2006] Stefan J. Wijnholds and Albert-Jan Boonstra, “A multisource calibration method for phased array radio telescopes,” 4th IEEE workshop on Sensor Array and Multichannel Processing (SAM), Waltham (MA), 12-14 July 2006

[Woestenburg & Dijkstra 2003] E.E.M. Woestenburg and K.F. Dijkstra, “Noise characterization of a phased array tile,” European Microwave Conference, Munich, Oct. 2003

Appendix A

Molecular Transitions Measured in the Laboratory

Table A.1: Transitions measured in laboratory

Molecular Species	Frequency (MHz)	Uncertainty (MHz)
$^{2}H^{16}O\,^{2}\Pi_{3/2}$	303.032	(0.002)
$^{40}Ca^{35}Cl\ ^{2}\Sigma$	303.860	(0.003)
$^{15}N^{16}O\ ^{2}\Pi_{1/2}$	309.226	(2E-4)
$^{2}H^{16}O\ ^{2}\Pi_{3/2}$	310.145	(0.001)
	310.215	(0.001)
	310.363	(0.001)
$^{88}Sr^{19}F\ ^{2}\Sigma_{1/2}$	312.928	(0.001)
	315.115	(0.001)
$^{18}O^{12}C^{32}S$	316.55685	(1E-3)
$^{2}H^{16}O\ ^{2}\Pi_{3/2}$	317.329	(0.004)
$^{32}S^{2}H\ ^{2}\Pi_{3/2}$	318.583	(0.002)
	318.640	(0.001)
	318.819	(0.001)
	318.833	(0.001)
	318.857	(0.001)
	319.052	(0.001)
	319.071	(0.001)
$^{7}Li^{16}OH$	321.068	(5E-3)
$^{40}Ca^{19}F\ ^{2}\Sigma_{1/2}$	322.396	(0.002)
$^{2}H^{16}O\ ^{2}\Pi_{3/2}$	322.480	(0.002)
$^{40}Ca^{35}Cl\ ^{2}\Sigma$	323.326	(0.003)
$^{40}Ca^{19}F\ ^{2}\Sigma_{1/2}$	326.746	(0.001)

continued on next page

Transitions measured in laboratory (cont'd)		
Molecular Species	**Frequency (MHz)**	**Uncertainty (MHz)**
	329.130	(0.001)
$^{16}O^{12}C^{34}S$	339.84058	(2E-3)
$^{40}Ca^{35}Cl\ ^{2}\Sigma$	343.070	(0.002)
$D^{13}C^{15}N$	344.083	(*)
$D^{12}C^{15}N$	352.153	(*)
$^{16}O^{12}C^{32}S$	356.22585	(1E-3)
$^{16}O^{13}C^{32}S$	364.42517	(6E-4)
$D^{13}C^{14}N$	364.580	(*)
DCCD	365.268	(0.001)
	365.278	(0.001)
	365.345	(0.001)
	365.421	(0.001)
	365.429	(0.001)
$^{40}Ca^{19}F\ ^{2}\Sigma_{1/2}$	367.881	(0.001)
$D^{12}C^{14}N$	372.374	(*1E-3)
$^{40}Ca^{35}Cl\ ^{2}\Sigma$	381.620	(0.002)
CD_4	385.310	(0.036)
$^{7}Li^{16}O\ ^{2}\Pi_{3/2}$	390.1	(0.1)
$^{40}Ca^{19}F\ ^{2}\Sigma_{1/2}$	398.848	(0.001)
$H^{13}C^{15}N$	404.702	(*)
$^{40}Ca^{19}F\ ^{2}\Sigma_{1/2}$	406.760	(0.001)
$^{18}O^{12}C^{32}S$	406.99756	(*7E-4)
$^{14}N^{16}O\ ^{2}\Pi_{1/2}$	411.206	(2E-4)
CH_4	423.02	(0.02)
$H^{12}C^{15}N$	423.878	(*)
$H^{13}C^{14}N$	429.666	(*)
$^{7}Li^{16}O\ ^{2}\Pi_{3/2}$	430.8	(0.2)
$^{14}N^{16}O\ ^{2}\Pi_{1/2}$	431.191	(2E-4)
$^{40}Ca^{19}F\ ^{2}\Sigma_{1/2}$	433.645	(0.001)
$H^{32}SD$	435.42	(*3.51)
$^{16}O^{12}C^{34}S$	436.93348	(1E-3)
$^{40}Ca^{19}F\ ^{2}\Sigma_{1/2}$	437.447	(0.001)
$^{32}S^{1}H\ ^{2}\Pi_{3/2}$	437.915	(0.002)
$^{88}Sr^{19}F\ ^{2}\Sigma_{1/2}$	438.109	(0.001)
$^{40}Ca^{19}F\ ^{2}\Sigma_{1/2}$	439.026	(0.001)
$^{88}Sr^{19}F\ ^{2}\Sigma_{1/2}$	440.485	(0.001)
$^{86}Sr^{19}F\ ^{2}\Sigma_{1/2}$	442.464	(0.001)
$^{32}S^{1}H\ ^{2}\Pi_{3/2}$	442.478	(0.001)
	442.628	(0.001)
$^{40}Ca^{19}F\ ^{2}\Sigma_{1/2}$	445.735	(0.002)

continued on next page

Transitions measured in laboratory (cont'd)		
Molecular Species	**Frequency (MHz)**	**Uncertainty (MHz)**
$^{32}S^{1}H\ ^{2}\Pi_{3/2}$	447.188	(0.002)
$H^{12}C^{14}N$	448.200	(3E-4)
	448.213	(5E-4)
	448.233	(6E-3)
	448.825	(3E-3)
	448.845	(4E-4)
	448.864	(3E-3)
	448.929	(3E-3)
	448.963	(1E-4)
	448.996	(3E-3)
	449.574	(3E-3)
	449.594	(4E-4)
	449.608	(2E-4)
	450.802	(3E-4)
	450.821	(5E-4)
$^{16}O^{12}C^{32}S$	457.99960	(1E-4)
$^{16}O^{13}C^{32}S$	468.54143	(6E-4)
$^{40}Ca^{19}F\ ^{2}\Sigma_{1/2}$	473.730	(0.003)
	476.208	(0.001)
	481.121	(0.001)
$^{15}N^{16}O\ ^{2}\Pi_{1/2}$	482.621	(2E-4)
$H^{16}OD$	486.266	(2E-3)
	486.450	(2E-3)
	486.487	(2E-3)
	486.528	(*2E-3)
	486.569	(2E-3)
	486.607	(2E-3)
$^{18}O^{12}C^{32}S$	508.74114	(*8E-4)
$^{40}Ca^{19}F\ ^{2}\Sigma_{1/2}$	515.090	(0.001)
	523.910	(0.001)
$^{88}Sr^{19}F\ ^{2}\Sigma_{1/2}$	533.823	(0.001)
$^{40}Ca^{81}Br\ ^{2}\Sigma_{1/2}$	534.380	(0.005)
$^{7}Li^{16}OH$	536.060	(5E-3)
$^{88}Sr^{19}F\ ^{2}\Sigma_{1/2}$	537.371	(0.001)
$^{86}Sr^{19}F\ ^{2}\Sigma_{1/2}$	539.349	(0.001)
$^{40}Ca^{19}F\ ^{2}\Sigma_{1/2}$	544.521	(0.001)
$^{40}Ca^{79}Br\ ^{2}\Sigma_{1/2}$	548.224	(0.002)
$^{40}Ca^{19}F\ ^{2}\Sigma_{1/2}$	554.070	(0.002)
$^{32}S^{2}H\ ^{2}\Pi_{3/2}$	554.834	(0.001)
$^{14}N^{16}O\ ^{2}\Pi_{1/2}$	560.854	(2E-4)
continued on next page		

Transitions measured in laboratory (cont'd)		
Molecular Species	**Frequency (MHz)**	**Uncertainty (MHz)**
$^{16}O^{12}C^{32}S$	572.49246	(2E-4)
$^{40}Ca^{19}F\ ^2\Sigma_{1/2}$	577.810	(0.002)
$^{16}O^{13}C^{32}S$	585.66942	(*3E-4)
$^{14}N^{16}O\ ^2\Pi_{1/2}$	587.747	(2E-4)
$^{40}Ca^{19}F\ ^2\Sigma_{1/2}$	588.029	(0.001)
$^{7}Li^{16}OH$	591.60	(0.02)
$^{7}Li^{16}OD$	597.44	(0.02)
$^{40}Ca^{19}F\ ^2\Sigma_{1/2}$	602.289	(0.001)
$^{18}O^{12}C^{32}S$	621.78683	(*1E-3)
$^{15}N^{16}O\ ^2\Pi_{1/2}$	622.569	(3E-4)
$^{14}N^{16}O\ ^2\Pi_{1/2}$	624.649	(2E-4)
$^{40}Ca^{19}F\ ^2\Sigma_{1/2}$	632.230	(0.001)
$^{40}Ca^{79}Br\ ^2\Sigma_{1/2}$	633.176	(0.001)
$^{14}N^{16}O\ ^2\Pi_{1/2}$	651.543	(2E-4)
$^{40}Ca^{81}Br\ ^2\Sigma_{1/2}$	653.570	(0.004)
$^{40}Ca^{79}Br\ ^2\Sigma_{1/2}$	656.616	(0.002)
$^{15}N^{16}O\ ^2\Pi_{1/2}$	670.708	(3E-4)
$^{7}Li^{16}O\ ^2\Pi_{3/2}$	686.1	(0.3)
$^{14}N^{16}O\ ^2\Pi_{1/2}$	693.828	(2E-4)
$^{13}CD_4$	698.843	(0.052)
$^{16}O^{12}C^{32}S$	699.70355	(2E-4)
CH X $^2\Pi_{3/2}$	701.677	(0.010)
$^{40}Ca^{19}F\ ^2\Sigma_{1/2}$	710.588	(0.001)
	714.500	(0.001)
$^{16}O^{13}C^{32}S$	715.80831	(*5E-4)
$^{40}Ca^{19}F\ ^2\Sigma_{1/2}$	720.112	(0.001)
CH X $^2\Pi_{3/2}$	724.789	(0.010)
$^{40}Ca^{79}Br\ ^2\Sigma_{1/2}$	739.422	(0.001)
$^{15}N^{16}O\ ^2\Pi_{1/2}$	742.836	(3E-4)
$^{18}O^{12}C^{32}S$	746.13378	(*1E-3)
$^{40}Ca^{79}Br\ ^2\Sigma_{1/2}$	751.380	(0.002)
$^{40}Ca^{81}Br\ ^2\Sigma_{1/2}$	755.172	(0.004)
$^{14}N^{16}O\ ^2\Pi_{1/2}$	758.911	(2E-4)
$^{88}Sr^{19}F\ ^2\Sigma_{1/2}$	760.960	(0.001)
$^{40}Ca^{35}Cl\ ^2\Sigma$	781.320	(0.002)
$^{15}N^{16}O\ ^2\Pi_{1/2}$	790.975	(3E-4)
$^{40}Ca^{35}Cl\ ^2\Sigma$	800.227	(0.001)
$^{14}N^{16}O\ ^2\Pi_{1/2}$	801.196	(2E-4)
$^{40}Ca^{35}Cl\ ^2\Sigma$	819.353	(0.001)
$^{40}Ca^{19}F\ ^2\Sigma_{1/2}$	821.338	(0.001)

continued on next page

Transitions measured in laboratory (cont'd)		
Molecular Species	**Frequency (MHz)**	**Uncertainty (MHz)**
$H^{16}OD$	824.478	(2E-3)
	824.507	(2E-3)
	824.525	(2E-3)
	824.549	(2E-3)
	824.569	(2E-3)
	824.604	(2E-3)
	824.671	(2E-3)
	824.742	(2E-3)
	824.773	(2E-3)
	824.790	(2E-3)
	824.814	(2E-3)
	824.834	(2E-3)
	824.864	(2E-3)
$^{40}Ca^{19}F\ ^2\Sigma_{1/2}$	828.368	(0.001)
$^{40}Ca^{79}Br\ ^2\Sigma_{1/2}$	832.920	(0.002)
	833.537	(0.001)
$^{40}Ca^{35}Cl\ ^2\Sigma$	838.632	(0.001)
$^{16}O^{12}C^{32}S$	839.63220	(2E-4)
$^{40}Ca^{81}Br\ ^2\Sigma_{1/2}$	840.730	(0.003)
$^{16}O^{13}C^{32}S$	858.95695	(*8E-4)
$^{32}S^2H\ ^2\Pi_{3/2}$	881.757	(0.002)
$^{18}O^{12}C^{32}S$	881.78105	(*2E-3)
$^{32}S^2H\ ^2\Pi_{3/2}$	881.788	(0.002)
	881.831	(0.001)
	881.959	(0.005)
$^{40}Ca^{37}Cl\ ^2\Sigma$	891.635	(0.001)
$H^{16}OD$	892.229	(*0.02)
$^{40}Ca^{37}Cl\ ^2\Sigma$	907.466	(0.001)
$^{13}CD_4$	911.938	(0.056)
$^{40}Ca^{35}Cl\ ^2\Sigma$	913.948	(0.001)
$^{40}Ca^{79}Br\ ^2\Sigma_{1/2}$	915.871	(0.001)
$^{13}CD_4$	923.452	(0.042)
$^{40}Ca^{37}Cl\ ^2\Sigma$	923.538	(0.002)
$^{7}Li^{16}O\ ^2\Pi_{3/2}$	926.9	(0.1)
$^{14}N^{16}O\ ^2\Pi_{1/2}$	929.259	(4E-3)
$^{40}Ca^{35}Cl\ ^2\Sigma$	933.047	(0.001)
$^{40}Ca^{37}Cl\ ^2\Sigma$	939.811	(0.001)
$^{40}Ca^{35}Cl\ ^2\Sigma$	952.340	(0.001)
$^{40}Ca^{19}F\ ^2\Sigma_{1/2}$	956.308	(0.001)
$^{15}N^{16}O\ ^2\Pi_{1/2}$	958.918	(3E-4)
continued on next page		

Transitions measured in laboratory (cont'd)

Molecular Species	Frequency (MHz)	Uncertainty (MHz)
$^{14}N^{16}O\ ^2\Pi_{1/2}$	964.023	(2E-3)
$^{40}Ca^{35}Cl\ ^2\Sigma$	971.773	(0.001)
$^{14}N^{16}O\ ^2\Pi_{1/2}$	991.734	(2E-4)
$^{16}O^{12}C^{32}S$	992.27600	(2E-3)
$^{40}Ca^{79}Br\ ^2\Sigma_{1/2}$	997.316	(0.002)
$^{16}O^{13}C^{32}S$	1015.11416	(*1E-3)
$^{15}N^{16}O\ ^2\Pi_{1/2}$	1015.415	(5E-4)
$D^{13}C^{15}N$	1032.205	(*)
$D^{12}C^{15}N$	1056.412	(*)
$^{40}Ca^{19}F\ ^2\Sigma_{1/2}$	1064.438	(0.001)
$^{14}N^{16}O\ ^2\Pi_{1/2}$	1072.596	(0.01)
$^{32}S^{1}H\ ^2\Pi_{3/2}$	1093.533	(0.002)
$D^{13}C^{14}N$	1093.690	(*)
$^{32}S^{1}H\ ^2\Pi_{3/2}$	1094.187	(0.001)
	1094.460	(0.001)
	1095.118	(0.002)
$^{40}Ca^{79}Br\ ^2\Sigma_{1/2}$	1100.665	(0.002)
$^{40}Ca^{19}F\ ^2\Sigma_{1/2}$	1105.143	(0.001)
$^{88}Sr^{19}F\ ^2\Sigma_{1/2}$	1105.708	(0.001)
$^{86}Sr^{19}F\ ^2\Sigma_{1/2}$	1110.438	(0.001)
$^{88}Sr^{19}F\ ^2\Sigma_{1/2}$	1112.194	(0.001)
$^{40}Ca^{19}F\ ^2\Sigma_{1/2}$	1114.016	(0.002)
$^{14}N^{16}O\ ^2\Pi_{1/2}$	1114.677	(0.02)
$^{86}Sr^{19}F\ ^2\Sigma_{1/2}$	1116.968	(0.001)
$D^{12}C^{14}N$	1117.070	(*3E-3)
$^{15}N^{16}O\ ^2\Pi_{1/2}$	1121.151	(3E-4)
$^{14}N^{16}O\ ^2\Pi_{1/2}$	1160.777	(3E-4)
$^{2}H^{16}O\ ^2\Pi_{3/2}$	1185.871	(0.001)
	1186.999	(0.003)
	1190.566	(0.002)
	1190.774	(0.002)
	1191.105	(0.002)
	1194.339	(0.001)
$^{40}Ca^{79}Br\ ^2\Sigma_{1/2}$	1195.735	(0.002)
$^{2}H^{16}O\ ^2\Pi_{3/2}$	1196.006	(0.003)
$^{88}Sr^{19}F\ ^2\Sigma_{1/2}$	1201.513	(0.001)
$^{86}Sr^{19}F\ ^2\Sigma_{1/2}$	1206.238	(0.001)
$^{88}Sr^{19}F\ ^2\Sigma_{1/2}$	1209.168	(0.001)
$^{40}Ca^{19}F\ ^2\Sigma_{1/2}$	1211.746	(0.001)
$^{86}Sr^{19}F\ ^2\Sigma_{1/2}$	1213.940	(0.001)

continued on next page

Transitions measured in laboratory (cont'd)		
Molecular Species	**Frequency (MHz)**	**Uncertainty (MHz)**
$H^{13}C^{15}N$	1214.054	(*)
$^{7}Li^{16}OH$	1221.06	(0.01)
$^{40}Ca^{19}F\ ^{2}\Sigma_{1/2}$	1222.038	(0.002)
$H^{32}SD$	1227.41	(*0.03)
CD_4	1243.318	(0.046)
CH_4	1246.55	(0.02)
$^{7}Li^{16}OD$	1260.47	(0.01)
$H^{12}C^{15}N$	1271.576	(*)
$^{40}Ca^{19}F\ ^{2}\Sigma_{1/2}$	1279.659	(0.001)
$H^{13}C^{14}N$	1288.939	(*)
$^{40}Ca^{19}F\ ^{2}\Sigma_{1/2}$	1290.252	(0.001)
	1300.811	(0.001)
$^{1}H^{17}O\ ^{2}\Pi_{3/2}$	1302.119	(0.01)
$^{40}Ca^{19}F\ ^{2}\Sigma_{1/2}$	1311.330	(0.001)
$^{1}H^{17}O\ ^{2}\Pi_{3/2}$	1322.464	(0.01)
$^{14}N^{16}O\ ^{2}\Pi_{1/2}$	1325.299	(1E-3)
$H^{12}C^{14}N$	1346.677	(5E-3)
	1346.796	(5E-3)
$^{14}N^{16}O\ ^{2}\Pi_{1/2}$	1348.459	(4E-3)
$^{1}H^{16}O\ ^{2}\Pi_{3/2}$	1371.377	(0.003)
$^{40}Ca^{19}F\ ^{2}\Sigma_{1/2}$	1383.275	(0.001)
	1395.281	(0.001)
	1407.255	(0.001)
$^{1}H^{16}O\ ^{2}\Pi_{3/2}$	1412.850	(0.003)
	1414.424	(0.003)
$^{1}H^{17}O\ ^{2}\Pi_{3/2}$	1418.202	(0.01)
$^{40}Ca^{19}F\ ^{2}\Sigma_{1/2}$	1419.191	(0.001)
$^{14}N^{16}O\ ^{2}\Pi_{1/2}$	1434.588	(1E-3)
$^{15}N^{16}O\ ^{2}\Pi_{1/2}$	1454.916	(5E-4)
$^{1}H^{17}O\ ^{2}\Pi_{3/2}$	1455.729	(0.01)
$^{1}H^{16}O\ ^{2}\Pi_{3/2}$	1455.896	(0.003)
$^{14}N^{16}O\ ^{2}\Pi_{1/2}$	1467.511	(1E-3)
$^{1}H^{16}O\ ^{2}\Pi_{3/2}$	1489.438	(0.003)
$^{14}N^{16}O\ ^{2}\Pi_{1/2}$	1514.768	(1E-3)
$^{1}H^{16}O\ ^{2}\Pi_{3/2}$	1536.944	(0.003)
	1538.702	(0.003)
$^{1}H^{18}O\ ^{2}\Pi_{3/2}$	1584.274	(0.002)
$^{1}H^{16}O\ ^{2}\Pi_{3/2}$	1586.213	(0.003)
$H^{32}SD$	1596.061	(*0.01)

Appendix B

SLAIM03: Spectral Line Atlas for Interstellar Molecules

by Frank J. Lovas, JPL

H2CCCC	300.270(	62)		142.143	26(2,24)-	26(2,25)				0.3019		
H2CNH	300.666(	9)		502.400	18(5,13)-	18(5,14)	17.0	- 17.0	.314	2.669	Kir73	
H2CNH	300.666(	9)		502.400	18(5,13)-	18(5,14)	19.0	- 19.0	.350	2.669	Kir73	
H2CNH	300.667(*	9)		502.400	18(5,13)-	18(5,14)			1.000	2.669	Kir73	
H2CNH	300.670(	9)		502.400	18(5,13)-	18(5,14)	18.0	- 18.0	.331	2.669	Kir73	
H2CO	300.871(	0)	300.870(1)	161.161	8(3, 5)-	8(3, 6)				2.1209	Cor80	
16OD 2P3/2	303.032(	1)	303.032(2)	-51.570	1. 5 -	1. 5	0.5	- 1.5		0.175	Bea78	
HDCO	303.339(	0)	303.300(100)	506.380	18(5,13)-	18(5,14)				2.6690	Glo78	
16OD 2P1/2	303.496(	394)		1098.781	9. 5 -	9. 5	8.5	- 9.5		0.000	Bea78	
HCCCHO	303.851(	2)		84.369	20(3,17)-	20(3,18)				0.8745		
H2CNH	305.441(	4)		254.319	12(4, 8)-	12(4, 9)	11.0	- 11.0	.305	2.546	Kir73	
H2CNH	305.442(	4)		254.319	12(4, 8)-	12(4, 9)	13.0	- 13.0	.358	2.546	Kir73	
H2CNH	305.444(*	4)		254.319	12(4, 8)-	12(4, 9)			1.000	2.546	Kir73	
H2CNH	305.448(	4)		254.319	12(4, 8)-	12(4, 9)	12.0	- 12.0	.329	2.546	Kir73	
16OD 2P1/2	307.652(	394)		1098.781	9. 5 -	9. 5	8.5	- 8.5		0.028	Bea78	
HDCO	308.531(	0)	308.900(500)	256.404	12(4, 8)-	12(4, 9)				2.5462	Glo78	
16OD 2P1/2	309.878(	292)		1098.781	9. 5 -	9. 5	9.5	- 10.5		0.000	Bea78	
16OD 2P3/2	310.144(	0)	310.145(1)	-51.570	1. 5 -	1. 5	0.5	- 0.5		0.219	Bea78	
16OD 2P3/2	310.215(	0)	310.215(1)	-51.570	1. 5 -	1. 5	1.5	- 1.5		0.424	Bea78	
16OD 2P3/2	310.363(	0)	310.363(1)	-51.570	1. 5 -	1. 5	2.5	- 2.5		0.993	Bea78	
16OD 2P1/2	314.285(	393)		1098.781	9. 5 -	9. 5	9.5	- 9.5		0.031	Bea78	
16OD 2P3/2	317.327(	1)	317.329(4)	-51.570	1. 5 -	1. 5	1.5	- 0.5		0.175	Bea78	
16OD 2P1/2	318.442(	394)		1098.781	9. 5 -	9. 5	9.5	- 8.5		0.000	Bea78	
H2CO-17	319.829(	22)		47.086	3(2, 1)-	3(2, 2)	5.5	- 4.5	.032	2.333		
H2CO-17	319.865(	18)		47.086	3(2, 1)-	3(2, 2)	4.5	- 3.5	.049	2.333		
H2CO-17	319.998(	14)		47.086	3(2, 1)-	3(2, 2)	3.5	- 2.5	.051	2.333		
H2CO-17	320.180(	10)		47.086	3(2, 1)-	3(2, 2)	2.5	- 1.5	.043	2.333		
H2CO-17	320.375(	6)		47.086	3(2, 1)-	3(2, 2)	1.5	- .5	.026	2.333		
H213CO	320.382(	0)		47.089	3(2, 1)-	3(2, 2)				2.3326		
H2CO-17	320.458(	0)		47.086	3(2, 1)-	3(2, 2)	4.5	- 4.5	.157	2.333		
H2CO-17	320.459(	0)		47.086	3(2, 1)-	3(2, 2)	3.5	- 3.5	.091	2.333		
H2CO-17	320.510(	0)		47.086	3(2, 1)-	3(2, 2)	2.5	- 2.5	.049	2.333		
H2CO-17	320.512(*	0)		47.086	3(2, 1)-	3(2, 2)			1.000	2.333		
H2CO-17	320.554(	0)		47.086	3(2, 1)-	3(2, 2)	5.5	- 5.5	.253	2.333		
H2CO-17	320.573(	0)		47.086	3(2, 1)-	3(2, 2)	1.5	- 1.5	.026	2.333		
H2CO-17	320.621(	0)		47.086	3(2, 1)-	3(2, 2)	.5	- .5	.021	2.333		
H2CO-17	320.819(	6)		47.086	3(2, 1)-	3(2, 2)	.5	- 1.5	.026	2.333		
H2CO-17	320.902(	10)		47.086	3(2, 1)-	3(2, 2)	1.5	- 2.5	.043	2.333		
H2CO-17	320.971(	14)		47.086	3(2, 1)-	3(2, 2)	2.5	- 3.5	.051	2.333		
H2CO-17	321.053(	18)		47.086	3(2, 1)-	3(2, 2)	3.5	- 4.5	.049	2.333		
H2CO-17	321.183(	22)		47.086	3(2, 1)-	3(2, 2)	4.5	- 5.5	.032	2.333		
16OD 2P1/2	321.544(	392)		1098.781	9. 5 -	9. 5	10.5	- 10.5		0.034	Bea78	
16OD 2P3/2	322.480(	1)	322.480(2)	-51.570	1. 5 -	1. 5	2.5	- 1.5		0.189	Bea78	
HCCCN	322.650(	270)		512.18	9, 1f -	9, 1e 1V6				.211	Laf78	
HNO	323.103(	474)		400.831	13(3,10)-	13(3,11)				1.3336		
SiC3	325.815(	14)		134.550	23(5,18)-	23(5,19)				2.0725		
16OD 2P1/2	325.951(	392)		1098.781	9. 5 -	9. 5	10.5	- 9.5		0.000	Bea78	
SiC3	326.607(	9)		70.209	16(4,12)-	16(4,13)				1.9096		
HCCCHO	326.627(	1)		2.419	1(1, 0)-	1(1, 1)				1.5000		
D2CO	327.772(	0)		819.325	25(7,18)-	25(7,19)				3.7132		
H213CO	330.381(	2)		858.968	23(5,18)-	23(5,19)				2.1042		
H2CO-17	330.617(	9)		858.947	23(5,18)-	23(5,19)	23.5	- 23.5	.168	2.104		
H2CO-17	330.618(	9)		858.947	23(5,18)-	23(5,19)	22.5	- 22.5	.161	2.104		
H2CO-17	330.619(	9)		858.947	23(5,18)-	23(5,19)	24.5	- 24.5	.175	2.104		
H2CO-17	330.621(	9)		858.947	23(5,18)-	23(5,19)	21.5	- 21.5	.154	2.104		

H2CO-17	330.621(* 9)		858.947	23(5,18)-	23(5,19)				1.000	2.104		
H2CO-17	330.623(9)		858.947	23(5,18)-	23(5,19)	25.5	- 25.5	.184	2.104			
H2CO-17	330.625(9)		858.947	23(5,18)-	23(5,19)	20.5	- 20.5	.148	2.104			
HC11_15N	332.791(0)		0.000	1 -	0				1.0000			
HCCCN	336.092(2)		230.92	7, 1f -	7, 1e 1V7				.268	Laf78		
HC11N	338.126(0)		0.000	1 -	0				1.0000			
HCCCN	339.310(650)		683.24	11, 1f -	11, 1e 1V5				.174	Laf78		
DOCO+	346.776(805)		147.494	16(2,14)-	16(2,15)				0.4852			
H2CCCC	348.278(71)		150.185	27(2,25)-	27(2,26)				0.2909			
H2CO	355.568(0)	355.568(0)	47.328	3(2, 1)-	3(2, 2)				2.3325	Cha77		
H2CNH	361.292(85)		2015.437	39(8,31)-	39(8,32)	38.0	- 38.0	.325	3.111	Kir73		
H2CNH	361.292(85)		2015.437	39(8,31)-	39(8,32)	40.0	- 40.0	.342	3.111	Kir73		
H2CNH	361.292(* 85)		2015.437	39(8,31)-	39(8,32)			1.000	3.111	Kir73		
H2CNH	361.293(85)		2015.437	39(8,31)-	39(8,32)	39.0	- 39.0	.333	3.111	Kir73		
HDCO	361.537(2)		2030.176	39(8,31)-	39(8,32)				3.1110			
H2CO	370.020(0)	370.019(1)	422.553	15(4,11)-	15(4,12)				2.0539	Cha81		
H2CS	375.896(1)		68.698	7(2, 5)-	7(2, 6)				1.0711			
H2CO	376.403(1)		1498.188	31(6,25)-	31(6,26)				2.2418			
H2CCO	377.414(2)	377.416(20)	9.726	1(1, 0)-	1(1, 1)				1.5000	Fab77		
H2CNH	379.205(24)		891.745	25(6,19)-	25(6,20)	24.0	- 24.0	.320	2.761	Kir73		
H2CNH	379.205(24)		891.745	25(6,19)-	25(6,20)	26.0	- 26.0	.346	2.761	Kir73		
H2CNH	379.206(* 24)		891.745	25(6,19)-	25(6,20)			1.000	2.761	Kir73		
H2CNH	379.208(24)		891.745	25(6,19)-	25(6,20)	25.0	- 25.0	.332	2.761	Kir73		
HDCO	381.813(1)		898.604	25(6,19)-	25(6,20)				2.7610			
H2CCC	384.674(10)		9.995	1(1, 0)-	1(1, 1)				1.5000			
H2CCO	390.753(175)		88.797	12(2,10)-	12(2,11)				0.6408			
D2CO	391.081(0)		167.502	10(4, 6)-	10(4, 7)				3.0247			
H2CNH	391.913(49)		1396.281	32(7,25)-	32(7,26)	31.0	- 31.0	.323	2.920	Kir73		
H2CNH	391.913(49)		1396.281	32(7,25)-	32(7,26)	33.0	- 33.0	.343	2.920	Kir73		
H2CNH	391.914(* 49)		1396.281	32(7,25)-	32(7,26)			1.000	2.920	Kir73		
H2CNH	391.915(49)		1396.281	32(7,25)-	32(7,26)	32.0	- 32.0	.333	2.920	Kir73		
H2CS	393.360(69)		299.974	19(3,16)-	19(3,17)				0.9218			
HDCO	393.529(1)		1406.750	32(7,25)-	32(7,26)				2.9205			
HCCCN	394.260(300)		515.22	10, 1f -	10, 1e 1V6				.191	Laf78		
HCCCN	394.871(10)		669.29	5, 1f -	5, 1e 3V7				.367	Laf78		
H2C18O	395.449(10)		900.362	24(5,19)-	24(5,20)				2.0165			
H2CCC	395.501(158)		91.316	12(2,10)-	12(2,11)				0.6408			
H213CO	398.552(4)		1544.936	32(6,26)-	32(6,27)				2.1720			
HCCCN	400.710(710)		686.90	12, 1f -	12, 1e 1V5				.160	Laf78		
H2CCCC	401.816(82)		158.524	28(2,26)-	28(2,27)				0.2807			
H2CNH	402.525(1)		109.112	7(3, 4)-	7(3, 5)	6.0	- 6.0	.283	2.403	Kir73		
H2CNH	402.527(1)		109.112	7(3, 4)-	7(3, 5)	8.0	- 8.0	.372	2.403	Kir73		
H2CNH	402.532(* 1)		109.112	7(3, 4)-	7(3, 5)			1.000	2.403	Kir73		
H2CNH	402.545(1)		109.112	7(3, 4)-	7(3, 5)	7.0	- 7.0	.322	2.403	Kir73		
H2CO	402.715(4)		2388.034	40(7,33)-	40(7,34)				2.3517			
HCCCHO	404.349(3)		90.908	21(3,18)-	21(3,19)				0.8330			
D2CO	406.430(0)		545.754	20(6,14)-	20(6,15)				3.4203			
HDCO	406.839(0)	406.930(100)	110.045	7(3, 4)-	7(3, 5)				2.4032	Glo78		
SiC3	407.342(37)		232.356	31(6,25)-	31(6,26)				2.1939			
H2CCHCN 1v15	407.687(8)		56.942	16(3,13)-	16(3,14)				1.0843			
H2CCHCN	408.904(0)		272.393	38(5,33)-	38(5,34)				1.2669			
D2CO	410.770(0)		1209.844	31(8,23)-	31(8,24)				3.8753			
H2C18O	411.374(3)		446.804	16(4,12)-	16(4,13)				1.9286			
HCCCHO	415.547(3)		22.448	9(2, 7)-	9(2, 8)				0.8432			
SiC3	415.779(9)		31.086	10(3, 7)-	10(3, 8)				1.7022			
H2CCHCN 1v15	416.645(2)		15.012	7(2, 5)-	7(2, 6)				1.0692			
H2CCHCN 1v11	423.629(1)		135.223	26(4,22)-	26(4,23)				1.1894			
H2C18O	429.658(27)		1593.798	33(6,27)-	33(6,28)				2.1062			
H2CO	430.153(1)		874.966	23(5,18)-	23(5,19)				2.1014			
H14N12C18O	430.677(3)			2(1, 1)-	2(1, 2)	2.0	- 2.0			Win76		
H14N12C18O	430.956(* 0)			2(1, 1)-	2(1, 2)					Win76		
H14N12C18O	431.036(1)			2(1, 1)-	2(1, 2)	3.0	- 3.0			Win76		
H14N12C18O	431.235(3)			2(1, 1)-	2(1, 2)	1.0	- 1.0			Win76		
H32SD	435.423(3512)		263.963	5(5, 1)-	6(4, 2)				0.096	Hel73		
H2CCHCN	436.784(0)		14.875	7(2, 5)-	7(2, 6)				1.0691			
DOCO+	439.178(1018)		158.872	17(2,15)-	17(2,16)				0.4574			
H2CCHCN 1v15	439.758(19)		144.470	27(4,23)-	27(4,24)				1.1461			
H2CCHCN	441.976(0)		56.605	16(3,13)-	16(3,14)				1.0837			
H2C18O	444.883(1)		178.410	9(3, 6)-	9(3, 7)				1.8953			
D2CO	447.942(0)		328.433	15(5,10)-	15(5,11)				3.1696			
H2CCCC	448.158(19)		11.178	3(1, 2)-	3(1, 3)				0.5833			
H2CCHCN 1v15	451.236(0)		1.845	1(1, 0)-	1(1, 1)				1.5000			
H2CCHCN 1v15	453.953(39)		285.851	39(5,34)-	39(5,35)				1.2337			
H15N12C16O	457.090(1)			2(1, 1)-	2(1, 2)					Win76		
H2CCHCN	457.283(0)		1.813	1(1, 0)-	1(1, 1)				1.5000			
H2CCCC	461.290(94)		167.161	29(2,27)-	29(2,28)				0.2712			
D2CO	464.984(1)		1677.715	37(9,28)-	37(9,29)				4.0686			
H2CCHCN 1v11	465.908(0)		14.808	7(2, 5)-	7(2, 6)				1.0689			
HCCCN	467.110(780)		690.83	13, 1f -	13, 1e 1V5				.148	Laf78		
H2CCHCN 1v11	468.694(0)		1.791	1(1, 0)-	1(1, 1)				1.5000			
HCCCN	470.672(2)		233.35	8, 1f -	8, 1e 1V7				.236	Laf78		
HCCCN	472.990(330)		518.56	11, 1f -	11, 1e 1V6				.174	Laf78		
CH3CH2CN	479.097(0)		1.064	1(1, 0)-	1(1, 1)				1.5000			
H2CCHCN 2v11	480.022(1)		1.771	1(1, 0)-	1(1, 1)				1.5000			
H14N12C16O	481.015(2)		32.270	2(1, 1)-	2(1, 2)	2.0	- 2.0	0.231	0.833	Win76		
H14N12C16O	481.293(* 0)		32.270	2(1, 1)-	2(1, 2)				0.833	Win76		
H14N12C16O	481.372(1)		32.270	2(1, 1)-	2(1, 2)	3.0	- 3.0	0.415	0.833	Win76		
H14N12C16O	481.571(2)		32.270	2(1, 1)-	2(1, 2)	1.0	- 1.0	0.150	0.833	Win76		

H14N13C16O	481.966(	4)				2(1, 1)-	2(1, 2)	2.0	- 2.0										Win76
H14N13C16O	482.242(*	1)				2(1, 1)-	2(1, 2)												Win76
H14N13C16O	482.321(	2)				2(1, 1)-	2(1, 2)	3.0	- 3.0										Win76
H14N13C16O	482.518(	4)				2(1, 1)-	2(1, 2)	1.0	- 1.0										Win76
CH3CH2CN	484.907(	13)			58.099	17(4,13)-	18(3,16)										2.7846		
H2CCHCN 2v11	485.440(	68)			135.216	26(4,22)-	26(4,23)										1.1879		
H16OD	486.521(	4)	486.528(	2)	480.243	5(4, 1)-	5(4, 2)										5.835	DeL74	
H2CCHCN 1v11	489.834(	5)			272.528	38(5,33)-	38(5,34)										1.2641		
H2CCHCN 1v11	490.369(	1)			56.525	16(3,13)-	16(3,14)										1.0830		
H2CCHCN	492.764(	0)			143.821	27(4,23)-	27(4,24)										1.1448		
SiC3	492.925(	22)			143.949	24(5,19)-	24(5,20)										1.9778		
H2CCHCN 2v11	495.628(	8)			14.749	7(2, 5)-	7(2, 6)										1.0687		
H213CO	497.746(	1)			453.709	16(4,12)-	16(4,13)										1.9273		
H2CO-17	498.129(	7)			453.702	16(4,12)-	16(4,13)	16.5	- 16.5		.167						1.927		
H2CO-17	498.131(	7)			453.702	16(4,12)-	16(4,13)	15.5	- 15.5		.156						1.927		
H2CO-17	498.133(	7)			453.702	16(4,12)-	16(4,13)	17.5	- 17.5		.178						1.927		
H2CO-17	498.137(*	7)			453.702	16(4,12)-	16(4,13)				1.000						1.927		
H2CO-17	498.138(	7)			453.702	16(4,12)-	16(4,13)	14.5	- 14.5		.148						1.927		
H2CO-17	498.144(	7)			453.702	16(4,12)-	16(4,13)	18.5	- 18.5		.190						1.927		
H2CO-17	498.149(	7)			453.702	16(4,12)-	16(4,13)	13.5	- 13.5		.140						1.927		
HNO	498.749(	727)			438.840	14(3,11)-	14(3,12)										1.2409		
CH3CH2CN	499.995(	2)			149.473	29(5,24)-	29(5,25)										1.6346		
HNO	500.411(	339)			109.151	5(2, 3)-	5(2, 4)		4.0-		5.0	0.011							
HNO	500.582(	282)			109.151	5(2, 3)-	5(2, 4)		6.0-		5.0	0.011							
HNO	501.327(	0)			109.151	5(2, 3)-	5(2, 4)		4.0-		4.0	0.262							
HNO	501.343(	0)			109.151	5(2, 3)-	5(2, 4)		6.0-		6.0	0.383							
HNO	501.381(	189)			109.151	5(2, 3)-	5(2, 4)										1.4663		
HNO	501.421(	0)			109.151	5(2, 3)-	5(2, 4)		5.0-		5.0	0.311							
H213CO	501.892(	3)			915.863	24(5,19)-	24(5,20)										2.0139		
HNO	502.182(	282)			109.151	5(2, 3)-	5(2, 4)		5.0-		6.0	0.011							
H2CO-17	502.237(	13)			915.842	24(5,19)-	24(5,20)	24.5	- 24.5		.168						2.014		
H2CO-17	502.238(	13)			915.842	24(5,19)-	24(5,20)	23.5	- 23.5		.161						2.014		
H2CO-17	502.240(	13)			915.842	24(5,19)-	24(5,20)	25.5	- 25.5		.175						2.014		
H2CO-17	502.242(	13)			915.842	24(5,19)-	24(5,20)	22.5	- 22.5		.155						2.014		
H2CO-17	502.242(*	13)			915.842	24(5,19)-	24(5,20)				1.000						2.014		
H2CO-17	502.246(	13)			915.842	24(5,19)-	24(5,20)	26.5	- 26.5		.183						2.014		
H2CO-17	502.249(	13)			915.842	24(5,19)-	24(5,20)	21.5	- 21.5		.149						2.014		
HNO	502.337(	339)			109.151	5(2, 3)-	5(2, 4)		5.0-		4.0	0.011							
H2CNH	512.134(	14)			543.100	19(5,14)-	19(5,15)	18.0	- 18.0		.315						2.524	Kir73	
H2CNH	512.134(	14)			543.100	19(5,14)-	19(5,15)	20.0	- 20.0		.350						2.524	Kir73	
H2CNH	512.136(*	14)			543.100	19(5,14)-	19(5,15)				1.000						2.524	Kir73	
H2CNH	512.140(	14)			543.100	19(5,14)-	19(5,15)	19.0	- 19.0		.332						2.524	Kir73	
H213CO	513.011(	0)			180.597	9(3, 6)-	9(3, 7)										1.8948		
H2CO-17	513.326(	3)			180.592	9(3, 6)-	9(3, 7)	9.5	- 9.5		.160						1.895		
H2CO-17	513.332(	3)			180.592	9(3, 6)-	9(3, 7)	8.5	- 8.5		.143						1.895		
H2CO-17	513.334(	3)			180.592	9(3, 6)-	9(3, 7)	10.5	- 10.5		.181						1.895		
H2CO-17	513.344(*	3)			180.592	9(3, 6)-	9(3, 7)				1.000						1.895		
H2CO-17	513.349(	3)			180.592	9(3, 6)-	9(3, 7)	7.5	- 7.5		.129						1.895		
H2CO-17	513.361(	3)			180.592	9(3, 6)-	9(3, 7)	11.5	- 11.5		.206						1.895		
H2CO-17	513.372(	3)			180.592	9(3, 6)-	9(3, 7)	6.5	- 6.5		.118						1.895		
HDCO	516.639(	0)	516.600(	50)	547.379	19(5,14)-	19(5,15)										2.5238	Glo78	
CH3CH2CN	516.649(	0)			9.361	6(2, 4)-	6(2, 5)										1.2318		
32SO2	521.458(	2)			583.167	39(7,33)-	38(8,30)										6.0117		
SiC3	524.036(	15)			76.859	17(4,13)-	17(4,14)										1.7922		
CH3CH2CN	524.239(	14)			94.947	22(5,17)-	23(4,20)										3.5768		
D2CO	524.974(	0)			74.770	6(3, 3)-	6(3, 4)										2.7720		
H2CCHCN	525.552(	1)			284.767	39(5,34)-	39(5,35)										1.2313		
H2CCCC	527.124(	108)			176.096	30(2,28)-	30(2,29)										0.2623		
HCCCHO	530.889(	4)			97.758	22(3,19)-	22(3,20)										0.7950		
H2CS	531.672(	92)			322.879	20(3,17)-	20(3,18)										0.8764		
H2CCO	532.763(	238)			97.557	13(2,11)-	13(2,12)										0.5931		
H2CNH	534.576(	121)			2100.983	40(8,32)-	40(8,33)	39.0	- 39.0		.325						3.020	Kir73	
H2CNH	534.576(	121)			2100.983	40(8,32)-	40(8,33)	41.0	- 41.0		.341						3.020	Kir73	
H2CNH	534.577(*	121)			2100.983	40(8,32)-	40(8,33)				1.000						3.020	Kir73	
H2CNH	534.578(	121)			2100.983	40(8,32)-	40(8,33)	40.0	- 40.0		.333						3.020	Kir73	
HDCO	534.815(	3)			2116.320	40(8,32)-	40(8,33)										3.0203		
HCCCN	538.500(	880)			695.08	14, 1f -	14, 1e 1V5										.138	Laf78	
H2CCC	539.238(	215)			100.328	13(2,11)-	13(2,12)										0.5931		
H2CCHCN 2v11	541.551(	33)			56.462	16(3,13)-	16(3,14)										1.0823		
H2CO	546.350(	2)			1575.905	32(6,26)-	32(6,27)										2.1669		
DOCO+	548.876(	1270)			170.919	18(2,16)-	18(2,17)										0.4326		
13CH3OH vt=1	551.523(	18)			235.555	3(1, 2)-	3(1, 3)	-+									0.4673		
HCCCN	552.807(	13)			671.13	6, 1f -	6, 1e 3V7										.310	Laf78	
HCCCN	558.830(	350)			522.21	12, 1f -	12, 1e 1V6										.160	Laf78	
D2CO	561.277(	0)			870.412	26(7,19)-	26(7,20)										3.5511		
CH3CH2CN	563.357(	1)			34.161	13(3,10)-	13(3,11)										1.3164		
H2CCHCN 1v11	568.195(	2)			143.812	27(4,23)-	27(4,24)										1.1432		
H213CO	571.779(	6)			1623.068	33(6,27)-	33(6,28)										2.1016		
H2CNH	574.433(	7)			282.153	13(4, 9)-	13(4,10)	12.0	- 12.0		.307						2.351	Kir73	
H2CNH	574.433(	7)			282.153	13(4, 9)-	13(4,10)	14.0	- 14.0		.356						2.351	Kir73	
H2CNH	574.437(*	7)			282.153	13(4, 9)-	13(4,10)				1.000						2.351	Kir73	
H2CNH	574.444(	7)			282.153	13(4, 9)-	13(4,10)	13.0	- 13.0		.330						2.351	Kir73	
12CH3OH vt=1	577.542(	9)			235.712	3(1, 2)-	3(1, 3)	-+									0.4669		
H2CCHCN 1v15	579.594(	47)			298.558	40(5,35)-	40(5,36)										1.1998		
HDCO	580.210(	0)	580.210(	100)	284.444	13(4, 9)-	13(4,10)										2.3509	Glo78	
H2CCHCN 1v15	580.726(	10)			62.335	17(3,14)-	17(3,15)										1.0203		
HC9N	581.037(	0)			0.000	1 -	0										1.0000		
H2CCHCN 1v15	583.524(	23)			153.362	28(4,24)-	28(4,25)										1.1031		

33SO2	587.987(	3)			57.237	12(2,10)-	11(3, 9)	12.5-	11.5	0.257		
HCCCN	588.313(	3)			236.09	9, 1f -	9, 1e 1V7				.211	Laf78
33SO2	588.470(	2)			57.237	12(2,10)-	11(3, 9)	11.5-	10.5	0.237		
SiC3	588.543(	54)			244.905	32(6,26)-	32(6,27)				2.1139	
33SO2	590.253(	17)			57.237	12(2,10)-	11(3, 9)				1.8779	
H2C18O	590.271(	14)			958.277	25(5,20)-	25(5,21)				1.9331	
33SO2	592.074(	2)			57.237	12(2,10)-	11(3, 9)	13.5-	12.5	0.280		
33SO2	592.558(	3)			57.237	12(2,10)-	11(3, 9)	10.5-	9.5	0.217		
CH3CH2CN	592.620(	1)			81.465	21(4,17)-	21(4,18)				1.4505	
H2CNH	596.054(	72)			1466.941	33(7,26)-	33(7,27)	32.0	- 32.0	.323	2.821	Kir73
H2CNH	596.054(	72)			1466.941	33(7,26)-	33(7,27)	34.0	- 34.0	.343	2.821	Kir73
H2CNH	596.055(*	72)			1466.941	33(7,26)-	33(7,27)			1.000	2.821	Kir73
H2CNH	596.057(	72)			1466.941	33(7,26)-	33(7,27)	33.0	- 33.0	.333	2.821	Kir73
HDCO	598.402(	2)			1477.914	33(7,26)-	33(7,27)				2.8210	
H2CCCC	599.752(	122)			185.328	31(2,29)-	31(2,30)				0.2539	
H2CO	600.742(	0)	600.740(	1)	183.048	9(3, 6)-	9(3, 7)				1.8942	Cha81
H2CNH	601.239(	36)			947.448	26(6,20)-	26(6,21)	25.0	- 25.0	.320	2.646	Kir73
H2CNH	601.239(	36)			947.448	26(6,20)-	26(6,21)	27.0	- 27.0	.345	2.646	Kir73
H2CNH	601.241(*	36)			947.448	26(6,20)-	26(6,21)			1.000	2.646	Kir73
H2CNH	601.244(	36)			947.448	26(6,20)-	26(6,21)	26.0	- 26.0	.332	2.646	Kir73
HDCO	605.291(	1)			954.710	26(6,20)-	26(6,21)				2.6463	
13CH3OH vt=0	605.764(	39)			275.567	17(3,14)-	17(3,15) -+				1.0053	
H2C18O	609.579(	35)			1672.445	34(6,28)-	34(6,29)				2.0397	
H2CO	614.687(	0)			461.476	16(4,12)-	16(4,13)				1.9257	
HCCCN	614.900(	1000)			699.63	15, 1f -	15, 1e 1V5				.129	Laf78
HCCCHO	622.730(	4)			25.558	10(2, 8)-	10(2, 9)				0.7619	
13CH3OH vt=1	626.102(	363)			447.884	17(2,16)-	17(2,15) -+				0.4372	
H2CS	626.290(	2)			77.861	8(2, 6)-	8(2, 7)				0.9440	
H2CCHCN 1v11	629.338(	6)			284.941	39(5,34)-	39(5,35)				1.2283	
H2CCHCN	629.466(	0)			61.992	17(3,14)-	17(3,15)				1.0196	
H2CNH	637.954(	1)			34.713	3(2, 1)-	3(2, 2)	2.0	- 2.0	.212	2.331	Kir73
H2CNH	637.954(	1)			34.713	3(2, 1)-	3(2, 2)	2.0	- 3.0	.026	2.331	Kir73
H2CNH	637.983(	1)			34.713	3(2, 1)-	3(2, 2)	4.0	- 3.0	.027	2.331	Kir73
H2CNH	637.983(	1)			34.713	3(2, 1)-	3(2, 2)	4.0	- 4.0	.402	2.331	Kir73
H2CNH	638.004(*	1)			34.713	3(2, 1)-	3(2, 2)			1.000	2.331	Kir73
H2CNH	638.066(	1)			34.713	3(2, 1)-	3(2, 2)	3.0	- 2.0	.026	2.331	Kir73
H2CNH	638.066(	1)			34.713	3(2, 1)-	3(2, 2)	3.0	- 3.0	.280	2.331	Kir73
H2CNH	638.066(	1)			34.713	3(2, 1)-	3(2, 2)	3.0	- 4.0	.027	2.331	Kir73
HDCO	644.903(	0)	644.893(	5)	35.029	3(2, 1)-	3(2, 2)				2.3311	Est63
H2CCHCN 2v11	650.905(	82)			143.830	27(4,23)-	27(4,24)				1.1415	
HCCCN	651.780(	390)			526.16	13, 1f -	13, 1e 1V6				.148	Laf78
SiC3	653.113(	7)			10.121	5(2, 3)-	5(2, 4)				1.4597	
H2CO	653.153(	1)			933.327	24(5,19)-	24(5,20)				2.0107	
H2CCHCN	653.695(	0)			152.702	28(4,24)-	28(4,25)				1.1017	
H2C18O	662.373(	5)			486.210	17(4,13)-	17(4,14)				1.8150	
HC11_15N	665.581(	0)			0.011	2 -	1				2.0000	
H2CCHCN	670.790(	1)			297.459	40(5,35)-	40(5,36)				1.1973	
D2CO	672.826(	0)			1272.730	32(8,24)-	32(8,25)				3.7303	
HC11N	676.252(	0)			0.011	2 -	1				2.0000	
13CH3OH vt=0	676.963(	22)			97.112	9(2, 7)-	9(2, 8) +-				0.6372	
DOCO+	677.891(	1565)			183.636	19(2,17)-	19(2,18)				0.4104	
H2CCCC	679.624(	138)			194.858	32(2,30)-	32(2,31)				0.2461	
13CH3OH vt=1	683.161(	23)			218.372	3(0, 3)-	4(1, 4)				2.2317	
H2CCHCN 1v15	686.891(	47)			87.089	22(2,20)-	21(3,19)				4.2011	
HCCCHO	688.501(	5)			104.920	23(3,20)-	23(3,21)				0.7602	
12CH3OH vt=1	688.670(	53)			453.605	17(2,16)-	17(2,15) -+				0.4486	
CH3CH2CN	692.051(	2)			158.465	30(5,25)-	30(5,26)				1.5723	
H2CCHCN 1v15	693.358(	4)			17.545	8(2, 6)-	8(2, 7)				0.9412	
HCCCN	696.100(	1300)			704.48	16, 1f -	16, 1e 1V5				.121	Laf78
H2CCHCN 1v11	698.245(	1)			61.928	17(3,14)-	17(3,15)				1.0188	
12CH 2PI 3/2	701.679(	4)	701.677(	10)		1.5 -	1.5	2 -	2			Ziu85
D14N12C16O	701.839(	5)			18.73	2(1, 1)-	2(1, 2)	2.0	- 2.0	0.231	0.833	Win76
D14N12C16O	702.097(*	1)			18.73	2(1, 1)-	2(1, 2)				0.833	Win76
D14N12C16O	702.171(	2)			18.73	2(1, 1)-	2(1, 2)	3.0	- 3.0	0.415	0.833	Win76
CH3CH2CN	702.266(	13)			94.964	23(4,19)-	22(5,18)				3.5837	
D14N12C16O	702.355(	5)			18.73	2(1, 1)-	2(1, 2)	1.0	- 1.0	0.150	0.833	Win76
12CH 2PI 3/2	704.201(	240)				1.5 -	1.5	2 -	1			Bog83
H2CS	708.123(	123)			346.927	21(3,18)-	21(3,19)				0.8351	
12CH3OH vt=0	709.316(	12)			281.347	17(3,14)-	17(3,15) -+				1.0086	
H2CCO	710.220(	318)			106.991	14(2,12)-	14(2,13)				0.5521	
H2CCC	718.853(	287)			110.034	14(2,12)-	14(2,13)				0.5521	
HCCCN	719.015(	4)			239.13	10, 1f -	10, 1e 1V7				.191	Laf78
12CH 2PI 3/2	722.478(	220)				1.5 -	1.5	1 -	2			Bog83
D2CO	722.646(	0)			587.013	21(6,15)-	21(6,16)				3.2416	
SiC3	723.762(	16)			35.381	11(3, 8)-	11(3, 9)				1.5470	
H2CCHCN 2v11	724.617(	173)			161.997	29(4,26)-	30(3,27)				5.4380	
12CH 2PI 3/2	724.791(	4)	724.789(	10)		1.5 -	1.5	1 -	1			Ziu85
H2CCHCN	726.805(	0)			17.404	8(2, 6)-	8(2, 7)				0.9410	
SiC3	731.988(	35)			153.745	25(5,20)-	25(5,21)				1.8890	
HCCCN	737.056(	17)			673.27	7, 1f -	7, 1e 3V7				.268	Laf78
D2CO	738.508(	1)			1752.362	38(9,29)-	38(9,30)				3.9341	
H2CCCC	746.925(	32)			12.365	4(1, 3)-	4(1, 4)				0.4500	
HNO	747.113(	1083)			479.561	15(3,12)-	15(3,13)				1.1601	
12CH3OH vt=0	747.569(	6)			98.799	9(2, 7)-	9(2, 8) +-				0.6432	
H213CO	748.888(	4)			975.135	25(5,20)-	25(5,21)				1.9302	
H2CO-17	749.383(	19)			975.114	25(5,20)-	25(5,21)	25.5	- 25.5	.168	1.930	
H2CO-17	749.384(	19)			975.114	25(5,20)-	25(5,21)	24.5	- 24.5	.161	1.930	
H2CO-17	749.386(	19)			975.114	25(5,20)-	25(5,21)	26.5	- 26.5	.175	1.930	

H2CO-17	749.389(*	19)		975.114	25(5,20)-	25(5,21)					1.000	1.930	
H2CO-17	749.390(	19)		975.114	25(5,20)-	25(5,21)	23.5	- 23.5	.155	1.930			
H2CO-17	749.394(	19)		975.114	25(5,20)-	25(5,21)	27.5	- 27.5	.182	1.930			
H2CO-17	749.399(	19)		975.114	25(5,20)-	25(5,21)	22.5	- 22.5	.150	1.930			
HCCCN	751.820(	440)		530.42	14, 1f -	14, 1e 1V6				.138	Laf78		
H2CCHCN 1v11	753.528(	2)		152.720	28(4,24)-	28(4,25)				1.0999			
DOCO+	765.931(	335)		16.110	2(1, 1)-	2(1, 2)				0.8333			
H2CCHCN 1v15	766.191(	28)		162.573	29(4,25)-	29(4,26)				1.0628			
H2CCCC	767.204(	156)		204.685	33(2,31)-	33(2,32)				0.2387			
H2CCHCN 2v11	770.955(	43)		61.881	17(3,14)-	17(3,15)				1.0179			
H2CCHCN 1v11	775.176(	1)		17.345	8(2, 6)-	8(2, 7)				0.9407			
H2CCHCN 1v11	778.530(	61)		263.277	40(1,39)-	39(3,36)				0.0208			
13CH3OH vt=1	781.921(	453)		476.083	18(2,17)-	18(2,16) -+				0.421			
HCCCN	782.300(	1600)		709.64	17, 1f -	17, 1e 1V5				.114	Laf78		
H2CO	783.292(	3)		1656.054	33(6,27)-	33(6,28)				2.0960			
13CH3OH vt=0	794.706(	1)		11.678	1(1, 0)-	1(1, 1) -+				1.2131			
H213CO	801.245(	1)		494.035	17(4,13)-	17(4,14)				1.8135			
H2CO-17	801.846(	10)		494.029	17(4,13)-	17(4,14)	17.5	- 17.5	.167	1.813			
H2CO-17	801.849(	10)		494.029	17(4,13)-	17(4,14)	16.5	- 16.5	.157	1.813			
H2CO-17	801.852(	10)		494.029	17(4,13)-	17(4,14)	18.5	- 18.5	.177	1.813			
H2CO-17	801.858(*	10)		494.029	17(4,13)-	17(4,14)			1.000	1.813			
H2CO-17	801.859(	10)		494.029	17(4,13)-	17(4,14)	15.5	- 15.5	.149	1.813			
H2CO-17	801.867(	10)		494.029	17(4,13)-	17(4,14)	19.5	- 19.5	.189	1.813			
H2CO-17	801.874(	10)		494.029	17(4,13)-	17(4,14)	14.5	- 14.5	.142	1.813			
H2CCHCN 1v15	810.270(	13)		68.047	18(3,15)-	18(3,16)				0.9628			
H213CO	810.829(	7)		1703.568	34(6,28)-	34(6,29)				2.0347			
SiC3	816.835(	25)		83.902	18(4,14)-	18(4,15)				1.6859			
H2CCHCN 2v11	824.524(	13)		17.293	8(2, 6)-	8(2, 7)				0.9404			
H16OD	824.672(	3)	824.671(2)	233.024	3(3, 0)-	3(3, 1)				5.238	DeL74		
H2C18O	824.678(	1)		201.586	10(3, 7)-	10(3, 8)				1.7118			
DOCO+	828.358(	1910)		197.021	20(2,18)-	20(2,19)				0.3903			
D2CO	832.211(	0)		189.070	11(4, 7)-	11(4, 8)				2.7482			
12CH3OH vt=0	834.285(	1)	834.267(10)	11.705	1(1, 0)-	1(1, 1) -+				1.2129	Rad72		
SiC3	839.382(	80)		257.852	33(6,27)-	33(6,28)				2.0373			
D2CO	846.706(	0)		359.849	16(5,11)-	16(5,12)				2.9607			
13CH3OH vt=0	846.730(	56)		303.877	18(3,15)-	18(3,16) -+				0.9697			
H2CNH	847.253(	22)		585.958	20(5,15)-	20(5,16)	19.0	- 19.0	.316	2.391	Kir73		
H2CNH	847.254(	22)		585.958	20(5,15)-	20(5,16)	21.0	- 21.0	.349	2.391	Kir73		
H2CNH	847.256(*	22)		585.958	20(5,15)-	20(5,16)			1.000	2.391	Kir73		
H2CNH	847.262(	22)		585.958	20(5,15)-	20(5,16)	20.0	- 20.0	.332	2.391	Kir73		
CH3CH2CN	848.108(	2)		88.056	22(4,18)-	22(4,19)				1.3784			
H2CCHCN	850.478(	1)		310.470	41(5,36)-	41(5,37)				1.1646			
32SO2 v2=1	851.336(	2)		125.746	18(3,15)-	17(4,14)				2.7884			
HDCO	854.621(	1)	854.940(500)	590.551	20(5,15)-	20(5,16)				2.3915	Glo78		
H2C18O	855.431(	43)		1753.404	35(6,29)-	35(6,30)				1.9765			
H2CCHCN	858.088(	1)		161.901	29(4,25)-	29(4,26)				1.0612			
HCCCN	858.930(	530)		534.98	15, 1f -	15, 1e 1V6				.129	Laf78		
12CH3OH vt=1	860.048(	65)		482.521	18(2,17)-	18(2,16) -+				0.4331			
H14N12C18O	861.622(	2)			3(1, 2)-	3(1, 3)	3.0	- 3.0			Win76		
H14N12C18O	861.901(*	1)			3(1, 2)-	3(1, 3)					Win76		
H14N12C18O	861.994(	2)			3(1, 2)-	3(1, 3)	4.0	- 4.0			Win76		
H14N12C18O	862.124(	3)			3(1, 2)-	3(1, 3)	2.0	- 2.0			Win76		
HCCCN	862.771(	4)		242.48	11, 1f -	11, 1e 1V7				.174	Laf78		
H2CCHCN 2v11	862.923(	97)		152.766	28(4,24)-	28(4,25)				1.0980			
H2CCCC	862.969(	175)		214.811	34(2,32)-	34(2,33)				0.2318			
CH3CH2CN	864.934(	1)		38.350	14(3,11)-	14(3,12)				1.2194			
H2C18O	866.625(	17)		1018.514	26(5,21)-	26(5,22)				1.8555			
HCCCN	873.400(	2000)		715.10	18, 1f -	18, 1e 1V5				.108	Laf78		
H2C18O	874.255(	0)		56.129	4(2, 2)-	4(2, 3)				1.7985			
H2CCHCN	878.104(	0)		67.696	18(3,15)-	18(3,16)				0.9621			
HCCCHO	882.865(	7)		112.393	24(3,21)-	24(3,22)				0.7281			
H2CNH	883.016(	3)		126.225	8(3, 5)-	8(3, 6)	7.0	- 7.0	.290	2.114	Kir73		
H2CNH	883.020(	3)		126.225	8(3, 5)-	8(3, 6)	9.0	- 9.0	.368	2.114	Kir73		
H2CNH	883.029(*	3)		126.225	8(3, 5)-	8(3, 6)			1.000	2.114	Kir73		
H2CNH	883.050(	3)		126.225	8(3, 5)-	8(3, 6)	8.0	- 8.0	.324	2.114	Kir73		
H16OD	892.229(	17)		942.549	8(5, 3)-	8(5, 4)				5.818	DeL74		
HDCO	892.448(	0)	892.600(500)	127.285	8(3, 5)-	8(3, 6)				2.1139	Glo78		
H2CNH	893.875(	103)		1539.758	34(7,27)-	34(7,28)	33.0	- 33.0	.323	2.726	Kir73		
H2CNH	893.875(	103)		1539.758	34(7,27)-	34(7,28)	35.0	- 35.0	.343	2.726	Kir73		
H2CNH	893.876(*	103)		1539.758	34(7,27)-	34(7,28)			1.000	2.726	Kir73		
H2CNH	893.879(	103)		1539.758	34(7,27)-	34(7,28)	34.0	- 34.0	.333	2.726	Kir73		
SiC3	896.051(	12)		1.445	1(1, 0)-	1(1, 1)				1.5000			
HDCO	897.226(	3)		1551.249	34(7,27)-	34(7,28)				2.7260			
HCCCHO	898.412(	6)		28.979	11(2, 9)-	11(2,10)				0.6948			
CH3CHO vt=0	909.890(	43)		112.586	17(-3,15)-	16(-4,13)				1.3491			
H15N12C16O	914.172(	2)			3(1, 2)-	3(1, 3)					Win76		
13CH3OH vt=1	918.973(	28)		241.831	4(1, 3)-	4(1, 4) -+				0.3580			
H2CCHCN 1v11	919.424(	34)		203.505	34(3,31)-	35(1,34)				0.0219			
CH3CH2CN	926.103(	1)		11.448	7(2, 5)-	7(2, 6)				1.0618			
13CH3OH vt=0	926.690(	62)		393.929	18(6,13)-	19(5,15)				4.7678			
H2CCO	928.543(	416)		117.098	15(2,13)-	15(2,14)				0.5163			
H2CS	930.613(	160)		372.120	22(3,19)-	22(3,20)				0.7975			
H2CNH	935.297(	53)		1005.310	27(6,21)-	27(6,22)	26.0	- 26.0	.321	2.539	Kir73		
H2CNH	935.297(	53)		1005.310	27(6,21)-	27(6,22)	28.0	- 28.0	.345	2.539	Kir73		
H2CNH	935.299(*	53)		1005.310	27(6,21)-	27(6,22)			1.000	2.539	Kir73		
H2CNH	935.303(	53)		1005.310	27(6,21)-	27(6,22)	27.0	- 27.0	.332	2.539	Kir73		
D2CO	939.087(	0)		923.497	27(7,20)-	27(7,21)				3.3980			
H2CCC	939.832(	375)		120.432	15(2,13)-	15(2,14)				0.5163			

```
HDCO            941.466(     2)                 1012.991  27(  6,21)-  27(  6,22)                                          2.5386
CH3CH2CN        946.284(     3)                  167.759  31(  5,26)-  31(  5,27)                                          1.5129
HCCCN           947.614(    23)                  675.71    8, 1f    -   8, 1e 3V7                                           .236  Laf78
H213CO          950.822(     0)                  204.313  10(  3, 7)-  10(  3, 8)                                          1.7111
H2CO-17         951.402(     5)                  204.309  10(  3, 7)-  10(  3, 8)    10.5     - 10.5       .162  1.711
H2CO-17         951.411(     5)                  204.309  10(  3, 7)-  10(  3, 8)     9.5     -  9.5       .146  1.711
H2CO-17         951.415(     5)                  204.309  10(  3, 7)-  10(  3, 8)    11.5     - 11.5       .181  1.711
H2CO-17         951.431(*    5)                  204.309  10(  3, 7)-  10(  3, 8)                          1.000  1.711
H2CO-17         951.436(     5)                  204.309  10(  3, 7)-  10(  3, 8)     8.5     -  8.5       .133  1.711
H2CO-17         951.455(     5)                  204.309  10(  3, 7)-  10(  3, 8)    12.5     - 12.5       .203  1.711
H2CO-17         951.472(     5)                  204.309  10(  3, 7)-  10(  3, 8)     7.5     -  7.5       .123  1.711
H2CO-17         960.315(    15)                   56.559   4(  2, 2)-   4(  2, 3)     5.5     -  4.5       .031  1.798
H2CO-17         960.316(    13)                   56.559   4(  2, 2)-   4(  2, 3)     4.5     -  3.5       .033  1.798
H2CO-17         960.442(    11)                   56.559   4(  2, 2)-   4(  2, 3)     3.5     -  2.5       .029  1.798
H213CO          960.465(     0)                   56.562   4(  2, 2)-   4(  2, 3)                                          1.7983
H2CO-17         960.508(    17)                   56.559   4(  2, 2)-   4(  2, 3)     6.5     -  5.5       .020  1.798
H2CO-17         960.635(     9)                   56.559   4(  2, 2)-   4(  2, 3)     2.5     -  1.5       .019  1.798
H2CO-17         960.750(     2)                   56.559   4(  2, 2)-   4(  2, 3)     4.5     -  4.5       .121  1.798
H2CO-17         960.767(     2)                   56.559   4(  2, 2)-   4(  2, 3)     5.5     -  5.5       .172  1.798
H2CO-17         960.819(     2)                   56.559   4(  2, 2)-   4(  2, 3)     3.5     -  3.5       .086  1.798
H2CO-17         960.852(*    2)                   56.559   4(  2, 2)-   4(  2, 3)                          1.000  1.798
H2CO-17         960.925(     2)                   56.559   4(  2, 2)-   4(  2, 3)     2.5     -  2.5       .063  1.798
H2CO-17         960.933(     2)                   56.559   4(  2, 2)-   4(  2, 3)     6.5     -  6.5       .239  1.798
H2CO-17         961.029(     2)                   56.559   4(  2, 2)-   4(  2, 3)     1.5     -  1.5       .056  1.798
H2CO-17         961.192(    17)                   56.559   4(  2, 2)-   4(  2, 3)     5.5     -  6.5       .020  1.798
H2CO-17         961.202(    15)                   56.559   4(  2, 2)-   4(  2, 3)     4.5     -  5.5       .031  1.798
H2CO-17         961.252(    13)                   56.559   4(  2, 2)-   4(  2, 3)     3.5     -  4.5       .033  1.798
H2CO-17         961.302(    11)                   56.559   4(  2, 2)-   4(  2, 3)     2.5     -  3.5       .029  1.798
H2CO-17         961.319(     8)                   56.559   4(  2, 2)-   4(  2, 3)     1.5     -  2.5       .019  1.798
H14N12C16O      962.298(     4)                   34.461   3(  1, 2)-   3(  1, 3)     3.0     -  3.0      0.280  0.583  Win76
12CH3OH vt=1    962.328(    15)                  242.143   4(  1, 3)-   4(  1, 4) -+                                        0.3574
H14N12C16O      962.576(*    1)                   34.461   3(  1, 2)-   3(  1, 3)                                          0.583  Win76
H14N12C16O      962.669(     2)                   34.461   3(  1, 2)-   3(  1, 3)     4.0     -  4.0      0.402  0.583  Win76
H14N12C16O      962.798(     3)                   34.461   3(  1, 2)-   3(  1, 3)     2.0     -  2.0      0.212  0.583  Win76
H14N13C16O      964.198(     5)                            3(  1, 2)-   3(  1, 3)     3.0     -  3.0                    Win76
H14N13C16O      964.474(*    2)                            3(  1, 2)-   3(  1, 3)                                          Win76
H14N13C16O      964.566(     3)                            3(  1, 2)-   3(  1, 3)     4.0     -  4.0                    Win76
H14N13C16O      964.695(     4)                            3(  1, 2)-   3(  1, 3)     2.0     -  2.0                    Win76
13CH3OH vt=1    964.965(   559)                  505.864  19(  2,18)-  19(  2,17) -+                                        0.4068
CH3CHO vt=2     965.873(  7496)                  446.455  21(  4,18)-  22(  3,19) --                                        4.6867
H2CCCC          967.411(   196)                  225.233  35(  2,33)-  35(  2,34)                                          0.2252
HCCCN           969.300(  2600)                  720.87   19, 1f    -  19, 1e 1V5                                          .103  Laf78
CH3CHO vt=1     969.553(     1)                  145.652   1(  1, 0)-   1(  1, 1) -+                                        9.6081
H2CCHCN         971.480(    16)                  275.496  41(  1,40)-  40(  3,37)                                          0.0203
HCCCN           973.100(   660)                  539.84   16, 1f    -  16, 1e 1V6                                          .121  Laf78
H2CCHCN 1v11    973.807(     2)                   67.650  18(  3,15)-  18(  3,16)                                          0.9611
H2CO            974.075(     2)                  994.128  25(  5,20)-  25(  5,21)                                          1.9265
HCCCHO          979.863(     4)                    3.030   2(  1, 1)-   2(  1, 2)                                          0.8333
H2CS            983.749(     3)                   88.169   9(  2, 7)-   9(  2, 8)                                          0.8438
H2CCHCN 1v11    988.787(     3)                  161.948  29(  4,25)-  29(  4,26)                                          1.0591
H2CO            989.139(     0)                  502.840  17(  4,13)-  17(  4,14)                                          1.8116
12CH3OH vt=0    991.360(    16)                  310.357  18(  3,15)-  18(  3,16) -+                                        0.9733
H2CCHCN 1v15    996.163(    34)                  172.102  30(  4,26)-  30(  4,27)                                          1.0248
HC11_15N        998.372(     1)                    0.033   3        -   2                                                   3.0000
HNO            1001.171(   397)                  125.448   6(  2, 4)-   6(  2, 5)          5.0-       6.0 0.008
HNO            1001.344(   339)                  125.448   6(  2, 4)-   6(  2, 5)          7.0-       6.0 0.008
HNO            1002.236(     0)                  125.448   6(  2, 4)-   6(  2, 5)          5.0-       5.0 0.274
HNO            1002.256(     0)                  125.448   6(  2, 4)-   6(  2, 5)          7.0-       7.0 0.377
HNO            1002.320(   376)                  125.448   6(  2, 4)-   6(  2, 5)                                          1.2375
HNO            1002.369(     0)                  125.448   6(  2, 4)-   6(  2, 5)          6.0-       6.0 0.318
HNO            1003.280(   339)                  125.448   6(  2, 4)-   6(  2, 5)          6.0-       7.0 0.008
HNO            1003.434(   396)                  125.448   6(  2, 4)-   6(  2, 5)          6.0-       5.0 0.008
H2C34S         1011.166(     8)                   10.256   1(  1, 0)-   1(  1, 1)                                          1.5000
CH3CH2CN       1013.342(    13)                  140.795  27(  6,22)-  28(  5,23)                                          4.3585
H12COOD        1013.70 (     1)                  128.357  16(  4,12)-  16(  4,13)                                          1.917  Wil80
HC11N          1014.378(     0)                    0.034   3        -   2                                                   3.0000
13CH3OH vt=0   1014.616(    34)                  112.848  10(  2, 8)-  10(  2, 9) +-                                        0.5662
HCCCN          1019.579(     5)                  246.13   12, 1f    -  12, 1e 1V7                                          .160  Laf78
CH3OCHO        1025.910(    37)                  132.262  20( 10,10)-  21(  9,12)  E                                      0.851  Oes99
H13COOH        1027.53 (     2)                  297.577  25(  5,20)-  25(  5,21)                                          1.905  Wil80
CH3CHO vt=0    1028.183(     6)                  218.878  26( -1,26)-  26(  0,26)                                          6.5E-8
H2CNH          1028.417(    11)                  312.141  14(  4,10)-  14(  4,11)    13.0     - 13.0       .309  2.181  Kir73
H2CNH          1028.418(    11)                  312.141  14(  4,10)-  14(  4,11)    15.0     - 15.0       .355  2.181  Kir73
H2CNH          1028.423(*   11)                  312.141  14(  4,10)-  14(  4,11)                          1.000  2.181  Kir73
H2CNH          1028.435(    11)                  312.141  14(  4,10)-  14(  4,11)    14.0     - 14.0       .330  2.181  Kir73
CH3OCHO        1028.917(    80)                  543.893  47( 13,34)-  47( 13,35)  E                                     12.516  Oes99
CH3OCHO        1034.310(    34)                  132.258  20( 10,11)-  21(  9,12)  A                                      0.851  Oes99
CH3OCHO        1036.245(    34)                  132.258  20( 10,10)-  21(  9,13)  A                                      0.851  Oes99
H2C18O         1036.940(     7)                  527.940  18(  4,14)-  18(  4,15)                                          1.7132
CH3OCHO        1038.592(     6)                  229.324  30(  9,21)-  30(  9,22)  E                                     11.975  Oes99
HDCO           1038.694(     0)                  314.653  14(  4,10)-  14(  4,11)                                          2.1812
CH3OCHO        1040.566(     6)                  229.326  30(  9,21)-  30(  9,22)  A                                     11.970  Oes99
H12COOH        1041.43 (     0)                   69.446  11(  3, 8)-  11(  3, 9)                                          1.552  Wil80
H12COOH        1042.11 (     0)                  163.850  18(  4,14)-  18(  4,15)                                          1.696  Wil80
H2CS           1046.488(     0)  1046.487(   1)   10.287   1(  1, 0)-   1(  1, 1)                                          1.5000 Joh71a
D12COOH        1056.46 (     0)                   13.571   4(  2, 2)-   4(  2, 3)                                          1.797  Wil80
H12COOH        1059.28 (     0)                   20.082   5(  2, 3)-   5(  2, 4)                                          1.461  Wil80
12CH3OH vt=1   1061.361(   800)                  513.037  19(  2,18)-  19(  2,17) -+                                        0.4196
```

```
CH3CHO vt=0    1065.076(     0)    1065.075(   5)    2.202   1(  1, 0)-   1(  1, 1) -+                                  9.4857 Got73
NH213CHO       1065.326(     2)                      18.657   5(  2, 3)-   5(  2, 4)          4.0-       5.0 0.011
NH213CHO       1065.375(     2)                      18.657   5(  2, 3)-   5(  2, 4)          6.0-       5.0 0.011
NH213CHO       1065.618(     0)                      18.657   5(  2, 3)-   5(  2, 4)          5.0-       5.0 0.311
NH213CHO       1065.747(   399)                      18.657   5(  2, 3)-   5(  2, 4)                                 1.4606
NH213CHO       1065.797(     0)                      18.657   5(  2, 3)-   5(  2, 4)          6.0-       6.0 0.383
NH213CHO       1065.833(     0)                      18.657   5(  2, 3)-   5(  2, 4)          4.0-       4.0 0.262
H2CO           1065.870(     0)    1065.871(   0)   57.042   4(  2, 2)-   4(  2, 3)                                 1.7981 Cha77
NH213CHO       1066.039(     2)                      18.657   5(  2, 3)-   5(  2, 4)          5.0-       6.0 0.011
NH213CHO       1066.125(     2)                      18.657   5(  2, 3)-   5(  2, 4)          5.0-       4.0 0.011
SiC3           1068.276(    53)                     163.938  26(  5,21)-  26(  5,22)                                 1.8055
32SO2 v2=1     1069.401(     2)                      83.005  15(  2,14)-  14(  3,11)                                 2.0344
HCCCN          1069.900(  3300)                     726.94   20, 1f    -  20, 1e 1V5                                  .098  Laf78
H2CCHCN 2v11   1074.929(    53)                      67.619  18(  3,15)-  18(  3,16)                                 0.9600
H2CCCC         1081.033(   219)                     235.954  36(  2,34)-  36(  2,35)                                 0.2190
D2CO           1082.509(     1)                    1337.616  33(  8,25)-  33(  8,26)                                 3.5913
NH2CHO         1085.311(     0)                     573.756  36(  7,29)-  37(  6,32)         35.0-      36.0 0.324
NH2CHO         1085.312(     0)                     573.756  36(  7,29)-  37(  6,32)         37.0-      38.0 0.342
NH2CHO         1085.328(    37)                     573.758  36(  7,29)-  37(  6,32)                                 5.8931
NH2CHO         1085.360(     0)                     573.756  36(  7,29)-  37(  6,32)         36.0-      37.0 0.333
H2CCHCN 1v15   1087.282(     6)                      20.394   9(  2, 7)-   9(  2, 8)                                 0.8400
HNO            1090.261(  1571)                     522.992  16(  3,13)-  16(  3,14)                                 1.0890
a-CH2=CHOH     1094.171(     0)                      16.805   5(  2, 3)-   5(  2, 4)                                 1.4596
HCCCN          1094.310(   860)                     545.01   17, 1f    -  17, 1e 1V6                                  .114  Laf78
D12COOH        1095.32 (     0)                     102.314  14(  4,10)-  14(  4,11)                                 2.193  Wil80
D12COOH        1096.55 (     2)                     466.158  32(  7,25)-  32(  7,26)                                 2.960  Wil80
H213CO         1099.054(     5)                    1036.784  26(  5,21)-  26(  5,22)                                 1.8521
H2CO-17        1099.749(    27)                    1036.764  26(  5,21)-  26(  5,22)    26.5     - 26.5       .168  1.852
H2CO-17        1099.751(    27)                    1036.764  26(  5,21)-  26(  5,22)    25.5     - 25.5       .162  1.852
H2CO-17        1099.753(    27)                    1036.764  26(  5,21)-  26(  5,22)    27.5     - 27.5       .175  1.852
H2CO-17        1099.757(*   27)                    1036.764  26(  5,21)-  26(  5,22)                        1.000  1.852
H2CO-17        1099.758(    27)                    1036.764  26(  5,21)-  26(  5,22)    24.5     - 24.5       .156  1.852
H2CO-17        1099.764(    27)                    1036.764  26(  5,21)-  26(  5,22)    28.5     - 28.5       .182  1.852
H2CO-17        1099.770(    27)                    1036.764  26(  5,21)-  26(  5,22)    23.5     - 23.5       .150  1.852
H2CCHCN 1v15   1109.750(    17)                      74.077  19(  3,16)-  19(  3,17)                                 0.9109
H2CO           1109.959(     4)                    1738.634  34(  6,28)-  34(  6,29)                                 2.0285
H2CO           1113.194(     0)    1113.190(   1)  207.372  10(  3, 7)-  10(  3, 8)                                 1.7103 Cha81
H2CCHCN        1115.291(     1)                     171.419  30(  4,26)-  30(  4,27)                                 1.0230
H12COOD        1118.53 (     1)                      56.532  10(  3, 7)-  10(  3, 8)                                 1.706  Wil80
HCCCHO         1120.347(    11)                     120.179  25(  3,22)-  25(  3,23)                                 0.6983
H2CCCC         1120.378(    48)                      13.848   5(  1, 4)-   5(  1, 5)                                 0.3667
12CH3OH vt=0   1120.381(     9)    1120.427(  50)  114.923  10(  2, 8)-  10(  2, 9) +-                                 0.5728 Bro81
NH2CHO         1123.033(     0)                     496.849  34(  6,28)-  34(  6,29)         34.0-      34.0 0.333
NH2CHO         1123.044(     7)                     496.849  34(  6,28)-  34(  6,29)                                 1.9921
NH2CHO         1123.049(     0)                     496.849  34(  6,28)-  34(  6,29)         33.0-      33.0 0.323
NH2CHO         1123.049(     0)                     496.849  34(  6,28)-  34(  6,29)         35.0-      35.0 0.343
H12COOD        1125.19 (     2)                     404.744  30(  6,24)-  30(  6,25)                                 2.297  Wil80
HC7N           1128.002(     0)                       0.000   1         -   0                                         1.0000
H2CCHCN 2v11   1131.904(   112)                     162.021  29(  4,25)-  29(  4,26)                                 1.0570
H2CCO          1132.236(     7)    1132.240(  20)   11.061   2(  1, 1)-   2(  1, 2)                                 0.8333 Fab77
CH3CHO vt=2    1135.778(  2724)                     311.623  12( -2,11)-  11( -3, 9)                                 0.0002
D2CO           1136.456(   103)                     932.496  29(  4,25)-  28(  6,22)                                 0.0475
H213CO         1137.249(     8)                    1786.438  35(  6,29)-  35(  6,30)                                 1.9710
CH3OCHO        1137.767(     6)                     174.380  26(  8,18)-  26(  8,19)  A                              11.146  Oes99
H13COOH        1138.18 (     0)                      19.808   5(  2, 3)-   5(  2, 4)                                 1.461  Wil80
CH3OCHO        1138.953(    10)                     174.379  26(  8,18)-  26(  8,19)  E                              11.085  Oes99
H2CCHCN        1139.582(     0)                      20.250   9(  2, 7)-   9(  2, 8)                                 0.8397
NH2CHO         1146.827(     0)                     300.833  26(  5,21)-  26(  5,22)         26.0-      26.0 0.332
NH2CHO         1146.842(     4)                     300.833  26(  5,21)-  26(  5,22)                                 1.8238
NH2CHO         1146.849(     0)                     300.833  26(  5,21)-  26(  5,22)         27.0-      27.0 0.345
NH2CHO         1146.850(     0)                     300.833  26(  5,21)-  26(  5,22)         25.0-      25.0 0.320
CH3OCHO        1148.438(     4)                      54.773  14(  5, 9)-  14(  5,10)  A                               8.568  Oes99
c-HCCCD        1148.893(   146)                      92.117  11(  3, 9)-  10(  4, 6)                                 0.0127
H2CCC          1154.015(    30)                     11.370   2(  1, 1)-   2(  1, 2)                                 0.8333
D2CO           1155.932(     2)                    1829.010  39(  9,30)-  39(  9,31)                                 3.8037
H12COOD        1158.13 (     1)                     246.861  23(  5,18)-  23(  5,19)                                 2.085  Wil80
CH3OCHO        1159.588(    10)                     457.240  43( 12,31)-  43( 12,32)  A                              13.487  Oes99
HC9N           1162.073(     0)                       0.019   2         -   1                                         2.0000
13CH3OH vt=0   1162.173(    77)                     333.756  19(  3,16)-  19(  3,17) -+                                0.9384
H2CCHCN 1v15   1171.451(    62)                     125.402  27(  2,26)-  26(  3,23)                                 4.0772
CH3OCHO        1172.199(    17)                      54.780  14(  5, 9)-  14(  5,10)  E                               8.200  Oes99
HCCCN          1175.400(  4200)                     733.31   21, 1f    -  21, 1e 1V5                                  .093  Laf78
CH3OCHO        1175.549(    82)                      30.000  10(  4, 6)-   9(  5, 5)  E                               0.144  Oes99
H13COOH        1176.07 (     1)                      68.792  11(  3, 8)-  11(  3, 9)                                 1.552  Wil80
13CH3OH vt=1   1178.173(   682)                     537.207  20(  2,19)-  20(  2,18) -+                                0.3943
SiC3           1182.408(   117)                     271.197  34(  6,28)-  34(  6,29)                                 1.9637
HCCCN          1184.474(    27)                     678.47    9, 1f    -   9, 1e 3V7                                  .211  Laf78
16OD 2P3/2     1185.871(     0)    1185.871(   1)   -5.198   2. 5     -   2. 5          2.5     -  3.5              0.054  Bea78
16OD 2P3/2     1187.000(     0)    1186.999(   3)   -5.198   2. 5     -   2. 5          1.5     -  2.5              0.053  Bea78
CH3CHO vt=2    1187.919(    17)                     259.169   1(  1, 0)-   1(  1, 1) -+                                9.1274
H2C18O         1188.043(    52)                    1836.675  36(  6,30)-  36(  6,31)                                 1.9163
HCCCN          1189.433(     6)                     250.09   13, 1f    -  13, 1e 1V7                                  .148  Laf78
16OD 2P3/2     1190.565(     0)    1190.566(   2)   -5.198   2. 5     -   2. 5          1.5     -  1.5              0.277  Bea78
16OD 2P3/2     1190.774(     0)    1190.774(   2)   -5.198   2. 5     -   2. 5          2.5     -  2.5              0.388  Bea78
16OD 2P3/2     1191.104(     0)    1191.105(   2)   -5.198   2. 5     -   2. 5          3.5     -  3.5              0.606  Bea78
CH3CH2CN       1192.517(     3)                      94.947  23(  4,19)-  23(  4,20)                                 1.3112
H2CCO          1193.528(   534)                     127.878  16(  2,14)-  16(  2,15)                                 0.4848
16OD 2P3/2     1194.340(     0)    1194.339(   1)   -5.198   2. 5     -   2. 5          2.5     -  1.5              0.053  Bea78
```

CH3OCHO	1195.435(	45)			457.236	43(12,31)-	43(12,32)	E									12.651	Oes99
16OD 2P3/2	1196.007(	1)	1196.006(	3)	-5.198	2. 5 -	2. 5		3.5	-	2.5						0.054	Bea78
SiC3	1197.898(	27)			40.068	12(3, 9)-	12(3,10)										1.4149	
H2CCHCN	1202.373(	0)			73.718	19(3,16)-	19(3,17)										0.9100	
CH3OCHO	1203.669(	6)			126.968	22(7,15)-	22(7,16)	A									10.292	Oes99
H2CCCC	1204.356(	243)			246.972	37(2,35)-	37(2,36)										0.2132	
H12COOH	1206.06 (	0)			319.125	26(5,21)-	26(5,22)										1.824	Wil80
H2CCC	1208.042(	482)			131.523	16(2,14)-	16(2,15)										0.4848	
H2CS	1208.173(	207)			398.456	23(3,20)-	23(3,21)										0.7630	
CH3OCHO	1212.747(	16)			126.969	22(7,15)-	22(7,16)	E									10.105	Oes99
H2CCHCN 1v11	1215.223(	1)			20.199	9(2, 7)-	9(2, 8)										0.8393	
CH3OCHO	1216.798(	4)			87.098	18(6,12)-	18(6,13)	A									9.424	Oes99
a-CH2=CHOH	1218.393(	1)			58.791	11(3, 8)-	11(3, 9)										1.5468	
D12COOH	1218.77 (	1)			315.154	26(6,20)-	26(6,21)										2.676	Wil80
HCCCN	1222.600(	1100)			550.48	18, 1f -	18, 1e 1V6										.108	Laf78
H32SD	1227.406(	33)			371.470	7(5, 2)-	7(5, 3)										6.528	Hel73
CH3OCHO	1234.230(	17)			87.101	18(6,12)-	18(6,13)	E									9.131	Oes99
a-CH2=CHOH	1234.314(	7)			255.563	25(5,20)-	25(5,21)										1.8885	
D2CO	1235.477(	0)			26.698	3(2, 1)-	3(2, 2)										2.3270	
H13COOH	1235.86 (	1)			162.633	18(4,14)-	18(4,15)										1.696	Wil80
H2CCHCN 1v11	1236.440(	23)			116.827	26(2,25)-	25(3,22)										3.9019	
H2CCHCN 2v11	1237.918(	43)			26.829	12(1,11)-	11(2,10)										2.6481	
SiC3	1240.455(	39)			91.340	19(4,15)-	19(4,16)										1.5888	
D12COOH	1245.10 (	1)			193.864	20(5,15)-	20(5,16)										2.412	Wil80
D2CO	1246.815(	0)			630.267	22(6,16)-	22(6,17)										3.0757	
CH3CHO vt=0	1252.287(	1)			19.794	6(2, 4)-	6(2, 5)	+-									7.7720	
H2C18O	1252.978(	21)			1081.072	27(5,22)-	27(5,23)										1.7830	
H213CO	1253.962(	2)			536.741	18(4,14)-	18(4,15)										1.7113	
H213CS	1254.646(	10241)			97.200	10(2, 8)-	10(2, 9)										0.7628	
H2CO-17	1254.878(	15)			536.736	18(4,14)-	18(4,15)		18.5	-	18.5		.167				1.711	
H2CO-17	1254.882(	15)			536.736	18(4,14)-	18(4,15)		17.5	-	17.5		.158				1.711	
H2CO-17	1254.886(	15)			536.736	18(4,14)-	18(4,15)		19.5	-	19.5		.177				1.711	
H2CO-17	1254.894(*	15)			536.736	18(4,14)-	18(4,15)						1.000				1.711	
H2CO-17	1254.895(	15)			536.736	18(4,14)-	18(4,15)		16.5	-	16.5		.150				1.711	
H2CO-17	1254.907(	15)			536.736	18(4,14)-	18(4,15)		20.5	-	20.5		.188				1.711	
H2CO-17	1254.917(	15)			536.736	18(4,14)-	18(4,15)		15.5	-	15.5		.143				1.711	
HCCCHO	1255.871(	7)			32.710	12(2,10)-	12(2,11)										0.6382	
34SO2 v2=1	1269.497(	98)			301.878	27(6,22)-	28(5,23)										4.2713	
CH3CH2CN	1279.030(	4)			177.354	32(5,27)-	32(5,28)										1.4561	
H2CCHCN 1v15	1283.184(	40)			181.949	31(4,27)-	31(4,28)										0.9888	
H2CCHCN 1v11	1284.653(	4)			171.495	30(4,26)-	30(4,27)										1.0207	
HCCCN	1285.500(	5200)			739.99	22, 1f -	22, 1e 1V5										.089	Laf78
CH3CH2CN	1286.949(	2)			42.838	15(3,12)-	15(3,13)										1.1336	
CH3OCHO	1288.446(	130)			502.617	40(19,21)-	41(18,23)	E									2.364	Oes99
H2CCHCN 2v11	1292.364(	19)			20.155	9(2, 7)-	9(2, 8)										0.8389	
12CH3OH vt=1	1295.839(	97)			543.153	20(2,19)-	20(2,18)	-+									0.4078	
SiC3	1300.234(	14)			12.454	6(2, 4)-	6(2, 5)										1.2267	
CH3CHO vt=0	1301.490(	7)			202.864	25(-1,25)-	25(0,25)										1.5E-7	
17OH 2P3/2	1302.119(M	50)	1302.119(	50)		1. 5 -	1. 5		2.5	3.0-	1.5	2.0	0.047					Bea78
D2CO	1305.646(	0)			88.473	7(3, 4)-	7(3, 5)										2.3891	
CH3OCHO	1316.496(	119)			502.612	40(19,22)-	41(18,23)	A									2.364	Oes99
CH3OCHO	1316.498(	119)			502.612	40(19,21)-	41(18,24)	A									2.364	Oes99
17OH 2P3/2	1322.464(M	50)	1322.464(	50)		1. 5 -	1. 5		3.5	3.0-	2.5	2.0	0.067					Bea78
H2CNH	1322.723(	146)			1614.733	35(7,28)-	35(7,29)		34.0	-	34.0		.324				2.635	Kir73
H2CNH	1322.723(	146)			1614.733	35(7,28)-	35(7,29)		36.0	-	36.0		.342				2.635	Kir73
H2CNH	1322.725(*	146)			1614.733	35(7,28)-	35(7,29)						1.000				2.635	Kir73
H2CNH	1322.730(	146)			1614.733	35(7,28)-	35(7,29)		35.0	-	35.0		.333				2.635	Kir73
CH3OCHO	1326.662(	123)			502.613	40(19,22)-	41(18,24)	E									2.365	Oes99
HDCO	1327.423(	3)			1626.758	35(7,28)-	35(7,29)										2.6351	
s-CH2=CHOH	1330.802(	1)			16.424	5(2, 3)-	5(2, 4)										1.4576	
HC11_15N	1331.162(	1)			0.067	4 -	3										4.0000	
H2CCHCN 1v11	1331.175(	37)			284.896	39(5,35)-	40(4,36)										7.2227	
H2CCHCN 1v11	1333.020(	2)			73.690	19(3,16)-	19(3,17)										0.9088	
H2CCCC	1337.910(	270)			258.287	38(2,36)-	38(2,37)										0.2076	
CH3CHO vt=2	1347.923(	41)			286.239	7(2, 5)-	7(2, 6)	+-									6.2575	
D12COOH	1349.99 (	0)			47.150	9(3, 6)-	9(3, 7)										1.891	Wil80
HC11N	1352.503(	0)			0.068	4 -	3										4.0000	
H2CCHCN 1v15	1353.687(	2)			2.464	2(1, 1)-	2(1, 2)										0.8333	
H2CCHCN	1354.359(	6)			116.662	25(3,22)-	26(2,25)										3.9814	
HCCCN	1357.800(	1500)			556.25	19, 1f -	19, 1e 1V6										.103	Laf78
12CH3OH vt=0	1360.498(	22)			340.974	19(3,16)-	19(3,17)	-+									0.9425	
CH3OCHO	1363.921(	8)			378.074	39(11,28)-	39(11,29)	A									12.816	Oes99
H2CNH	1365.087(	33)			630.977	21(5,16)-	21(5,17)		20.0	-	20.0		.317				2.270	Kir73
H2CNH	1365.088(	33)			630.977	21(5,16)-	21(5,17)		22.0	-	22.0		.348				2.270	Kir73
H2CNH	1365.092(*	33)			630.977	21(5,16)-	21(5,17)						1.000				2.270	Kir73
H2CNH	1365.100(	33)			630.977	21(5,16)-	21(5,17)		21.0	-	21.0		.332				2.270	Kir73
H2CCHCN	1371.826(	0)			2.431	2(1, 1)-	2(1, 2)										0.8333	
HCCCN	1372.329(	6)			254.35	14, 1f -	14, 1e 1V7										.138	Laf78
H2C34S	1373.811(	13853)			98.498	10(2, 8)-	10(2, 9)										0.7628	
HDCO	1376.815(	1)			635.899	21(5,16)-	21(5,17)										2.2701	
13CH3OH vt=1	1378.025(	37)			249.675	5(1, 4)-	5(1, 5)	-+									0.2891	
a-CH2=CHOH	1378.471(	3)			139.457	18(4,14)-	18(4,15)										1.6854	
CH3CH2CN	1379.517(	13)			140.783	27(6,21)-	28(5,24)										4.3569	
CH3OCHO	1379.826(	24)			378.070	39(11,28)-	39(11,29)	E									12.481	Oes99
H2CCHCN 1v11	1382.052(	21)			26.808	11(2,10)-	12(1,11)										2.6338	
s-CH2=CHOH	1384.927(	2)			126.609	17(4,13)-	17(4,14)										1.7800	
H2CCHCN 1v11	1387.464(	36)			214.822	36(1,35)-	35(3,32)										0.0221	
CH3CHO vt=1	1395.763(	43)			144.949	2(1, 2)-	1(-1, 0)										0.0170	

```
HCCCN          1400.400(  6500)                  746.97   23, 1f    -  23, 1e 1V5                                          .085  Laf78
D14N12C16O     1403.907(     6)                   20.76    3(  1, 2)-   3(  1, 3)     3.0     -  3.0      0.280  0.583  Win76
D14N12C16O     1404.165(*    2)                   20.76    3(  1, 2)-   3(  1, 3)                                         0.583  Win76
D14N12C16O     1404.251(     3)                   20.76    3(  1, 2)-   3(  1, 3)     4.0     -  4.0      0.402  0.583  Win76
D14N12C16O     1404.371(     6)                   20.76    3(  1, 2)-   3(  1, 3)     2.0     -  2.0      0.212  0.583  Win76
H2CCHCN 1v11   1406.058(     1)                    2.410   2(  1, 1)-   2(  1, 2)                                         0.8333
HCCCHO         1408.038(    15)                  128.275  26(  3,23)-  26(  3,24)                                         0.6707
17OH 2P3/2     1418.202(M   50)  1418.202(  50)            1. 5     -   1. 5          1.5  2.0-  0.5  1.0  0.029        Bea78
13CH3OH vt=1   1424.617(   825)                  570.109  21(  2,20)-  21(  2,19) -+                                      0.3834
H2CO           1428.682(     2)  1428.685(   5) 1057.369  26(  5,21)-  26(  5,22)                                         1.8480 Boc96
H2CNH          1429.312(    76)                 1065.334  28(  6,22)-  28(  6,23)    27.0     - 27.0       .321  2.437  Kir73
H2CNH          1429.312(    76)                 1065.334  28(  6,22)-  28(  6,23)    29.0     - 29.0       .345  2.437  Kir73
H2CNH          1429.315(*   76)                 1065.334  28(  6,22)-  28(  6,23)                          1.000  2.437  Kir73
H2CNH          1429.321(    76)                 1065.334  28(  6,22)-  28(  6,23)    28.0     - 28.0       .333  2.437  Kir73
H2CCHCN        1436.127(     1)                  181.255  31(  4,27)-  31(  4,28)                                         0.9868
H14N12C18O     1436.203(     4)                           4(  1, 3)-   4(  1, 4)     4.0     -  4.0                      Win76
H14N12C18O     1436.482(*    1)                           4(  1, 3)-   4(  1, 4)                                         Win76
H14N12C18O     1436.584(     2)                           4(  1, 3)-   4(  1, 4)     5.0     -  5.0                      Win76
H14N12C18O     1436.682(     3)                           4(  1, 3)-   4(  1, 4)     3.0     -  3.0                      Win76
CH3CH2CN       1437.258(     0)                    1.645   2(  1, 1)-   2(  1, 2)                                         0.8333
HDCO           1438.527(     2)                 1073.449  28(  6,22)-  28(  6,23)                                         2.4372
H2C18O         1439.711(     2)                  227.084  11(  3, 8)-  11(  3, 9)                                         1.5597
H2CCHCN 2v11   1440.043(     3)                    2.391   2(  1, 1)-   2(  1, 2)                                         0.8333
12CH3OH vt=1   1443.034(    21)                  250.180   5(  1, 4)-   5(  1, 5) -+                                      0.2884
HCCCN          1447.630(    32)                  681.53   10, 1f    -  10, 1e 3V7                                          .191  Laf78
17OH 2P3/2     1455.729(M   50)  1455.729(  50)            1. 5     -   1. 5          2.5  2.0-  1.5  1.0  0.052        Bea78
H2CCHCN        1460.289(     6)                  297.459  41(  4,37)-  40(  5,36)                                         7.4380
13CH3OH vt=0   1464.095(    48)                  130.154  11(  2, 9)-  11(  2,10) +-                                      0.5068
15NH2CHO       1465.420(   134)                    2.737   1(  1, 0)-   1(  1, 1)                                         1.5000
H2CCHCN 2v11   1469.963(   128)                  171.597  30(  4,26)-  30(  4,27)                                         1.0183
H2CCHCN 2v11   1470.982(    65)                   73.677  19(  3,16)-  19(  3,17)                                         0.9076
s-CH2=CHOH     1471.830(     5)                  237.780  24(  5,19)-  24(  5,20)                                         1.9573
H2CS           1474.811(     4)                   99.620  10(  2, 8)-  10(  2, 9)                                         0.7627
H2CCCC         1482.240(   299)                  269.900  39(  2,37)-  39(  2,38)                                         0.2023
a-CH2=CHOH     1492.414(     0)                    2.396   1(  1, 0)-   1(  1, 1)                                         1.5000
H2CCHCN 1v15   1494.619(    20)                   80.424  20(  3,17)-  20(  3,18)                                         0.8637
HCCCN          1500.100(  1900)                  562.33   20, 1f    -  20, 1e 1V6                                          .098  Laf78
H13COOH        1500.22 (     3)                  317.145  26(  5,21)-  26(  5,22)                                         1.824  Wil80
NH2CHO         1501.177(     0)                  167.910  19(  4,15)-  19(  4,16)          19.0-       19.0 0.332
NH2CHO         1501.205(     3)                  167.910  19(  4,15)-  19(  4,16)                                         1.6006
NH2CHO         1501.219(     0)                  167.910  19(  4,15)-  19(  4,16)          20.0-       20.0 0.350
NH2CHO         1501.221(     0)                  167.910  19(  4,15)-  19(  4,16)          18.0-       18.0 0.315
H2CCO          1511.335(   676)                  139.332  17(  2,15)-  17(  2,16)                                         0.4569
H12COOD        1516.40 (     0)                   18.238   5(  2, 3)-   5(  2, 4)                                         1.461  Wil80
CH3OCHO        1517.701(     6)                   15.646   7(  3, 4)-   7(  3, 5)  A                                      6.189  Oes99
HCCCN          1519.800(  8000)                  754.25   24, 1f    -  24, 1e 1V5                                          .082  Laf78
H15N12C16O     1523.599(     3)                           4(  1, 3)-   4(  1, 4)                                         Win76
CH3OCHO        1528.771(    12)                   15.657   7(  3, 4)-   7(  3, 5)  E                                      6.086  Oes99
H2CCC          1529.719(   611)                  143.307  17(  2,15)-  17(  2,16)                                         0.4570
DOCO+          1531.844(   664)                   18.106   3(  1, 2)-   3(  1, 3)                                         0.5833
D2CO           1533.804(     0)                  393.253  17(  5,12)-  17(  5,13)                                         2.7724
SiC3           1533.864(    81)                  174.527  27(  5,22)-  27(  5,23)                                         1.7264
CH3CH2CN       1534.180(     1)                   13.833   8(  2, 6)-   8(  2, 7)                                         0.9307
D2CO           1537.411(     0)                  978.582  28(  7,21)-  28(  7,22)                                         3.2526
NH2CHO         1538.108(     3)  1538.110(  10)    2.754   1(  1, 0)-   1(  1, 1)           1.0-        1.0 0.083
NH2CHO         1538.676(     2)  1538.674(  10)    2.754   1(  1, 0)-   1(  1, 1)           1.0-        2.0 0.139
NH2CHO         1539.264(     2)  1539.269(  10)    2.754   1(  1, 0)-   1(  1, 1)           2.0-        1.0 0.139
NH2CHO         1539.527(     4)  1539.526(  10)    2.754   1(  1, 0)-   1(  1, 1)           1.0-        0.0 0.111
NH2CHO         1539.544(     0)  1539.544(  10)    2.754   1(  1, 0)-   1(  1, 1)                                         1.5000 Gar80
NH2CHO         1539.832(     0)  1539.833(  10)    2.754   1(  1, 0)-   1(  1, 1)           2.0-        2.0 0.417
NH2CHO         1540.998(     4)  1540.991(  10)    2.754   1(  1, 0)-   1(  1, 1)           0.0-        1.0 0.111
H2CO           1547.363(     1)  1547.359(   5)  546.645  18(  4,14)-  18(  4,15)                                         1.7091 Boc96
HNO            1548.079(    33)                   57.034   5(  1, 5)-   6(  0, 6)           5.0-        6.0 0.324
HNO            1548.778(   458)                   57.034   5(  1, 5)-   6(  0, 6)           6.0-        6.0 0.009
HNO            1549.384(   119)                   57.034   5(  1, 5)-   6(  0, 6)                                         2.6065
HNO            1549.457(   524)                   57.034   5(  1, 5)-   6(  0, 6)           5.0-        5.0 0.009
HNO            1549.958(    17)                   57.034   5(  1, 5)-   6(  0, 6)           6.0-        7.0 0.385
HNO            1550.299(    12)                   57.034   5(  1, 5)-   6(  0, 6)           4.0-        5.0 0.273
H2CS           1551.061(   264)                  425.936  24(  3,21)-  24(  3,22)                                         0.7312
HNO            1554.816(  2225)                  569.133  17(  3,14)-  17(  3,15)                                         1.0259
H2CO           1555.551(     5)                 1823.647  35(  6,29)-  35(  6,30)                                         1.9642
NH2CHO         1566.403(     0)                  521.766  35(  6,29)-  35(  6,30)          35.0-       35.0 0.333
NH2CHO         1566.417(     9)                  521.766  35(  6,29)-  35(  6,30)                                         1.9242
NH2CHO         1566.423(     0)                  521.766  35(  6,29)-  35(  6,30)          36.0-       36.0 0.342
NH2CHO         1566.424(     0)                  521.766  35(  6,29)-  35(  6,30)          34.0-       34.0 0.324
12CH3OH vt=1   1566.857(   116)                  578.867  21(  2,20)-  21(  2,19) -+                                      0.3975
HCCCN          1568.260(     7)                  258.91   15, 1f    -  15, 1e 1V7                                          .129  Laf78
H2CCCC         1568.513(    68)                   15.628   6(  1, 5)-   6(  1, 6)                                         0.3095
NH213CHO       1569.078(     4)  1569.082(  10)    2.697   1(  1, 0)-   1(  1, 1)           1.0-        1.0 0.083        Gar80
13CH3OH vt=0   1569.176(   106)                  365.202  20(  3,17)-  20(  3,18) -+                                      0.9108
NH213CHO       1569.650(     2)  1569.644(  10)    2.697   1(  1, 0)-   1(  1, 1)           1.0-        2.0 0.139        Gar80
NH213CHO       1570.236(     2)  1570.244(  10)    2.697   1(  1, 0)-   1(  1, 1)           2.0-        1.0 0.139        Gar80
NH213CHO       1570.507(     4)  1570.508(  10)    2.697   1(  1, 0)-   1(  1, 1)           1.0-        0.0 0.111        Gar80
NH213CHO       1570.519(    27)  1570.520(  10)    2.697   1(  1, 0)-   1(  1, 1)                                         1.5000 Gar80
NH213CHO       1570.807(     0)  1570.805(  10)    2.697   1(  1, 0)-   1(  1, 1)           2.0-        2.0 0.417        Gar80
NH213CHO       1571.973(     4)  1571.970(  10)    2.697   1(  1, 0)-   1(  1, 1)           0.0-        1.0 0.111        Gar80
CH3OCHO        1578.149(     8)                  306.411  35( 10,25)-  35( 10,26)  A                                    12.082  Oes99
H213CO         1578.512(    10)                 1871.678  36(  6,30)-  36(  6,31)                                         1.9102
```

CH3OCHO	1580.685(	12)		306.408	35(10,25)-	35(10,26)	E					12.003	Oes99
H2C18O	1583.011(	9)		571.996	19(4,15)-	19(4,16)						1.6212	
CH3OCHO	1583.740(	24)		563.957	48(13,35)-	48(13,36)	A					13.420	Oes99
18OH 2P3/2	1584.275(	0)	1584.274(	2)	-38.203	1. 5 -	1. 5	1.0	- 2.0			0.144	Bea78
H12COOH	1584.88 (	0)			178.157	19(4,15)-	19(4,16)					1.601	Wil80
H213CO	1588.287(	6)			1100.811	27(5,22)-	27(5,23)					1.7792	
H2CO-17	1589.243(	38)			1100.791	27(5,22)-	27(5,23)	27.5	- 27.5	.168		1.779	
H2CO-17	1589.246(	38)			1100.791	27(5,22)-	27(5,23)	26.5	- 26.5	.162		1.779	
H2CO-17	1589.249(	38)			1100.791	27(5,22)-	27(5,23)	28.5	- 28.5	.174		1.779	
H2CO-17	1589.255(*	38)			1100.791	27(5,22)-	27(5,23)			1.000		1.779	
H2CO-17	1589.256(	38)			1100.791	27(5,22)-	27(5,23)	25.5	- 25.5	.156		1.779	
H2CO-17	1589.263(	38)			1100.791	27(5,22)-	27(5,23)	29.5	- 29.5	.181		1.779	
H2CO-17	1589.272(	38)			1100.791	27(5,22)-	27(5,23)	24.5	- 24.5	.151		1.779	
s-CH2=CHOH	1595.750(	1)			2.289	1(1, 0)-	1(1, 1)					1.5000	
H32SD	1596.061(	10)			100.130	3(3, 0)-	3(3, 1)					5.212	Hel73